Deformed SYK & Holography

Sheorey, Sam

Awarding institution:
King's College London

Deformed SYK & Holography

Sameer U. Sheorey

A Dissertation
Presented for the Degree
of Doctor of Philosophy
in the Subject of
Theoretical Physics

Advisor: Dionysios Anninos

Department of Mathematics
King's College London
United Kingdom
July 2024

Abstract

Motivated by the search for a microscopic description of spacetime and the study of quantum chaos, this thesis explores deformations of the Sachdev-Kitaev-Ye (SYK) model. These deformed models exhibit a rich holographic landscape and provide rare examples of strongly coupled systems with non-trivial and tractable thermal RG flows. We start by studying thermodynamics properties the flows. We find that, under certain circumstances, the thermal RG flow in the strongly coupled infrared phase exhibits two regions of linear-in-temperature entropy, which we interpret in terms of Schwarzian actions. We also find a novel model dependent zero temperature entropy for a certain family of deformations. Conformal perturbation theory affords us analytical control over the flows away from the near-conformal fixed point of the original Hamiltonian. We show how this can potentially be used to engineer holographic geometries that contain a portion of de Sitter space, if we allow our deformations to be non-Hermitian. We then turn to more dynamical probes of the deformed models, focussing on Krylov complexity, which has recently been proposed as a diagnostic of quantum chaos. By computing and comparing Krylov and Lyapunov exponents in these deformed models we are able to show that, in all studied examples, while the Lyapunov exponent can have non-monotonic behaviour the Krylov exponent behaves monotonically, and in many cases provides a poor bound for Lyapunov exponent. We speculate on the possibility that this monotonicity might be a generic feature of the Krylov exponent in quantum systems evolving under unitary evolution.

To Dad and Mothiaai

Acknowledgements

This thesis would not have been possible without the help of many people, and I would like to extend my gratitude to at least a few of them now.

First, I would like to thank my supervisor, Dionysios. Thank you for inspiring me to take on the PhD, persuading me to push through the difficult periods and encouraging me to find my own research path. Thank you also for your remarkable generosity in sharing both your time and vast knowledge with me. Your infectious enthusiasm for physics never ceases to amaze me and has provided constant encouragement. I have been extraordinarily lucky to have been your student.

In terms of academic guidance, I ended up being doubly blessed during my PhD. Damián, your meticulous support and unending patience have been invaluable. Thank you for all that you have taught me and helping me reach my potential as a young researcher. I will certainly miss camping out in your office and discussing our latest calculations. Most of all, thank you for your advice and friendship.

Next, I would like to thank the rest of my wonderful collaborators: Shira Chapman, Saskia Demulder, Ellie Harris, Osher Shoval and David Vegh. It has been a pleasure to work with and learn from each of you.

I also cannot go without mentioning all the incredible PhD students and postdocs I have had the pleasure of getting to know over the past few years. Thank you for your camaraderie, for the lighter moments, and most of all, for our many pub trips.

Finally, I am especially indebted to my wife Nikki, my mother Bharati and brother Nik, for their encouragement, love and patience throughout this four year journey.

Contents

1 Introduction

This thesis is motivated by two distinct but deeply connected problems in theoretical physics. The first is the search for a microscopic description of spacetime and the second is the study of signatures of chaos in many body quantum systems. In this work we will explore both topics in the context of simple but concrete models, where we are able to perform precise calculations both analytically and numerically.

Motivation 1: A microscopic description of spacetime

A theory describing the thermodynamic properties of substances was known before a theory describing their particulate nature was fully developed. Nevertheless, the deep physical principle that matter is made of particles had long been suspected. The application of mechanical laws to these hypothesised particles, initiated by Bernoulli in 1738 [1] and with pivotal contributions by Maxwell and Boltzmann in the mid-19th century [2, 3], resulted in the dramatic mathematical realisation of this principle. For the first time we saw the macroscopic properties of substances as emerging in a precise way from the behaviour of their particulate constituents. Many of the great developments in physics since then have come from revising the laws that should be applied to these particles in light of ever developing observational and theoretical evidence.

It is possible that we find ourselves in an analogous situation with an entirely different kind of 'substance' - spacetime itself. A compelling reason to think along these lines goes as follows. In statistical mechanics we can compute the partition function of a thermal ensemble from the Euclidean path integral of the theory. In the case of Einstein's theory of gravity we can analogously compute 'thermodynamic properties' of spacetimes via the gravitational path integral [4]. In this scheme we compute the Euclidean path integral of the gravitational action and interpret the results as thermodynamic quantities. We can speculate that these quantities are more than just an analogy and picture the gravitational action as an effective action for some underlying theory containing microscopic degrees of freedom. In other words we may think of spacetime as emerging from 'particles'.

Though this idea may seem superficial at first, there has been strong theoretical evidence in support of it. The story of combining thermodynamics with general relativity began with the

study of black hole thermodynamics, initiated by Bekenstein [5] and Hawking [6]. Their arguments, which were independent of the gravitational path integral, led to the conclusion that black holes are thermodynamic objects that carry an entropy proportional to one quarter the area of their horizon

$$S_{\rm BH} = \frac{A_{\rm hor}}{4}\left(\frac{k_b c^3}{\hbar G}\right) + \cdots \ . \tag{1.1}$$

Notably, the entropy of a black hole is a factor of $\sim 10^{19}$ times greater than that of a star of the same mass. Though it is not clear how we should interpret this entropy, its enormous value suggests that it is counting more than the states of ordinary matter that could be associated to the black hole. Moreover, as the appearance of both $\hbar$ and G in the formula suggests, this entropy must combine both gravitational and quantum mechanical effects. It is also telling that, to leading order, the entropy of black holes as calculated from the gravitational path integral gives the same result. Such a calculation provides quantum corrections that any candidate theory of quantum gravity should be able to predict.

The fact that the entropy of a black hole scales with its area and not its volume led to the conjecture of the holographic principle [7, 8], that the information content of a region of space can be encoded on its boundary. The most famous realisation of this principle in a concrete model is called the AdS/CFT correspondence [9]. The AdS/CFT correspondence claims a 1-1 correspondence between states in a string theory containing gravity in $\mathrm{AdS}_5 \times S^5$ and $\mathcal{N} = 4$ Super Yang-Mills, a conformal field theory without gravity that lives on the AdS_5 boundary. It is hoped that other dualities exist along the lines of the AdS/CFT correspondence that can provide a new way to understand theories of gravity and the emergence of spacetime. Of particular interest would be to find a holographic dual to de Sitter space, providing a microscopic model in which test ideas about our own expanding universe. Despite various proposals, the lack of natural boundary at infinity to anchor the dual theory makes this a particularly difficult problem and a definitive framework remains elusive; see [10] for a recent review.

The pursuit of a microscopic description of spacetime is more than just a theoretical curiosity. Firstly, a description of spacetime, based on the theory of General Relativity, is known to break down in regimes of high energy or short distances (UV). Most famously General Relativity predicts singularities at the centre of black holes and at the beginning of the universe. Such problems cannot be resolved by an effective theory of quantum gravity based on quantising the Einstein Hilbert action

and it is likely that a microscopic UV completion will be needed. But it is not only in the UV that a microscopic description of spacetime might be crucial. Problems such as eternal inflation [11, 12], the black hole information paradox [13, 14] and the cosmological constant problem [15, 16] all hint at a possible breakdown of effective field theory low energies or long distances (IR) and the need of a microscopic model to shine a light on these problems. The cosmological constant problem is a particularly illustrative example of this. This constant, needed to describe the accelerating expansion of our universe, has a current measured value of [17]

$$\Lambda = 1.1056 \times 10^{-52}\,\mathrm{m}^{-2}\ , \tag{1.2}$$

which differs from the naive quantum field theory estimate by ~ 120 orders of magnitude [15, 16]. This small positive constant is thought to account for $\sim$70% of the energy content of the universe, and yet we have not found a fundamental explanation for its observed value. Nonetheless, the thermodynamics of de Sitter space give a deep clue that a microscopic description is needed. The leading term of the entropy of de Sitter, found by the gravitational path integral, is found to proportional to the area of the cosmological horizon,

$$S_{\mathrm{dS}} = \frac{A_{\mathrm{hor.}}}{4}\left(\frac{k_B c^3}{\hbar G}\right) + \cdots = \frac{3\pi}{\Lambda}\left(\frac{k_B c^3}{\hbar G}\right) + \cdots\ . \tag{1.3}$$

This remarkable formula binds the value of the cosmological constant to a microscopic description of spacetime, and just as in the case of the black hole, the fact that it follows an area law hints that this description should be holographic.

Motivation 2: Diagnosing quantum chaos

In classical systems, chaos is diagnosed by exponential sensitivity to the initial conditions of a system. Quantum mechanics however is governed by a linear equation, excluding the possibility of such a definition. Nonetheless, given that chaos can exist in the classical limit of quantum systems, it is natural to ask what the underlying signatures of chaos are in quantum systems. The study of such signatures falls under the umbrella of quantum chaos.

In quantum many body systems diagnosing chaos presents a further challenge: dynamical probes are typically hard to compute, in part due to the fact that the Hilbert space grows exponentially

with the number of constituents. This difficulty is even more pronounced in quantum systems that are strongly coupled and quantum chaotic. Despite significant progress in the area [18], defining a good quantum signature of chaos valid for all time scales can be difficult. The situation improves when the quantum system has some intrinsically small parameter, such as in large N theories or those with a semi-classical limit. Following the use of the exponential growth of the Poisson bracket as a function of time [19] to diagnose classical chaos, one might hope that in a quantum theory with a semi-classical limit, the commutator of simple (local) operators might be related to quantum chaos. Indeed, in such systems the square of the commutator [20] was found to grow exponentially with a growth rate λ_L, known as the Lyapunov exponent. Further, it was shown in [21] in local, unitary quantum systems the Lyapunov exponent satisfies,

$$\lambda_L \leq \frac{2\pi}{\beta}, \tag{1.4}$$

thus setting a bound on quantum chaotic behaviour. There are, of course, other interesting quantities to diagnose quantum chaos, such as the onset of random matrix statistics [22], the spectral form factor [23] or quantum circuit complexity [24, 25].

Another related quantum signature of chaos comes from the idea of operator growth. The intuition is that, if the Hamiltonian is chaotic, an initially simple operator will grow exponentially in complexity under Heisenberg time evolution. As opposed to the Lyapunov exponent, this concept does not require a small parameter. Recently, the use of Krylov subspace methods has been proposed to quantify this idea of operator growth [26].

Since their conception in 1931, Krylov methods have played an important role in mathematics and theoretical physics [27]. Their main feature is to project a higher-dimensional (computationally hard) problem to a lower-dimensional one (approximate, but computationally more accessible). Typical examples involve matrix diagonalisation or eigenvalue problems. In the case of operator growth, the idea is to find the minimal subspace needed to follow the time-evolution of an operator, without the need of diagonalising the full Hamiltonian. This is done by considering the subspace spanned by the set of nested commutators of the operator with the Hamiltonian. The nested commutators are said to form a basis of the Krylov subspace. It was conjectured that the properties of this subspace can be used to diagnose whether the quantum system is chaotic or not by using the *operator growth hypothesis* [26]. Since then a critical amount of work has been devoted to

understand and test this hypothesis in different quantum systems. See [28], and references therein, for a comprehensive review of recent results on the subject.

As a quantitative measure of operator growth, the concept of Krylov complexity was coined in [26]. Under certain assumptions that we will discuss later, this complexity grows exponentially with time in chaotic systems, and it was conjectured that the exponent, called the Krylov exponent λ_K, would serve as a tighter bound for the Lyapunov exponent (when this one is well-defined), namely,

$$\lambda_L \leq \lambda_K \leq \frac{2\pi}{\beta} \ . \tag{1.5}$$

As we will see, while the Lyapunov exponent appears require the computation of the four-point out-of-time-ordered correlator, the computation of the Krylov exponent only requires knowledge of the two-point function of the operator. Then, if the left bound turns out to be tight, this gives a computational advantage to λ_K as a probe of quantum chaos. Given this potential advantage and the fact that a semi-classical or large N limit is not needed, it is important to understand whether Krylov complexity can serve as a more general diagnosis of chaos.

A tractable model at the intersection of holography and quantum chaos

Whilst the AdS/CFT correspondence was a significant achievement, its computational challenges limit its usefulness as a tool for understanding quantum gravity. At the same time studies of many body chaos are hampered by the complexity of the systems involved. Fortunately, there is a model that lies at the intersection of these two fields that is complex enough to capture their essential features while still being simple enough to remain highly solvable. This model is called the Sachdev-Kitaev-Ye (SYK) model.

The SYK model is a many body quantum mechanical model in $0+1$ dimensions, consisting of Majorana fermions with random all-to-all interactions. A version of the model was originally proposed by Sachdev and Ye in 1992 who used the model to study strongly correlated materials [29]. The model was later revisited by Kitaev in 2015 who proposed using a simplified version of the model in the context of AdS_2 holography [30]. Moreover, Kitaev showed the SYK model to be maximally chaotic at low temperatures by virtue of it saturating the chaos bound (1.4) [30,31].

Extending Kitaev's insights, an explicit duality between the SYK and AdS_2 dilaton gravity (JT gravity) was found [32–34]. As well as describing the AdS_2 black hole, this theory has quantum

fluctuations coming from boundary dynamics that are described by the SYK model. It is also worth noting that since JT gravity universally describes the near horizon behaviour of near-extremal black holes in higher dimensions, the duality should also capture important properties of astrophysical black holes; see *e.g.,* [33, 35] for a discussion. From the holographic perspective, the saturation of the chaos bound provides evidence towards black holes being the fastest scramblers in nature [36].

A new direction in SYK research and holography

Studying the SYK model at strong coupling has been extremely fruitful, yielding many insights in the context of both holography and many body chaos [26, 31, 37–45]. Nonetheless, the need for concrete and tractable models in both quantum chaos and holography remains. In this thesis we look to address this problem by opening a new chapter in the study of deformed SYK models and holography. Our goal is to perform a systematic study of relevant deformations of the SYK model, examining their rich thermodynamic and chaotic behaviours and exploring the new holographic possibilities that they present. We will do so by employing cutting-edge numerical methods (see section 3) alongside innovative analytical techniques to extract a collection of precise and insightful results.

Concretely, the SYK model admits a rich landscape of relevant deformations that take the form of another SYK Hamiltonian with fewer fermions in each interaction term [46–55]. These deformed models can have highly non-trivial behaviour in the infrared. We will examine the Hamiltonian

$$H_q = i^{\frac{q}{2}} \sum_{1\leq i_1<i_2<\cdots<i_q\leq N} J_{i_1 i_2 \cdots i_q} \psi_{i_1}\psi_{i_2}\cdots\psi_{i_q} \ , \qquad q \in 2\mathbb{Z}^+ \ , \tag{1.6}$$

deformed by an operator $s\, H_{\tilde{q}_i}$ with $\tilde{q} < q$, where s is a dimensionless coupling and ψ_i are N Majorana fermions. The couplings of both H_q and $H_{\tilde{q}}$ are drawn from a Gaussian ensemble. For such a deformation, provided that s is small enough, as we flow towards the IR of the theory we first reach the IR fixed point of the original SYK model described by JT gravity before flowing to a new fixed point in the deep IR of the model. Studying these deformed models along their thermal RG flow we uncover a diverse and noteworthy set of behaviours. These include, for example, a zero temperature entropy that varies continuously with model parameters, and the possibility for a worldline theory residing in the interior of their holographic bulk [54].

We further enhance the richness of the flows by considering deformations built from concate-

nating multiple SYK Hamiltonians. This opens up a vast landscape of holographic geometries that could potentially be realised by these models. By developing new techniques in *relevant* conformal perturbation theory, we gain analytical control over these flows in the vicinity of their first fixed point. We exploit this to explore the possibility of engineering new holographic geometries, including ones that contain a portion of de Sitter space [56, 57]. This could perhaps open new avenues for exploring the holographic nature of our own expanding universe, providing a complementary approach to active research in this direction [58–60].

The flows also include the possibility of transitions between different regions of near-maximal chaos or transitions between near-maximally chaotic and integrable behaviour. This provides a unique opportunity to test out signatures of quantum chaos in the context of these highly non-trivial behaviours. We make use of this to test the robustness of Krylov complexity as a diagnostic for quantum chaos that has recently attracted significant research attention [26, 28, 61–69]. This leads us to make a novel conjecture about the growth of the Krylov exponent, which sharply contrasts it to that of the better established Lyapunov exponent [70].

These deformed SYK models offer a unique example of strongly coupled systems with complex yet tractable thermal RG flows. We hope this new chapter in their study can continue to provide new and interesting insights into the nature of chaos and holography.

Outline of the thesis

The thesis is structured as follows. In section 2 we review the relevant background material needed to motivate and develop the results of this thesis. In section 3 we give an overview of key methodologies used in the thesis by detailing the numerical techniques used to investigate the deformed models. The main results of the thesis are then presented in the following three sections.

In section 4 we study deformed SYK models with a single unitary deformation. These models correspond holographically to flow geometries that interpolate between two Euclidean near-AdS_2 spacetimes with different radii. We significantly generalise the study of these deformed models beyond the analytically solvable regime studied in previous work [52, 53], establishing new insights including a non-trivial model dependent zero temperature entropy and the fact that relevant conformal perturbation theory can be used to describe the flow.

In section 5 we extend our analysis to multiple deformations and allow for non-unitary models.

From the holographic perspective, these deformed SYK models open up a far richer set of bulk geometries. JT gravity can be generalised to a set of dilaton gravity theories that describe a much more general set of two-dimensional spacetimes than just AdS_2 [71]. In particular these can describe a geometry that is asymptotically AdS_2 but flows to dS_2 in the interior [56, 57, 72]. In this section we provide evidence towards the idea that deformed SYK models may be able to realise such geometries, if we allow ourselves to consider non-Hermitian models.

In section 6 we return to considering single, unitary deformations, and use the flows to test Krylov complexity as a diagnostic for quantum chaos. We find that while the Lyapunov exponent can have non-monotonic behaviour along the flows as a function of temperature, in all studied examples the Krylov exponent behaves monotonically. Moreover, we show that although in undeformed SYK model the Krylov exponent is found to equal the Lyapunov exponent at all temperatures, in the case of the deformed model the two can diverge significantly, rendering the Krylov exponent a poor measure for diagnosing chaos in such models.

Finally, in section 7 we present our main conclusions and outlook. In particular, we speculate on the need for open quantum systems in the context of de Sitter holography. Further, we conjecture that (as long as it is well-defined) the Krylov exponent has a monotonic behaviour along thermal RG flows. It is hoped that these ideas could open up new directions in the study of chaos and holography.

This thesis is based on the following published work and work in preparation.

- D. Anninos, D. A. Galante, S. U. Sheorey, *Renormalisation Group Flows of the SYK Model*, JHEP 11 (2023) 197 [2212.04944].
- S. Chapman, S. Demulder, D. A. Galante, S. U. Sheorey, O. Shoval *Krylov complexity and chaos in deformed SYK models*, (2024) arXiv:2407.09604.
- D. Anninos, D. A. Galante, S. U. Sheorey, *(Non-)Hermitian deformations of the Sachdev-Ye-Kitaev model and their holographic duals* [in preparation].

The author has also published the following work during their PhD program, which does not form part of this thesis.

- S. Chapman, D. A. Galante, E. Harris, S. U. Sheorey, D. Vegh, *Complex geodesics in de Sitter space*, JHEP 03 (2023) 006 [2212.01398]

2 Preliminaries

2.1 Quantum chaos

Dynamical information about a quantum system is encoded in its spectrum. This is therefore a natural place to search for statistical signatures of chaos. In 1984, Bohigas, Giannoni and Schmit stated the famous BGS conjecture that the spectral statistics of chaotic quantum system should be described by random matrix theory (RMT) [73]. RMT was introduced initially by Wigner, and later developed by Dyson and Metha [74–76]. The idea was that the eigenvalue statistics of heavy nuclei are well described by that of random Hamiltonians - in particular by Hamiltonians whose matrix elements are drawn from Gaussian distributions. Gaussian ensembles of $n \times n$ matrices have probability density functions of the form

$$p(\{H_{ij}\}) = \mathcal{N}_{\beta_D} e^{-\frac{\beta_D}{4}\mathrm{Tr}(H^2)} , \qquad \beta_D = 1,\, 2 \text{ or } 4 , \tag{2.1}$$

where $\mathcal{N}_{\beta_D}$ is a normalisation constant and β_D is known as the Dyson index. There are three Gaussian ensembles, often denoted by their Dyson index. These are the Gaussian Orthogonal Ensemble (GOE) with $\beta_D = 1$, Gaussian Unitary Ensemble (GUE) with $\beta_D = 2$ and Gaussian Symplectic Ensemble (GSE) with $\beta_D = 4$. These ensembles are defined on the spaces of real symmetric, Hermitian and Hermitian quaternionic matrices respectively and the β_D dependence in (2.1) ensures that their probablity densities are invariant under orthogonal, unitary and symplectic similarity transformations respectively. The BGS conjecture extends the idea of RMT to state that any quantum system that displays chaotic behaviour in its classical limit should have the same spectral properties as predicted by random matrices models defined by (2.1). In particular the eigenvalue distribution of such models is given by [77]

$$P(\{\lambda_i\}) = \mathcal{N}_{\beta_D} \exp\left(-\frac{\beta_D}{4}\sum_{i=1}^{n}\lambda_i^2\right)\prod_{i<j}|\lambda_i - \lambda_j|^{\beta_D} . \tag{2.2}$$

We observe that the exponential term stops the eigenvalues form spreading too far from the origin whilst the product term stops any two eigenvalues from getting too close to each other. A notable consequence of the conjecture is that the distribution of the spacing between eigenvalues, s, expected

for chaotic systems goes like $p(s) \sim se^{-s^2/4\sigma^2}$ whilst that of an integrable system follows Poisson statistics, $p(s) \sim e^{-s}$. The SYK model has been shown to have spectral statistics corresponding to each of the GOE, GUE and GSE ensembles depending on the number of Majorana fermions, N, in the model [41].

In many body systems another important signature of chaos is the growth of simple (few body) operators into complex (many body) ones. An important diagnostic for this effect is the double commutator. For a system at finite temperature β^{-1}, the double commutator for Hermitian operators V and W is defined as [20, 21]

$$\mathcal{C}(t) = \langle -[W(t), V(0)]^2 \rangle_\beta \ , \tag{2.3}$$

where $\langle \bullet \rangle_\beta = Z_\beta^{-1} \mathrm{tr}(e^{-\beta H} \bullet)$ is the thermal average. For fermionic systems the commutator is replaced by an anti-commutator. The idea behind this diagnostic is that in a chaotic system the operator $W(t)$ spreads across the system in such a way that it will quickly fail to commute with any simple operator in the system V. More precisely, in chaotic systems, after an initial dissipation time $t_d \sim \beta$ the double commutator is conjectured to grow exponentially at early times before saturating to its late time average. Within this time frame we can write the growth of the double commutator for a chaotic system as

$$\mathcal{C}(t) \sim \varepsilon e^{\lambda_L t} + \cdots \ , \tag{2.4}$$

where ε is a small parameter, typically either proportional to $\hbar$ in the case of systems with a semi-classical limit, or $1/N$ for systems permitting a large N limit like the SYK. The rate of early time growth is governed by λ_L, known as the quantum Lyapunov exponent. The time at which saturation occurs is called the scrambling time, $t_s = (1/\lambda_L) \log(1/\varepsilon)$. Note that for the Lyapunov exponent to be meaningful, this timescale has to be much larger than the dissipation time $t_d \sim \beta$, which is guaranteed as long as $N \gg 1$ with $\beta \sim O(1)$.

We can gain an intuition for the double commutator by taking the semi-classical limit of a single particle quantum system with $W(t) = q(t)$ and $V = p$. The double commutator then becomes a

Poisson bracket which we can write as [20, 21]

$$-(i\hbar\{q(t),p\})^2 = \hbar^2\left(\frac{\partial q(t)}{\partial q(0)}\right)^2 . \tag{2.5}$$

This quantity measures the sensitivity of trajectories to the initial position of the system, and is precisely the quantity we expect to grow exponentially for classically chaotic systems. When W and V are Hermitian and unitary we can rewrite the double commutator as

$$\mathcal{C}(t) = 2\left(1 - \mathrm{Re}\left(\mathrm{OTOC}(t)\right)\right) \ , \tag{2.6}$$

where the out of time order correlator is defined as $\mathrm{OTOC}(t) = \langle W(t)V(0)W(t)V(0)\rangle_\beta$. Therefore, in such cases, the OTOC contains the same information as the double commutator and is often computed instead. In a quantum chaotic system with a small parameter, that we will now take to be $1/N$, this correlator generically behaves as [21]

$$\mathrm{OTOC} = f_0 - \frac{f_1}{N}\exp\lambda_L t + \cdots , \tag{2.7}$$

where $f_{0,1}$ are order one numbers that are theory dependent and λ_L is the Lyapunov exponent. It was shown in [21] that in local, unitary quantum systems, $f_{0,1} > 0$ and

$$\lambda_L \leq \frac{2\pi}{\beta}, \tag{2.8}$$

which we will refer to as the chaos bound. Since the OTOC can have divergences one often computes a regularised OTOC

$$\mathrm{OTOC}(t) = \mathrm{Tr}\left(\rho^{\frac{1}{4}}W(t)\rho^{\frac{1}{4}}V(0)\rho^{\frac{1}{4}}W(t)\rho^{\frac{1}{4}}V(0)\right) \ , \qquad \rho = \frac{1}{Z(\beta)}e^{-\beta H} \ . \tag{2.9}$$

It has be shown in the case of the SYK that the Lyapunov exponent does not depend on the choice of regularisation [44, 78]. The Lyapunov exponent of the SYK model can be computed analytically at low temperatures and is found to saturate the chaos bound [30, 31], rendering the model maximally chaotic in this regime.

2.2 Krylov complexity

In this section we review the notion of Krylov complexity and its relation to chaos in quantum systems. We will be interested in the growth of a simple operator $\mathcal{O}$ under Heisenberg time evolution. Heisenberg time evolution spreads the operator through a series of nested commutators, which can be written in terms of the Liouvillian operator $\mathcal{L} := [H, \cdot]$ as

$$\mathcal{O}(t) = e^{iHt}\mathcal{O}e^{-iHt} = \sum_{n=0}^{\infty} \frac{(it)^n}{n!}\mathcal{L}^n\mathcal{O} \ . \tag{2.10}$$

In the following we will always assume the Hamiltonian and the operator $\mathcal{O}$ to be Hermitian. To describe the operator spreading, we first consider the vector space spanned by the nested commutators

$$\mathcal{H}_{\mathcal{O}} = \text{span}\{\mathcal{O}, [H, \mathcal{O}], [H, [H, \mathcal{O}]], \ldots\} \ . \tag{2.11}$$

This operator space is called the Krylov subspace and it contains the time-evolved operator $\mathcal{O}(t)$ for all t. In order to quantify the operator growth within this subspace one defines an inner product acting on operators in the theory. The inner product used at infinite temperature is given by

$$(\mathcal{O}_1|\mathcal{O}_2) := \frac{\text{Tr}(\mathcal{O}_1^\dagger \mathcal{O}_2)}{\text{Tr}(I)}, \tag{2.12}$$

where I is the identity operator. One can also consider the system at finite inverse temperature β, for which it is usually useful to use the Wightman inner product,

$$(\mathcal{O}_1|\mathcal{O}_2)_\beta^W := \frac{1}{Z}\text{Tr}\left(e^{-\beta H/2}\mathcal{O}_1^\dagger e^{-\beta H/2}\mathcal{O}_2\right) \ , \tag{2.13}$$

where $Z = \text{Tr}\left(e^{-\beta H}\right)$. Taking the $\beta \to 0$ limit recovers the inner product at infinite temperature. One can then find an orthonormal basis with respect to the inner product via the Gram-Schmidt procedure. We will refer to this basis as the Krylov basis. For a Hermitian operator, the Gram-Schmidt procedure applied to (2.10) is described in [26] as follows. First define

$$|\mathcal{O}_0) := |\mathcal{O}) \, , \ b_1 = (\mathcal{O}_0\mathcal{L}|\mathcal{L}\mathcal{O}_0) \, , \ |\mathcal{O}_1) := b_1^{-1}\mathcal{L}\,|\mathcal{O}_0) \ . \tag{2.14}$$

Then, for $n > 1$, carry out the following recursive algorithm

$$\begin{cases} |A_n) & := \mathcal{L}|\mathcal{O}_{n-1}) - b_{n-1}|\mathcal{O}_{n-2}) \ , \\ b_n & := (A_n|A_n)^{1/2} \ , \\ |\mathcal{O}_n) & := b_n^{-1}|A_n) \ . \end{cases} \tag{2.15}$$

For finite dimensional Hilbert spaces, the recursive algorithm stops for some $n = D_K$ known as the Krylov dimension.

The b_n's are called Lanczos coefficients and from (2.15) it is easy to see that the Liouvillian operator is tridiagonal with respect to the Krylov basis with the upper and lower diagonal entries corresponding to the Lanczos coefficients,

$$(\mathcal{O}_n|\mathcal{L}|\mathcal{O}_m) = \begin{pmatrix} 0 & b_1 & 0 & 0 & \cdots \\ b_1 & 0 & b_2 & 0 & \cdots \\ 0 & b_2 & 0 & b_3 & \cdots \\ 0 & 0 & b_3 & 0 & \ddots \\ \vdots & \vdots & \vdots & \ddots & \ddots \end{pmatrix} \ . \tag{2.16}$$

The time-dependent operator admits the following expansion,

$$\mathcal{O}(t) = \sum_{n=0}^{D_K-1} i^n \varphi_n(t)|\mathcal{O}_n) \, , \tag{2.17}$$

where all the time-dependence has been completely transferred to "wavefunctions" $\varphi_n(t)$ of the Schrödinger equation of an effective one dimensional tight-binding chain

$$\partial_t \varphi_n(t) = b_n \varphi_{n-1}(t) - b_{n+1}\varphi_{n+1}(t) \, , \qquad \varphi_n(0) = \delta_{n0} \, , \quad \varphi_{-1}(t) = 0. \tag{2.18}$$

From this one can directly infer that the spread of the operator in time over the Krylov basis is determined by the Lanczos coefficients. The faster the Lanczos coefficients grow with n, the faster the operator will spread over the Krylov basis.

In [26], it was noted that in non-integrable many body systems the Lanczos coefficients are

asymptotically linear in n,[1]

$$b_n \sim \alpha\, n + \gamma \ , \tag{2.19}$$

where the slope $\alpha > 0$ and γ are constant real numbers. When the system is integrable, the Lanczos coefficients will grow with a fractional power $b_n \sim n^\delta$, for $0 < \delta < 1$. A linear growth in the Lanczos coefficients[2] is expected to lead to an exponential growth in the Krylov complexity that is defined as,

$$C_K \equiv \sum_{n=0}^{D_K-1} n|\varphi_n|^2 \quad {}^{b_n \sim \alpha\, n}_{\sim} \quad e^{\lambda_K t} \, , \tag{2.20}$$

where we defined the Krylov exponent as follows[3]

$$\lambda_K \equiv 2\alpha \, . \tag{2.21}$$

Note that the form of the exponential growth in (2.20) has not been proved for all cases of coefficients with linear asymptotic growth. Nonetheless, it has been checked analytically and numerically for a large range of cases and is expected to hold in general [26]. The Krylov complexity C_K measures the average position of the operator in the tight-binding chain, which effectively describes the spread of the operator over the Krylov basis. Note that, as a consequence, in integrable quantum systems, the Krylov complexity typically does not grow exponentially. See [28] for different known behaviours. In such cases the Krylov exponent is not well-defined.

For chaotic systems where (2.19) holds and the Lyapunov exponent is also well-defined, it was proposed that the Krylov exponent could provide an upper bound for the Lyapunov exponent, see (1.5) that we recall here,

$$\lambda_L \leq \lambda_K \leq \frac{2\pi}{\beta} \ . \tag{2.22}$$

[1]Note that for one-dimensional systems, there could be a logarithmic correction to the linear growth [28]. This correction is not present in SYK-like models.

[2]This assumes that the dependence of the Lanczos coefficients on n is smooth.

[3]One should note that there are known examples where the exponential of the Krylov complexity λ_K does not satisfy this relation with the slope of the Lanczos coefficients α. This was shown to happen in thermal quantum field theory, where the Lanczos coefficients split into separate branches for even and an odd n [79,80], where the staggering was proposed to be related to the mass gap in the power spectrum. We will indeed see such a splitting for the finite q SYK, but both even and odd coefficients will be linear with the same slope and the staggering effect will be very small in all the cases we study. Therefore, we will assume that $\lambda_K = 2\alpha$. We leave a full evaluation of λ_K for future work.

The left inequality was proved at infinite temperature in [26], and follows from properties of the Krylov basis. In [26] the inequality was further conjectured to hold at finite temperature so long as the Wightman inner product (2.13) is used. This conjecture was evidenced by the study of the SYK model in a certain scaling limit, where the inequality was found to be saturated. It is worth noting that while the Lyapunov exponent requires the computation of the four-point OTOC, the Krylov exponent only requires the two-point autocorrelation function (see section 6.2). It is not obvious why these two distinct correlators should be related in this manner and moreover whether the bound should be tight. We will explore the tightness of this bound and how reliable λ_K is as a means for diagnosing chaos in section 6. Under the assumption of certain analytic and smoothness properties of the Lanczos coefficients n, the right inequality was proved at finite temperature in [26,61,62]. It is worth noting that Krylov complexity was generalised to study the spread of states rather than operators both in unitary [63–65,68] and non-unitary systems [66,67,69].

2.3 The SYK model

Having explored general ideas about quantum chaos we know turn our attention to the main protagonist of the thesis - the SYK model. The SYK model is a quantum mechanical model with random, q-local interactions. See [31,35,81–83], for instance, for some reviews of the model. The observables of the theory are built from N Majorana fermions, ψ_i, obeying equal time anti-commutation relations

$$\{\psi_i, \psi_j\} = \delta_{ij} \ , \qquad i,j = 1, \ldots, N \ . \tag{2.23}$$

The model consists of an ensemble of Hamiltonians

$$H_q = (i)^{\frac{q}{2}} \sum_{1 \leq i_1 < i_2 < \ldots < i_q \leq N} J_{i_1 i_2 \ldots i_q} \psi_{i_1} \psi_{i_2} \ldots \psi_{i_q} \ , \qquad q \in 2\mathbb{Z}^+ \ , \tag{2.24}$$

where the coupling constants $J_{i_1 i_2 \ldots i_q}$ of the theory are independent and identically distributed random variables drawn from a Gaussian distribution with

$$\langle J_{i_1 i_2 \cdots i_q} \rangle = 0 \ , \qquad \langle J^2_{i_1 i_2 \cdots i_q} \rangle = \frac{2^{q-1}}{q} \frac{\mathcal{J}^2 (q-1)!}{N^{q-1}} \ . \tag{2.25}$$

At finite N, the dimensionality of the Hilbert space is $2^{N/2}$, which makes it computationally hard to exactly diagonalise the Hamiltonian for $N \gtrsim 36$. In this regime, it can already be observed that the spectrum of the theory is chaotic for all values of $q \geq 4$, and integrable for $q = 2$ [31, 35].

Large N limit

From the perspective of the path integral, it is useful to express the theory in terms of bi-local fields $G(\tau_1, \tau_2)$, $\Sigma(\tau_1, \tau_2)$ [31, 40, 84]. For a detailed derivation the reader may refer to appendix A. The Euclidean time coordinate $\tau \sim \tau + \beta$ is periodically identified with period given by the inverse temperature β. Physically, $G(\tau_1, \tau_2)$ computes the (time-ordered) thermal two-point function

$$G(\tau_1, \tau_2) = \frac{1}{N} \sum_{i=1}^{N} \langle T\psi_i(\tau_1)\psi_i(\tau_2)\rangle_\beta \,, \tag{2.26}$$

In terms of G and Σ the action reads

$$I = -\frac{1}{2}\log\det\left(\delta(\tau_1-\tau_2)\partial_{\tau_2} - \Sigma(\tau_1,\tau_2)\right) + \frac{1}{2}\int_0^\beta\int_0^\beta d\tau_1 d\tau_2 \left(\Sigma(\tau_1,\tau_2)G(\tau_1,\tau_2) - \mathcal{J}^2\frac{2^{q-1}}{q^2}G(\tau_1,\tau_2)^q\right) \,, \tag{2.27}$$

and the disorder averaged partition function of the theory is given by

$$\langle Z(\beta)\rangle_J = \int [DGD\Sigma] e^{-NI[G,\Sigma]} \,, \tag{2.28}$$

where we indicate a disorder average by $\langle \bullet \rangle_J$. At large N, the theory permits a saddle point approximation. The resulting Schwinger-Dyson equations are the following integro-differential equations

$$\begin{cases} G^{-1}(\tau_1,\tau_2) = \delta(\tau_1-\tau_2)\partial_{\tau_2} - \Sigma(\tau_1,\tau_2) \,, \\ \Sigma(\tau_1,\tau_2) = \mathcal{J}^2\frac{2^{q-1}}{q}G(\tau_1,\tau_2)^{q-1} \,. \end{cases} \tag{2.29}$$

The above equations can be solved numerically using a recursive algorithm and the fast Fourier transform [31] or the Legendre spectral method [85]. Details of these procedures are given in section 3.2. In the IR of the theory, given by $|\tau_1 - \tau_2| \gg 1/\mathcal{J}$, we can self-consistently drop the $\delta(\tau_1 - \tau_2)\partial_{\tau_2}$

term in (2.29), resulting in an effective theory described by the equations

$$\begin{cases} \int_0^\beta d\tau' \, G(\tau_1,\tau')\Sigma(\tau',\tau_2) = -\delta(\tau_1-\tau_2) \ , \\ \Sigma(\tau_1,\tau_2) = \frac{2^{q-1}}{q}\mathcal{J}^2 G(\tau_1,\tau_2)^{q-1} \ . \end{cases} \tag{2.30}$$

Provided $\Delta = 1/q$ these above equations are invariant under the transformations

$$\begin{cases} G(\tau_1,\tau_2) \to \tilde{G}(\tau_1,\tau_2) = \phi'(\tau_1)^\Delta \, G(\phi(\tau_1),\phi(\tau_2)) \, \phi'(\tau_2)^\Delta \ , \\ \Sigma(\tau_1,\tau_2) \to \tilde{\Sigma}(\tau_1,\tau_2) = \phi'(\tau_1)^{\Delta(q-1)} \, \Sigma(\phi(\tau_1),\phi(\tau_2)) \, \phi'(\tau_2)^{\Delta(q-1)} \ , \end{cases} \tag{2.31}$$

with $\phi(\tau)$ a smooth, monotonically increasing function that maps the thermal circle to the thermal circle with single unit of winding. The structure of $\phi(\tau)$ is that of a reparameterisation of the circle to itself.

In the IR, the SYK model is approximated by a one-dimensional conformal field theory [31, 40]. The fermions ψ_i transform as primary operators of conformal weight $\Delta = 1/q$. At the level of the action, the low-energy effective description is given by

$$I_{\text{CFT}} = -\frac{1}{2}\log\det(-\Sigma(\tau_1,\tau_2)) + \frac{1}{2}\int_0^\beta \int_0^\beta d\tau_1 d\tau_2 \left(\Sigma(\tau_1,\tau_2)G(\tau_1,\tau_2) - \mathcal{J}^2 \frac{2^{q-1}}{q^2} G(\tau_1,\tau_2)^q \right) . \tag{2.32}$$

The solution to the IR Schwinger-Dyson equations (2.30) is given by

$$G_\phi(\tau_1,\tau_2) = \phi'(\tau_1)^\Delta \, b \, \text{sgn}(\tau_1-\tau_2) \left(\frac{\pi}{\beta\mathcal{J}\sin\left(\frac{\pi(\phi(\tau_1)-\phi(\tau_2))}{\beta}\right)} \right)^{2\Delta} \phi'(\tau_2)^\Delta \ , \tag{2.33}$$

with

$$b = \frac{1}{2}\left(\frac{(1-2\Delta)\tan(\pi\Delta)}{\pi\Delta} \right)^\Delta \ . \tag{2.34}$$

All solutions G_ϕ have the same action when evaluated on the conformal action (2.32). As such, the saddle approximation naively diverges as the volume of the reparameterisation group. To get a finite answer we must account for the effect of the leading 'irrelevant' correction away from the

conformal action. It is given by the Schwarzian action [31]

$$I_{\text{Sch}} = -\frac{\alpha(q)}{2\mathcal{J}} \int_0^\beta d\tau \left(\left(\frac{2\pi}{\beta} \right)^2 \phi'(\tau)^2 - \left(\frac{\phi''(\tau)}{\phi'(\tau)} \right)^2 \right) . \tag{2.35}$$

The constant $\alpha(q)$ has to be determined numerically by solving the full Schwinger-Dyson equations, as discussed further in appendix B, as its precise value does not follow from IR considerations. The Schwarzian action explicitly breaks the reparametrisation symmetry of the conformal action down to an unphysical $SL(2,\mathbb{R})$ reparametrisation group. The final path integral must still be divided by the volume of the residual $SL(2,\mathbb{R})$ to be made sense of [86, 87].

Given the Schwarzian theory (2.35), one can compute thermodynamic quantities to leading order in the saddle point approximation. For instance, given the on-shell solution $\phi(\tau) = \tau$, the free energy F_{Sch} is found by taking the Schwarzian action on shell

$$-\frac{\beta F_{\text{Sch}}}{N} = \frac{2\pi^2 \alpha(q)}{\beta \mathcal{J}} , \tag{2.36}$$

and is found to be quadratic in the temperature. Given an expression for free energy F, the thermodynamic entropy S can be computed as

$$S = (1 - \beta\partial_\beta)(-\beta F) . \tag{2.37}$$

It is straightforward from (2.36) to verify that the entropy of the Schwarzian theory is linear in the temperature,

$$\frac{S_{\text{Sch}}}{N} = \frac{4\pi^2 \alpha(q)}{\beta \mathcal{J}} . \tag{2.38}$$

Additionally, the zero temperature entropy of the SYK can be computed explicitly [31, 40] such that the entropy of the SYK model admits the following small temperature expansion

$$\frac{S}{N} = \left(S_0^{\text{free}} - \int_0^{1/q} dx\, \pi \left(\frac{1}{2} - x \right) \tan \pi x \right) + \frac{4\pi^2 \alpha(q)}{\beta \mathcal{J}} + \cdots , \tag{2.39}$$

where $S_0^{\text{free}} \equiv \log 2/2$ is the zero temperature entropy of a free fermion.

Large q limit

The SYK model admits further computational control if, after taking the large N limit, we also take the large q limit.[4] In this case, we can expand the two-point function $G(\tau_1, \tau_2) = G(\tau_1 - \tau_2)$ as

$$G(\tau) = \frac{\text{sgn}(\tau)}{2}\left(1 + \frac{g(\tau)}{q} + \mathcal{O}(1/q^2)\right) . \tag{2.40}$$

To leading order in q, the Schwinger-Dyson equations (2.29) become a single ordinary differential equation for $g(\tau)$, namely

$$\partial_\tau^2 g(\tau) = 2\mathcal{J}^2 e^{g(\tau)} . \tag{2.41}$$

Imposing thermal boundary conditions, $g(0) = g(\beta) = 0$, we find that,

$$e^{g(\tau)} = \frac{\cos^2\nu}{\cos^2\left(2\nu\left(\frac{1}{2} - \frac{\tau}{\beta}\right)\right)} , \qquad \beta\mathcal{J} = \frac{2\nu}{\cos\nu} . \tag{2.42}$$

Given $g(\tau)$, we can compute the complete thermodynamics of the theory by evaluating the action (2.27) on-shell to leading order in the large q expansion,

$$\frac{\beta F}{N} = -S_0^{\text{free}} - \frac{\beta}{8q^2}\int_0^\beta d\tau \left[\frac{1}{2}\left(\partial_\tau g(\tau)\right)^2 + 2\mathcal{J}^2 e^{g(\tau)}\right] + \cdots . \tag{2.43}$$

At low temperatures, the parameter ν can be expanded as follows,

$$\nu = \frac{\pi}{2} - \frac{\pi}{\beta\mathcal{J}} + \frac{2\pi}{(\beta\mathcal{J})^2} - \frac{\pi\left(24 + \pi^2\right)}{6(\beta\mathcal{J})^3} + O(\beta\mathcal{J})^{-4} , \tag{2.44}$$

while at large temperatures $\nu \sim \beta\mathcal{J}/2 + \cdots$. Using (2.44) with (2.42) and (2.43) one can extract the low-temperature thermodynamic behaviour of the theory. In particular, the thermal entropy at low temperatures reads [54]

$$\frac{S}{N} = \left(S_0^{\text{free}} - \frac{\pi^2}{4q^2}\right) + \frac{\pi^2}{q^2}\frac{1}{\beta\mathcal{J}} + \cdots . \tag{2.45}$$

By comparing (2.45) with (2.38), we see that $\alpha(q) \to 1/4q^2$ as $q \to \infty$. Next order corrections in the large q limit have been studied in [90].

[4] Another solvable case is known as the double-scaled SYK model, obtained by taking both the large N and large q limit, but with N/q^2 fixed. See, for instance, [88, 89].

Chaos exponent

One of the salient features of the SYK model is that there is enough computational control to compute dynamical quantities such as the OTOC at large N and in the strongly-coupled regime. At infinitely low temperatures, where conformal symmetry is emergent, it can be checked that the SYK model saturates the maximal chaos bound [21]. The leading order correction away from maximal chaos can also be computed analytically and it gives, *e.g.,* for $q = 4$, $q = 6$, and $q \to \infty$ [31],

$$\lambda_C \equiv (\lambda_L)_{\beta\mathcal{J}\gg 1} \approx \begin{cases} \frac{2\pi}{\beta}\left(1 - \frac{4.28}{\beta\mathcal{J}} + \dots\right), & q = 4\,, \\ \frac{2\pi}{\beta}\left(1 - \frac{3.11}{\beta\mathcal{J}} + \dots\right), & q = 6\,, \\ \frac{2\pi}{\beta}\left(1 - \frac{2}{\beta\mathcal{J}} + \dots\right), & q \to \infty\,. \end{cases} \tag{2.46}$$

Away from this limit, the Lyapunov exponent can be computed numerically, see section 3.4. In the large q limit, it is possible to compute it analytically for all temperatures, obtaining $\lambda_L = \frac{4\nu}{\beta}$.

2.4 Deformed SYK models

A *relevant* question is whether the SYK model admits deformations away from its near-conformal infrared fixed point. Simple operators in the SYK model are mostly irrelevant [81]. However, it is possible to deform the SYK model with deformations that take the form of the SYK Hamiltonian itself, but with a different number of fermions. Namely, it is possible to consider the following theory,

$$H_{\text{def}} = H_q + sH_{\tilde{q}}\,, \tag{2.47}$$

where s is a tunable dimensionless parameter and the Hamiltonian H_x denotes the Hamiltonian (independent random) ensemble (2.24)-(2.25) of a single SYK model with x-fermion interactions.[5] Note that the Hamiltonian is built from the same N fermions.

In this thesis, we will assume that $q > \tilde{q}$. A naive power counting argument indicates that this is required for the second term to be relevant. The argument goes as follows. Near the conformal fixed point of the first SYK, the fermions acquire a scaling dimension of $\Delta = 1/q$, so the second SYK Hamiltonian, thought of as a disordered operator [53, 54], has a naive scaling dimension of $\Delta = \tilde{q}/q < 1$, and will become dominant in the infrared. In section 4.3.3 we will carry out a more

[5] Similar deformations have been recently considered in the double-scaling limit [91, 92].

careful analysis of this intuition and demonstrate that it is indeed correct.

Large N limit and large q limits

Similar to the single SYK case, in the large N limit, the deformed action can be described in terms of bi-local fields [52, 53]

$$I = -\frac{1}{2}\log\det(\partial_\tau - \Sigma) + \frac{1}{2}\int_0^\beta \int_0^\beta d\tau_1 d\tau_2 \left(\Sigma G - \mathcal{J}^2\left(\frac{2^{q-1}}{q^2}G^q + s^2\frac{2^{\tilde{q}-1}}{\tilde{q}^2}G^{\tilde{q}}\right)\right) , \tag{2.48}$$

from which we get a set of deformed Schwinger-Dyson equations

$$\begin{cases} G^{-1}(\tau_1,\tau_2) = \delta(\tau_1-\tau_2)\partial_{\tau_2} - \Sigma(\tau_1,\tau_2) , \\ \Sigma(\tau_1,\tau_2) = \mathcal{J}^2\left(\frac{2^{q-1}}{q}G(\tau_1,\tau_2)^{q-1} + s^2\frac{2^{\tilde{q}-1}}{\tilde{q}}G(\tau_1,\tau_2)^{\tilde{q}-1}\right) . \end{cases} \tag{2.49}$$

A case of special interest is $\tilde{q} = 2$. The deformation then consists of an integrable Hamiltonian, often referred to as mass-deformed SYK, and has been broadly studied in the context of quantum chaotic to integrable transitions [46–51].

The deformed SYK model can also be studied in the large-$q, \tilde{q}$ limit [52–55]. It is convenient to define the ratio $\mathfrak{n} \equiv q/\tilde{q} > 1$ and take both q and $\tilde{q}$ to infinity, while keeping $\mathfrak{n}$ fixed. In this case, the Schwinger-Dyson equations (2.49) reduce to

$$\partial_\tau^2 g(\tau) = 2\mathcal{J}^2\left(e^{g(\tau)} + \mathfrak{n}s^2 e^{g(\tau)/\mathfrak{n}}\right) . \tag{2.50}$$

In general, this differential equation (supplemented with thermal boundary conditions) can be solved numerically using standard shooting methods [54], see section 3.3 for details.

An analytically solvable deformation

Notably, there is at least one case that can be solved analytically for all values of $\beta\mathcal{J}$ and s. This is when $\mathfrak{n} = 2$, which means that the number of fermions in the relevant deformation is half of that in the original Hamiltonian [52, 53]. In this case, the two-point function is given by

$$e^{g(\tau)} = \frac{4\nu^4}{\left(\sqrt{(\beta\mathcal{J})^2\nu^2 + s^4(\beta\mathcal{J})^4}\cos\left(\nu\left(\frac{2\tau}{\beta}-1\right)\right) + s^2(\beta\mathcal{J})^2\right)^2} , \tag{2.51}$$

where the parameter ν is defined as

$$\cos\nu = \frac{2\nu^2 - s^2(\beta\mathcal{J})^2}{\sqrt{(\beta\mathcal{J})^2\nu^2 + s^4(\beta\mathcal{J})^4}}. \tag{2.52}$$

Paralleling the analysis of the single SYK model, we can compute the thermodynamic behaviour of this model. To leading order in the large q and $\tilde{q}$ expansion, the free energy of the deformed model is given by

$$\frac{\beta F}{N} = -S_0^{\text{free}} - \frac{\beta}{8q^2}\int_0^\beta d\tau \left[\frac{1}{2}\left(\partial_\tau g(\tau)\right)^2 + \mathcal{J}^2\left(2\mathfrak{n}^2 s^2 e^{g(\tau)/\mathfrak{n}} + 2e^{g(\tau)}\right)\right] . \tag{2.53}$$

Of particular interest is low temperature thermodynamics of the model. Provided that $s \ll 1$, there turns out to be two regimes in which the theory is nearly conformal and the entropy becomes (nearly) linear in the temperature. We refer to these two regimes as the **intermediate** ($1/s^2 \gg \beta\mathcal{J} \gg 1$) and the **deep** infrared ($\beta\mathcal{J} \gg 1/s^2$) of the theory.

To extract the intermediate infrared behaviour analytically, we expand the parameter ν above for small values of s and large values of $\beta\mathcal{J}$ such that $\beta\mathcal{J}s$ is kept fixed (of order one). This expansion yields

$$\begin{aligned}\nu_{\text{Int IR}} =& \frac{\pi}{2} + \frac{2(\beta\mathcal{J}s)^2 - \pi^2}{\pi\beta\mathcal{J}} + \frac{2}{\pi^3}\frac{\left(\pi^4 - 4(\beta\mathcal{J}s)^4\right)}{(\beta\mathcal{J})^2} \\ &+ \frac{16\left(24-\pi^2\right)(\beta\mathcal{J}s)^6 - 96\pi^2(\beta\mathcal{J}s)^4 + 6\pi^6(\beta\mathcal{J}s)^2 - \pi^6\left(24+\pi^2\right)}{6\pi^5(\beta\mathcal{J})^3} + \cdots .\end{aligned} \tag{2.54}$$

In this case we obtain for the entropy [53][6]

$$\text{Intermediate IR:}\quad \frac{S}{N} = \left(S_0^{\text{free}} - \frac{\pi^2}{4q^2}\right) + \frac{\pi^2}{q^2}\frac{1}{\beta\mathcal{J}} - \frac{2s^2\beta\mathcal{J}}{q^2} + \cdots , \tag{2.55}$$

which has the linear-in-temperature behaviour expected for a single SYK theory with H_q, and s will only appear as a small correction away from this intermediate near fixed point. For lower temperatures, the theory develops a new near fixed point, that can be studied analytically by doing

[6]The model studied in in [53] has fermions with two different flavours and so effectively, the number q of fermionic interactions in each term of the Hamiltonian was twice the one considered here. One can recover the thermodyamic formulas in [53] by simply taking $q \to 2q$ in our expressions.

the following expansion,

$$\nu_{\text{Deep IR}} = \pi - \frac{\pi\sqrt{1+4s^2}}{s^2\beta\mathcal{J}} + \frac{\pi(4s^2+1)}{s^4}\frac{1}{(\beta\mathcal{J})^2} + \frac{\pi^3\left(-2s^4+2s^2+1\right)-3\pi\left(4s^2+1\right)^2}{3s^6\sqrt{4s^2+1}}\frac{1}{(\beta\mathcal{J})^3} + \cdots , \tag{2.56}$$

in this case the entropy becomes

$$\text{Deep IR:}\quad \frac{S}{N} = \left(S_0^{\text{free}} - \frac{\pi^2}{4\tilde{q}^2}\right) + \bar{\aleph}\frac{\pi^2}{\tilde{q}^2}\frac{1}{s\beta\mathcal{J}} + \cdots , \tag{2.57}$$

where

$$\bar{\aleph} = \frac{\sqrt{1+4s^2}}{2s} . \tag{2.58}$$

We can compare (2.57) to the IR behaviour of the single SYK model, $sH_{\tilde{q}}$, which is (2.45) with $q \to \tilde{q}$ and $\mathcal{J} \to s\mathcal{J}$. While the zero temperature entropy is unchanged, the deformed model changes dramatically the coefficient of the entropy that is linear in the temperature. This is parameterised by the constant $\bar{\aleph}$. Note that in the limit $s \to \infty$, $\bar{\aleph} \to 1$ and we recover the single SYK result, as expected.

The full behaviour of the thermal entropy can also be computed [53]. In figure 1 we plot the entropy as a function of temperature for different values of s^2. We see that for values of s^2 sufficiently small the entropy interpolates between the two near-conformal fixed points described by (2.55) and (2.57).

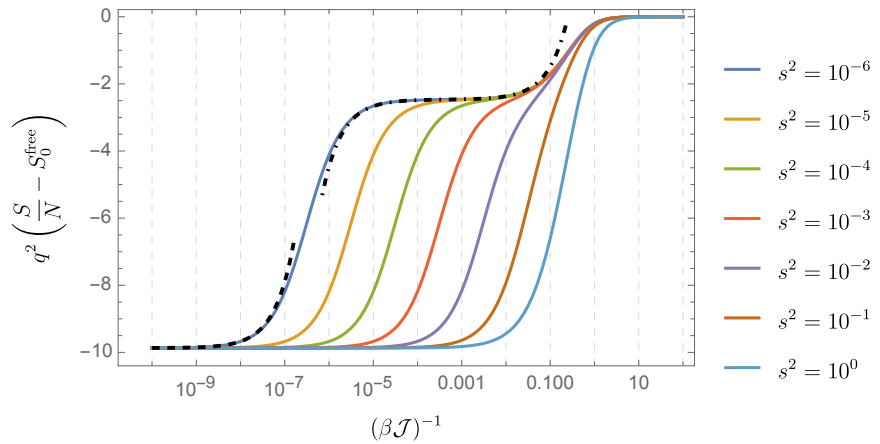

Fig. 1: The entropy as a function of temperature (in logarithmic scale) for the deformed SYK model at large N and large q with $\mathfrak{n} = 2$. The black dashed-dotted curve gives the intermediate IR entropy (2.55) for $s^2 = 10^{-6}$ whilst the black dashed curve gives the deep IR entropy (2.57) for $s^2 = 10^{-6}$.

Chaos exponent

As with the single SYK, in this model it is also possible to compute dynamical quantities associated with quantum chaos. In particular, for the case $\mathfrak{n} = 2$, the Lyapunov exponent can be computed analytically around both near fixed points [52],

$$\lambda_L = \begin{cases} \frac{2\pi}{\beta}\left(1 - \frac{2}{\beta\mathcal{J}} - \left(\frac{1}{2} - \frac{4}{\pi^2}\right) s^2\beta\mathcal{J} + \cdots\right), & \text{Intermediate IR}, \\ \frac{2\pi}{\beta}\left(1 - \frac{1}{s^2\beta\mathcal{J}} + \cdots\right), & \text{Deep IR}. \end{cases} \tag{2.59}$$

This shows, that close enough to both fixed points the system becomes maximally chaotic, while in between the Lyapunov exponent decreases to non-maximal values. Away from these limits, the full behaviour of the Lyapunov exponent was also found numerically in [52], which we reproduce in section 6.4.1.1 and compare to the Krylov computations.

2.5 Dilaton gravity theories

We close the preliminary material by giving a brief review of JT gravity and its thermodynamics. As we shall describe, JT gravity is the holographic dual to the SYK model. We refer the reader to [35, 82, 93] for more detailed reviews. The natural action to write for 2d gravity is the Einstein-Hilbert action

$$S_{EH} = \frac{1}{2\kappa}\int_{\mathcal{M}} d^2x\,\sqrt{g}(R - 2\Lambda)\ . \tag{2.60}$$

In two dimensions however, the Einstein tensor vanishes identically and so the theory is topological. This can be seen directly by invoking the Gauss-Bonnet theorem which tells us that the Einsten-Hilbert action in two dimensions evaluates to the Euler characteristic of the manifold on which it is defined. In order to generate a non-trivial theory Jackiw and Teitelboim proposed introducing a scalar field, ϕ, called the dialton field, that couples to the Ricci scalar [94, 95]. Since we are interested in the thermodynamics of the theory we will work in Euclidean signature and consider the action

$$S_E = -S_0 - \frac{1}{2\kappa}\int_{\mathcal{M}} d^2x\sqrt{g}\phi\,(R - 2\Lambda) - \frac{1}{\kappa}\int_{\partial\mathcal{M}}\sqrt{h}\phi K\ . \tag{2.61}$$

We consider the theory on a disc topology with boundary $\partial\mathcal{M}$ that we will describe later. The final term in the action is called the Gibbons-York-Hawking (GYH) boundary term and is included to

make the variational principle well defined. We have also chosen to supplement the action with an Einsten-Hilbert term

$$S_0 \equiv \frac{\phi_0}{2\kappa}\int_{\mathcal{M}} d^2x\sqrt{g}R + \frac{\phi_0}{\kappa}\int_{\partial\mathcal{M}}\sqrt{h}K = \frac{2\pi\phi_0}{\kappa}\chi(\mathcal{M}) = \frac{2\pi\phi_0}{\kappa}\ , \tag{2.62}$$

where we have used that the Euler Characteristic, $\chi(\mathcal{M})$, evaluates to 1 for the disc topology and ϕ_0 is a free parameter that sets the zero temperature entropy of the theory. We now focus on the case $\Lambda = -1$ which classically gives rise to AdS_2 space. In Poincaré coordinates the AdS_2 metric is given by

$$ds^2 = \frac{dz^2 + dt^2}{z^2}\ . \tag{2.63}$$

We will allow our boundary to fluctuate and parametrise it by a trajectory $(t(u), z(u))$ where u denotes the time along the boundary curve, as shown in figure 2.

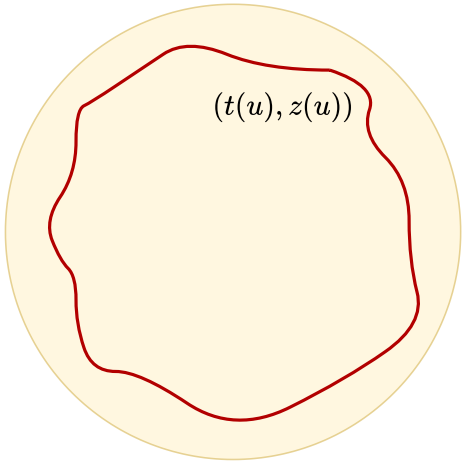

Fig. 2: The circle is the hyperbolic disc representing Euclidean AdS_2. We consider the space within the boundary curve parametised by $(t(u), z(u))$.

We compute the thermodynamics of the theory by taking a gravitational path integral with the following boundary conditions for the metric and dilaton field

$$ds^2|_{\text{bdry}} = \frac{t'(u)^2 + z'(u)^2}{z(u)^2} = \frac{1}{\varepsilon^2}du^2, \qquad \phi|_{\text{bdry}} = \frac{\tilde{\phi}}{\varepsilon}\ . \tag{2.64}$$

Note that the boundary condition on the metric fixes the z coordinate on the boundary curve in

terms of the t coordinate

$$z(u) = \varepsilon t'(u) + \mathcal{O}(\varepsilon^3) \ . \tag{2.65}$$

We now compute the thermal partition function by taking path integral

$$\begin{aligned} Z(\beta) &= e^{S_0} \int [Dg][D\phi]\, e^{\frac{1}{2\kappa}\int_{\mathcal{M}} \sqrt{g}\phi(R+2) + \frac{1}{\kappa}\int_{\partial\mathcal{M}} \sqrt{h}\phi(K-1)} \\ &= e^{S_0} \int [Dg]\, \delta(R+2)\, e^{\frac{1}{\kappa}\int_{\partial\mathcal{M}} \sqrt{h}\phi(K-1)} \ . \end{aligned} \tag{2.66}$$

In the second line we have integrated over the dilaton field. This reduces the path integral to one over boundary action, and restricts geometries to those with $R = -2$ and hence with bulk metric (2.63). To write the boundary action explicitly we first compute the extrinsic curvature to find

$$K = \frac{t'\left(t'^2 + z'^2 + z'z''\right) - zz't''}{\left(t'^2 + z'^2\right)^{3/2}} = 1 + \varepsilon^2\, \mathrm{Sch}(t,u) + \mathcal{O}(\varepsilon^4) \ , \tag{2.67}$$

where $\mathrm{Sch}(t,u)$ is the Schwarzian derivative defined by

$$\mathrm{Sch}(t,u) \equiv \frac{t'''(u)}{t'(u)} - \frac{3}{2}\left(\frac{t''(u)}{t'(u)}\right)^2 \ . \tag{2.68}$$

Then, using the boundary conditions (2.64) we find that the boundary action is given by the Schwarzian action

$$I_{\mathrm{Sch}} = -\frac{1}{\kappa}\int_{\partial\mathcal{M}} \sqrt{h}\phi(K-1) = -\frac{\tilde{\phi}}{\kappa}\int du\ \mathrm{Sch}(t,u) \ . \tag{2.69}$$

Since we are considering a thermal system it is more natural to use the Rindler frame, which we can find by making the transformation

$$t = \tan\frac{\pi\tau}{\beta} \ . \tag{2.70}$$

Note that $\tau \sim \tau + \beta$ and the period β carries the physical interpretation of being the inverse temperature of the spacetime. We then find that the Schwarzian action can be written as

$$I_{\mathrm{Sch}} = -\frac{\tilde{\phi}}{2\kappa}\int_0^\beta d\tau\ \left(\left(\frac{2\pi}{\beta}\right)^2 \tau'(u)^2 - \left(\frac{\tau''(u)}{\tau'(u)}\right)^2\right) \ . \tag{2.71}$$

Note that this is the same action that governs the IR dynamics the SYK model (2.35) upon making

the identification $\tilde{\phi}/\kappa = \alpha(q)/\mathcal{J}$, revealing the duality between the two models. The partition function then becomes a path integral purely over reparametrisations, $\tau \in \text{Diff}(S^1)$, of the boundary curve, whose action is given by the Schwarzian action (2.71)

$$Z(\beta) = e^{S_0} \int_{\text{Diff}(S^1)/SL(2,\mathbb{R})} [\mathcal{D}\tau]\, e^{-I_{\text{Sch}}} \ . \tag{2.72}$$

Here, it is important to note that overall translations and rotations do not change the shape of the boundary curve, and so the path integral must be quotiented over reparametrisations in the $SL(2,\mathbb{R})$ subgroup. The saddle solution to the Schwarzian action is given by $\tau(u) = u$ and leads to the following thermodynamics

$$S_{\text{JT}} = S_0 + \frac{4\pi^2\tilde{\phi}}{\kappa}\frac{1}{\beta} \ , \tag{2.73}$$

which is the analogue of the SYK entropy at low temperatures (2.39). Going beyond the thermodynamics one can also explore the chaotic behaviour of the model by computing the OTOC of the boundary modes [32, 33]. As with the SYK one finds that the model saturates the maximal chaos bound.

Finally we can consider generalisations to JT gravity by including a potential, $U(\phi)$, for the dilaton field [71]. The action is then given by

$$S_E = -S_0 - \frac{1}{2\kappa}\int_{\mathcal{M}} d^2x\sqrt{g}\,(\phi R + U(\phi)) - \frac{1}{\kappa}\int_{\partial\mathcal{M}} \sqrt{h}\phi K \ . \tag{2.74}$$

Taking $U(\phi) = -2\Lambda\phi$ recovers the JT action (2.61). This theory permits general black hole solutions of the form

$$ds^2 = f(r)dt^2 + \frac{dr^2}{f(r)}, \quad f(r) = \frac{1}{\tilde{\phi}}\int_{r_h}^{r} dr' U(\phi(r')) \ , \quad \phi(r) = \tilde{\phi}r \ , \tag{2.75}$$

where r_h is the position of the horizon which is located at the origin of the disc. The thermodynamics of the theory are then given by

$$\beta^{-1} = \frac{|U(\phi(r_h))|}{4\pi\tilde{\phi}}, \quad S = \frac{2\pi\phi_0}{\kappa} + \frac{2\pi\tilde{\phi}}{\kappa}r_h \ . \tag{2.76}$$

We shall explore the connection between these more general dilaton gravity theories and deformed SYK models later in the thesis.

3 Manual for numerical methods

In this section we provide an overview of the numerical methods used in this thesis. We will review the relevant equations to solve, outline the numerical algorithms used, and point reader to existing code that can be readily implemented. For simplicity we will focus on the case of the SYK model with a single deformation, which we recall is defined by

$$H_{\text{def}} = H_q + sH_{\tilde{q}} \ , \tag{3.1}$$

where s is a dimensionless tunable parameter and the Hamiltonian of the each SYK is defined by

$$H_q = (i)^{\frac{q}{2}} \sum_{1\leq i_1<i_2<\ldots<i_q\leq N} J_{i_1 i_2 \ldots i_q} \psi_{i_1} \psi_{i_2} \ldots \psi_{i_q} \ , \tag{3.2}$$

with $q \in 2\mathbb{Z}^+$. The coupling constants of the theory independently drawn from a Gaussian distribution that satisfies

$$\langle J_{i_1 i_2 \cdots i_q} \rangle = 0 \ , \qquad \langle J^2_{i_1 i_2 \cdots i_q} \rangle = \frac{2^{q-1}}{q} \frac{\mathcal{J}^2 (q-1)!}{N^{q-1}} \ . \tag{3.3}$$

Code for this section written by the author can be found on GitHub via the following URL

https://github.com/sameersheorey/Deformed-SYK-Numerics (3.4)

Though the code provided here applies for a single deformation, it can be easily adapted to handle multiple deformations as considered in section 5. This code is written in `Python` and `Mathematica`.

3.1 Finite N methods for the SYK

The SYK model (3.1) can be solved at finite N by exact diagonalisation methods. To do so we first need an explicit matrix representation of the Hamiltonian. In all cases the matrices are built from Majorana fermions obeying anti-commutation relations (2.23), and so we look for matrix representations of these operators. For simplicity we focus on the case of there being an even number of fermions, $N = 2K$. In this case we can pair up our fermions ($1 \leftrightarrow 2, 3 \leftrightarrow 4$ etc) and for

each pair of fermions we define a new operator χ_i such that

$$\chi_i = \frac{1}{\sqrt{2}}(\psi_{2i-1} - i\psi_{2i}) \ , \qquad i = 1, 2, ..., K \ . \tag{3.5}$$

We then have that the χ_i obey the anti-commutation relations for $K = N/2$ Dirac fermions

$$\{\chi_i, \chi_j^\dagger\} = \delta_{ij} \ , \qquad \{\chi_i, \chi_j\} = 0 \ , \qquad \{\chi_i^\dagger, \chi_j^\dagger\} = 0 \ . \tag{3.6}$$

For $K = 1$ it is well known that we have a two state space with basis we label by $\{|0\rangle, |1\rangle\}$ such that

$$\begin{aligned} \chi_1|0\rangle = 0, \qquad & \chi_1|1\rangle = |0\rangle \ , \\ \chi_1^\dagger|0\rangle = |1\rangle, \qquad & \chi_1^\dagger|1\rangle = 0 \ . \end{aligned} \tag{3.7}$$

Representing our basis states as vectors

$$|0\rangle = \begin{pmatrix} 1 \\ 0 \end{pmatrix} , \qquad |1\rangle = \begin{pmatrix} 0 \\ 1 \end{pmatrix} , \tag{3.8}$$

and using (3.7) we find that

$$\chi_1 = \begin{pmatrix} 0 & 1 \\ 0 & 0 \end{pmatrix} , \qquad \chi_1^\dagger = \begin{pmatrix} 0 & 0 \\ 1 & 0 \end{pmatrix} , \tag{3.9}$$

from which it follows that

$$\psi_1^{(K=1)} = \frac{1}{\sqrt{2}} \begin{pmatrix} 0 & 1 \\ 1 & 0 \end{pmatrix} , \qquad \psi_2^{(K=1)} = \frac{1}{\sqrt{2}} \begin{pmatrix} 0 & -i \\ i & 0 \end{pmatrix} , \tag{3.10}$$

For $K > 1$, the Hilbert space can be represented as matrices acting in a tensor product space of K such Hilbert spaces. The dimension of the Hilbert space of the model is therefore 2^K and we can define our basis elements to be

$$(\chi_1^\dagger)^{n_1}(\chi_2^\dagger)^{n_2} \cdots (\chi_K^\dagger)^{n_K}|0\rangle \ , \qquad n_k = 0, 1 \ . \tag{3.11}$$

Starting from the case $K = 1$ where the fermions are given by (3.10), we can extend the matrix representation to $K > 1$ with the following iterative procedure. For $K = 2, 3, \ldots$ we recursively build the following matrices

$$\begin{aligned} \psi_i^{(K)} &= \psi_i^{(K-1)} \otimes \begin{pmatrix} -1 & 0 \\ 0 & 1 \end{pmatrix}, \qquad i = 1, \ldots, N-2 \ , \\ \psi_{N-1}^{(K)} &= \frac{1}{\sqrt{2}} I_{2^{K-1}} \otimes \begin{pmatrix} 0 & 1 \\ 1 & 0 \end{pmatrix}, \qquad \psi_N^{(K)} = \frac{1}{\sqrt{2}} I_{2^{K-1}} \otimes \begin{pmatrix} 0 & -i \\ i & 0 \end{pmatrix} . \end{aligned} \tag{3.12}$$

Once one has obtained the fermions in matrix form they can be multiplied together to construct the Hamiltonian (3.2), which can then be diagonalised using standard numerical libraries. However, the direct diagonalisation of the Hamiltonian becomes computationally expensive for large N. In particular, the SYK Hamiltonian is a $2^{N/2} \times 2^{N/2}$ matrix and is not sparse. The computational complexity of diagonalising the Hamiltonian is $\mathcal{O}(2^{3N/2})$ and so grows exponentially with N [44,96]. One trick to speed up the procedure is to take advantage of the fact that both the single and deformed SYK Hamiltonians preserve the parity of the Dirac fermion number operator

$$Q \equiv \sum_i^K \left(\chi_i^\dagger \chi_i \right) \ . \tag{3.13}$$

This means that basis (3.11) can be split into and even and odd parity sectors and the Hamiltonian can be made block diagonal. One can then diagonalise the Hamiltonian in each sector separately. This was enough to diagonalise the Hamiltonian for $N = 30$ in ~ 15 mins. In section 5.3 we use results up to $N = 30$ as the basis for an extrapolation to large N. The code we used to diagonalise the Hamiltonian is based on a `Mathematica` implementation that is available at https://fidel-schaposnik.github.io/mathematica/. To get to significantly larger N more sophisticated techniques need to be used, such as parallel processing, using GPU's and using approximate techniques where the error can be ignored. One package that is able to reach $N = 46$ is available at https://github.com/guygurari/syk. It has also been reported [44] that correlation functions with $N = 60$ fermions could be computed using the Dynamite package which can be found at https://github.com/GregDMeyer/dynamite.

3.2 Large N Schwinger Dyson equations

Here we describe numerical methods used to solve the Schwinger-Dyson equations for the deformed SYK model, which we recall are given by

$$G^{-1}(\tau_1,\tau_2) = \delta(\tau_1-\tau_2)\partial_{\tau_2} - \Sigma(\tau_1,\tau_2)\ , \tag{3.14}$$

$$\Sigma(\tau_1,\tau_2) = \mathcal{J}^2\left(\frac{2^{q-1}}{q}G(\tau_1,\tau_2)^{q-1} + s^2\frac{2^{\tilde{q}-1}}{\tilde{q}}G(\tau_1,\tau_2)^{\tilde{q}-1}\right)\ . \tag{3.15}$$

We describe two methods for solving these. The first involves solving the Schwinger-Dyson equations in Matsubara frequency space [31] and allows for inverse temperatures of $\beta\mathcal{J}\sim 10^2$ to be reached. A second method introduced in [85] involves writing G and Σ as Legendre series. This method allows for even larger inverse temperature of $\beta\mathcal{J}\sim 10^4$ to be reached.

Matsubara Frequency Method

The idea behind this method is to start with the free solution of the single SYK as an initial seed for an iterative algorithm that has fast convergence properties. For the numerical procedure, it is convenient to write (3.14) in frequency space, so that at finite temperature it becomes

$$\frac{1}{G(\omega_n)} = -i\omega_n - \Sigma(\omega_n)\ , \tag{3.16}$$

where $\omega_n = 2\pi\left(n+1/2\right)/\beta$ are Matsubara frequencies and β is the inverse temperature. At each step in the procedure we update $G(\omega_n)$ by a proportion of the error in (3.16),

$$G_{j+1}(\omega_n) = G_j(\omega_n) + a\left(\frac{1}{-i\omega_n - \Sigma_j(\omega_n)} - G_j(\omega_n)\right)\ , \tag{3.17}$$

where the weight a is initially set to $a=0.5$. We then use (3.15) to get an update for $\Sigma(\omega_n)$, using the fast Fourier transform (FFT) to switch between frequency and position space. The iteration is continued until the error in (3.16) is deemed to be sufficiently small. We implemented the algorithm in `python` using the inbuilt `FFT`, and `IFFT` functions from the `NumPy` module.

To get good convergence, it is important to discretise the τ-interval into many points, particularly near 0 and β where we found the most error from the expected solution. 20,000 points is enough to see good plots, but we could go up to 2,000,000 and still run the algorithm in reasonable

time. This allowed us to reach inverse temperatures of the order of $\beta\mathcal{J} \sim 10^2$. To reach much larger $\beta\mathcal{J}$ requires significant time and memory.

Another important aspect in the numerical code is to keep track of the full absolute error squared, $\sum_n |G_{j+1}(\omega_n) - G_j(\omega_n)|^2$, at each iteration. In the case it increases, we half the value of the weighting parameter a. We found that around 50 iterations was sufficient to get convergence to the solution.

Legendre Spectral Method

For this method we expand the G and Σ fields as Legendre series and iteratively update their Legendre coefficients. To solve the Schwinger-Dyson equations we take the following steps. We first discretise our time interval $\tau \in [0, \beta]$ by $\tau_i = \beta(x_i + 1)/2$ for $i = 0, ..., N$ where x_i are Legendre points. On this discretised interval we approximate our G and Σ fields by the first $N + 1$ terms of their Legendre series

$$G(\tau_i) \approx \sum_{\ell=0}^{N} G_\ell L_\ell(x_i) \ , \qquad \Sigma(\tau_i) \approx \sum_{\ell=0}^{N} \Sigma_\ell L_\ell(x_i) \ . \tag{3.18}$$

We will need be able to transform back from Σ_ℓ to $\Sigma(\tau_i)$. This is implemented as

$$\Sigma_\ell = \sum_{i=0}^{N} S_{\ell i} \Sigma(\tau_i) \ , \quad S_{\ell i} = \frac{2\ell + 1}{2} \omega_i L_\ell(x_i) \ , \tag{3.19}$$

where $w_i = \frac{2}{N(N+1)} \frac{1}{[L_N(x_i)]^2}$ are the Legendre weights. The equation (3.14) can be written as

$$\sum_{\ell=0}^{N} \left(D_{k\ell} - \frac{\beta^2}{4} [\Sigma *]_{k\ell} \right) G_\ell = 0 \ , \tag{3.20}$$

$$\sum_{\ell=0}^{N} \left((-1)^\ell + 1 \right) G_\ell = 1 \ . \tag{3.21}$$

Here the condition (3.21) comes from the delta function in the Schwinger-Dyson equation (3.14). In (3.20) the derivative matrix $D_{k\ell}$ is given by $D_{k\ell} = (2k + 1)$ if $k + \ell$ is odd and $k < \ell$ and the convolution matrix $[\Sigma *]_{k\ell}$ is found by the following recursive algorithm. First we compute the first

two columns of the matrix using the relations

$$
\begin{aligned}
[\Sigma*]_{0,0} &= -\frac{2\Sigma_1}{3} \ , & [\Sigma*]_{k,0} &= 2\left(\frac{\Sigma_{k-1}}{2k-1} - \frac{\Sigma_{k+1}}{2k+3}\right), \quad k \geq 1 \ , \\
[\Sigma*]_{0,1} &= -\frac{[\Sigma*]_{1,0}}{3} \ , & [\Sigma*]_{k,1} &= \frac{[\Sigma*]_{k-1,0}}{2k-1} - \frac{[\Sigma*]_{k+1,0}}{2k+3}, \quad k \geq 1 \ .
\end{aligned}
\tag{3.22}
$$

We then compute the lower triangular part of the matrix, where $k \geq l$ using the relations

$$
[\Sigma*]_{k,\ell+1} = -\frac{2\ell+1}{2k+3}[\Sigma*]_{k+1,\ell} + \frac{2\ell+1}{2k-1}[\Sigma*]_{k-1,\ell} + [\Sigma*]_{k,\ell-1} \ . \tag{3.23}
$$

Finally we compute the upper triangular part of the matrix, where $k < l$ using the relation

$$
[\Sigma*]_{k,\ell} = (-1)^{\ell+k}\frac{2k+1}{2\ell+1}[\Sigma*]_{\ell,k} \ . \tag{3.24}
$$

Equations (3.20) and (3.21) are then implemented as a single matrix equation

$$
\sum_{\ell=0}^{N} M_{k\ell} G_\ell = \delta_{kN} \ , \tag{3.25}
$$

where the M is a $(N+1)\times(N+1)$ matrix whose first N rows are given by $M_{kl} = D_{k\ell} + \frac{\beta^2}{4}[\Sigma*]_{k\ell}$ and final row is $M_{Nl} = (-1)^l + 1$. The algorithm is then implemented as follows

1. Initialise to the free solution $G_\ell^{(0)} = \frac{1}{2}\delta_{\ell 0}$.

2. Use (3.18) to compute $G(\tau_i)$, and then (3.15) to compute $\Sigma(\tau_i)$. Then use (3.19) to compute Σ_ℓ.

3. Compute the convolution matrix $[\Sigma*]_{k\ell}$ using the recursive algorithm (3.22)-(3.24) and then solve the equation (3.25) for G_ℓ using a linear solver.

4. Make the weighted update: $G_\ell^{(j+1)} = G_\ell^{(j)} + u\left(\text{solution to equation (3.25)} - G_\ell^{(j)}\right)$, where initially $u = 0.5$.

5. Compute $\sum_\ell |G_\ell^{(j+1)} - G_\ell^{(j)}|$. In the case it increases, we half the value of the weighting parameter u. Repeat steps 2-5 until the sum converges within a desired tolerance.

For more details on the derivation of the algorithm see appendix A in [85].

3.3 Large q shooting method

In the large q limit of the deformed SYK model we send both q and $\tilde{q}$ to infinity while keeping their ratio, $\mathfrak{n} = q/\tilde{q}$ finite and fixed. We recall that substituting the large q expansion,

$$G(\tau) = \frac{\text{sgn}(\tau)}{2}\left(1 + \frac{g(\tau)}{q} + \mathcal{O}(1/q^2)\right) \ , \tag{3.26}$$

into large N Schwinger-Dyson equations (3.14) and (3.15) reduces them to a single, second order differential equation

$$\partial_\tau^2 g(\tau) = 2\mathcal{J}^2\left(e^{g(\tau)} + \mathfrak{n}s^2 e^{g(\tau)/\mathfrak{n}}\right) \ . \tag{3.27}$$

where at finite temperature the equation has thermal boundary conditions, $g(0) = g(\beta) = 0$. Our goal will be to solve this equation numerically. Before discussing the boundary value problem we first review how to solve the equation (3.27) when given initial conditions $g(0) = a$ and $g'(0) = b$ instead. The first step is to package the second order differential equation as a first order vector differential equation

$$\vec{y}\,'(\tau) = \vec{F}(\tau, \vec{y}(\tau)) \ , \tag{3.28}$$

where $\vec{y}(\tau) = (g(\tau), g'(\tau))$ and the function $\vec{F}(\tau, \vec{y}(\tau)) = (g'(\tau), f(\tau, g(\tau)))$ with

$$f(\tau, g(\tau)) = 2\mathcal{J}^2\left(e^{g(\tau)} + \mathfrak{n}s^2 e^{g(\tau)/\mathfrak{n}}\right) \ . \tag{3.29}$$

We then discretise our space into into intervals of size h and solve the differential equation iteratively at points $\tau_i = ih$ for $i \in \mathbb{N}$. The simplest way to do this is to use the Euler method, for which we take

$$\vec{y}(\tau_{i+1}) = \vec{y}(\tau_i) + h\vec{F}(\tau_i, \vec{y}(\tau_i)) \ , \tag{3.30}$$

with the initial condition $\vec{y}(\tau_0) = (a, b)$. The Euler method (3.30) has an error of order h^2 at each step. It can be improved by adding higher order corrections in h. For our purposes we will use the fourth order Runge-Kutta method which has an error of order h^5 at each step [97]. For this method we take

$$\vec{y}(\tau_{i+1}) = \vec{y}(\tau_i) + \frac{1}{6}\left(\vec{K}_0 + 2\vec{K}_1 + 2\vec{K}_2 + \vec{K}_3\right) \ , \tag{3.31}$$

where

$$\begin{cases} \vec{K}_0 = h\vec{F}(\tau_i, \vec{y}(\tau_i)) \ , \\ \vec{K}_1 = h\vec{F}\left(\tau_i + h/2, \vec{y}(\tau_i) + \vec{K}_0/2\right) \ , \\ \vec{K}_2 = h\vec{F}\left(\tau_i + h/2, \vec{y}(\tau_i) + \vec{K}_1/2\right) \ , \\ \vec{K}_3 = h\vec{F}\left(\tau_i + h, \vec{y}(\tau_i) + \vec{K}_2\right) \ . \end{cases} \tag{3.32}$$

We now consider the boundary value problem of solving (3.27) with boundary conditions $g(0) = g(\beta) = 0$. We solve this using a standard numerical procedure called the shooting method. The idea behind this method is as follows. We don't know the value of $g'(0)$ that will give us the correct solution, satisfying our boundary conditions. Instead we guess a value $g'(0) = u$ and iteratively solve the differential equation using the Runge-Kutta method described above until we reach $\tau = \beta$ at the other end of the interval. We then check how close the value of $g(\beta)$ is to the boundary condition $g(\beta) = 0$. The strategy is to then tune the value of u until we satisfy this boundary condition within some pre-specified tolerance. If we define a function $H(u)$ that gives the value of $g(\beta)$ for a given initial condition u, then the shooting method is equivalent to finding the root of $H(u)$. This can be done using any root finding algorithm. In practice, to ensure convergence we found it best to use the bisection method.

As we go to smaller temperatures the magnitude gradient of the solution $g(\tau)$ becomes larger near the edges, $\tau = 0$ and $\tau = \beta$. This means that to ensure convergence of the method at low temperatures we need to take a small interval h, and so the shooting method can be slow to run. One way to speed up the convergence is to observe that the solution always satisfies $g'(\beta/2) = 0$. We can therefore re-define $H(u)$ to give the value of $g'(\beta/2)$ for a given initial condition u. Once we have found a solution u by the bisection method, we compute the $g(\tau)$ on the whole interval with this u and check the solution is consistent with $g(\beta) = 0$. This cuts down the interval we need to apply the Runge-Kutta method over by half. A second way to speed up the method is to use variable step sizes, h_i, in the Runge-Kutta method. In particular we can use a smaller spacings near the edges and a larger spacings in the middle of the interval. This is because the gradient of the solution is small in the middle of the interval and so we don't need as much resolution here. We found that using the Legendre points to set the spacings h_i works well.

3.4 Lyapunov exponent in the deformed SYK

In this appendix we discuss the numerical method used to find the Lyapunov exponent for the deformed SYK model at finite $q > 2$ and large q. In both cases we will be concerned with the regularised OTOC defined by

$$\text{OTOC}\left(t_1, t_2\right) = \frac{1}{N^2} \sum_{i,j=1}^{N} \text{Tr}\left(\rho^{\frac{1}{4}} \psi_i(t_1) \rho^{\frac{1}{4}} \psi_j(0) \rho^{\frac{1}{4}} \psi_i(t_2) \rho^{\frac{1}{4}} \psi_j(0)\right), \quad \rho = \frac{1}{Z(\beta)} e^{-\beta H} \ . \tag{3.33}$$

At large N we can write the OTOC as

$$\text{OTOC}(t_1, t_2) = F_0(t_1, t_2) + \frac{1}{N} F(t_1, t_2) + \cdots \ . \tag{3.34}$$

The $1/N$ contribution to the OTOC is described by a set of ladder diagrams that satisfy the equation [31]

$$F\left(t_1, t_2\right) = \int dt_3 dt_4 \ K\left(t_1, t_2, t_3, t_4\right) F\left(t_3, t_4\right) \ , \tag{3.35}$$

where the Kernel $K\left(t_1, t_2, t_3, t_4\right)$ is given by

$$K\left(t_1, t_2, t_3, t_4\right) = G^R(t_{13}) G^R(t_{24}) \mathcal{J}^2 \left(\frac{2^{q-1}}{q} (q-1) G^W(t_{34})^{q-2} + s^2 \frac{2^{\tilde{q}-1}}{\tilde{q}} (\tilde{q}-1) G^W(t_{34})^{\tilde{q}-2} \right) \ , \tag{3.36}$$

where $t_{ij} \equiv t_i - t_j$. Here $G^R(t)$ is the retarded propagator and $G^W(t)$ is the Wightman propagator defined between two real time folds separated by half the thermal circle. These are defined by the following relations

$$\begin{cases} G^R(t) = \frac{1}{N} \sum_i \theta(t) \langle \psi_i(t) \psi_i(0) + \psi_i(0) \psi_i(t) \rangle_\beta = \theta(t) \left(G(it + \varepsilon) - G(it - \varepsilon) \right) \ , \\ G^W(t) = G(\beta/2 + it) \ . \end{cases} \tag{3.37}$$

Finite q

To find the Lyapunov exponent at finite q we first make the growth ansatz

$$F(t_1, t_2) = e^{\lambda_L (t_1 + t_2)/2} f(t_{12}) \ . \tag{3.38}$$

Writing (3.35) in frequency space gives

$$f\left(\omega'\right)=\int d\omega\; M(\omega',\omega)f(\omega), \tag{3.39}$$

where

$$\begin{cases} M(\omega',\omega) & =\frac{\mathcal{J}^2}{2\pi}\left|G^R\left(\omega'+i\frac{\lambda_L}{2}\right)\right|^2\; m(\omega',\omega)\;, \\ m(\omega',\omega) & =\int dt\; e^{i(\omega'-\omega)t}\left(\frac{2^{q-1}}{q}(q-1)G^W(t)^{q-2}+s^2\frac{2^{\tilde{q}-1}}{\tilde{q}}(\tilde{q}-1)G^W(t)^{\tilde{q}-2}\right)\;. \end{cases} \tag{3.40}$$

We can find the Lyapunov exponent numerically by discretising ω and treating (3.39) as a matrix equation. We then search for a value of λ_L such that $M(\omega',\omega)$ has an eigenvalue of 1. We do this using binary search to find the value of λ_L for which the largest eigenvalue of M crosses 1. To compute the matrix $M(\omega',\omega)$ we first numerically compute the spectral function $\rho(\omega)$ defined by

$$\rho(\omega)=\frac{G^{>}(\omega)}{2\pi}(1+e^{-\beta\omega})\;,\quad G^{>}(t)=\frac{1}{N}\sum_i\langle\psi_i(t)\psi_i(0)\rangle_\beta=G(it+\varepsilon)\;. \tag{3.41}$$

The numerical computation of $\rho(\omega)$ is given in appendix 3.5. From $\rho(\omega)$ we can find $G^R(t)$ and $G^W(t)$ by the following relations

$$\begin{cases} G^R(t) & =\theta(t)\int d\omega\;\rho(\omega)\cos(\omega t)\;, \\ G^W(t) & =\int d\omega\; e^{-\omega\left(it+\frac{\beta}{2}\right)}\frac{\rho(\omega)}{1+e^{-\beta\omega}}\;. \end{cases} \tag{3.42}$$

We can then compute $G^R\left(\omega'+i\frac{\lambda_L}{2}\right)$ from (3.42) by performing a Fourier transform with frequencies shifted by $i\lambda_L/2$. For the single SYK one can check the numerical computation of $G^R(t)$ and $G^W(t)$ by comparing to their conformal solutions and leading corrections given by [31],

$$\begin{cases} G^R_C(t) & =2\,b\cos(\pi\Delta)\theta(t)\left(\frac{\pi}{\beta\mathcal{J}\sinh\frac{\pi t}{\beta}}\right)^{2\Delta}\left(1-\frac{\alpha_G(q)}{\beta\mathcal{J}}\left(2-\frac{\pi\tan(\pi\Delta)+\frac{2\pi t}{\beta}}{\tanh\left(\frac{\pi t}{\beta}\right)}\right)\right)\;, \\ G^W_C(t) & =b\left(\frac{\pi}{\beta\mathcal{J}\cosh\frac{\pi t}{\beta}}\right)^{2\Delta}\left(1-\frac{\alpha_G(q)}{\beta\mathcal{J}}\left(2-\frac{2\pi t}{\beta}\tanh\left(\frac{\pi t}{\beta}\right)\right)\right)\;, \end{cases} \tag{3.43}$$

where $\Delta = 1/q$, $\alpha_G(q)$ is a q dependent constant that must be fitted numerically and

$$b = \frac{1}{2}\left(\frac{(1-2\Delta)\tan(\pi\Delta)}{\pi\Delta}\right)^{\Delta} . \tag{3.44}$$

In figure 3 we show plots with numerical computations of $G^R(t)$ and $G^W(t)$ against their respective conformal solutions (3.43) for $q = 6$ at inverse temperature $\beta\mathcal{J} = 10$. For these plots we use the numerical value of $\alpha_G(6) = 0.1737$ given in [31].

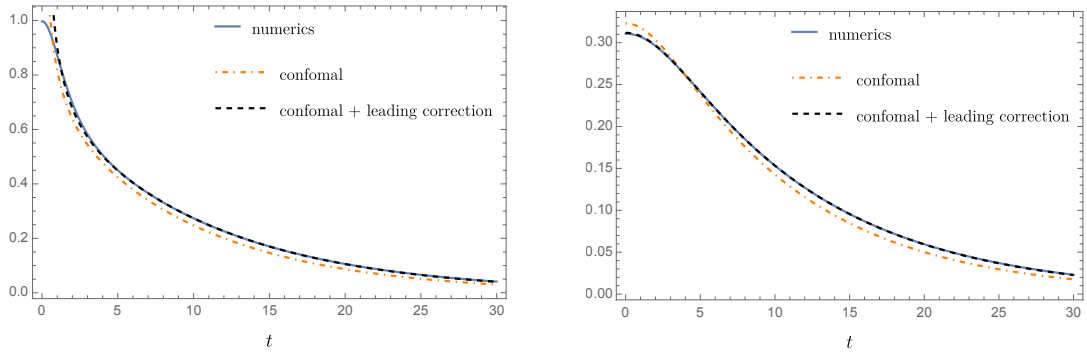

(a) $G^R(t)$ (b) $G^W(t)$

Fig. 3: Numerical computations of $G^R(t)$ and $G^W(t)$ for $q = 6$ at inverse temperature $\beta\mathcal{J} = 10$. The numerics (solid lines) are plotted against the conformal solution (dashed-dotted lines) and the conformal solution with leading correction (dashed lines).

Large q

Using (3.37) along with (3.26) we find that to leading order in the large q limit the kernel (3.36) is given by

$$K(t_1,t_2,t_3,t_4) = 2\mathcal{J}^2\theta(t_{13})\theta(t_{24})\left(e^{g(\beta/2+it)} + s^2 e^{\frac{g(\beta/2+it)}{\mathfrak{n}}}\right) . \tag{3.45}$$

Substituting this into (3.35) with the growth ansatz (3.38) and applying $\partial_{t_1}\partial_{t_2}$ to both sides of the equation gives

$$\left(\frac{\lambda_L}{4} - \partial_t^2\right) f(t) = 2\mathcal{J}^2\left(e^{g(\beta/2+it)} + s^2 e^{\frac{g(\beta/2+it)}{\mathfrak{n}}}\right) f(t) . \tag{3.46}$$

We can then find λ_L by looking for a normalisable solution to this equation. This can be done numerically by solving the equation with the Runge-Kutta method starting at $t = 0$ and going up to some large value of t. From (3.33) and (3.34) we see that $F(t_1,t_2) = F(t_2,t_1)$, which in turn means that $f(t_{12})$ is an even function. This gives us the initial condition $f'(0) = 0$. The initial

value of $f(0)$ can be any positive real number for the procedure since the value of the Lyapunov exponent does not depend on the overall normalisation of f. We then do a binary search for λ_L looking for the solution to cross zero at the end of the interval. To compute the plots in figure 31 we used initial conditions $f(0) = 0.01, f'(0) = 0$ and applied the Runge-Kutta method on the interval $t \in [0, 3\beta]$.

3.5 Spectral function in the deformed SYK

In this appendix we describe the numerical method used to compute the spectral function of $G(t)$, labelled by $\rho(\omega)$ and defined by (3.41). The method we use follows that described in [98, 99] for an SYK Lindbladian model, though it is also applicable for unitary deformed SYK models. The procedure involves numerically solving a system of equations involving $\rho(\omega)$ and the analogously defined spectral function of $\Sigma(t)$, which we label by $\sigma(\omega)$. Specifically, after passing to real time and Fourier transforming (see supplementary materials of [98] for a detailed derivation), the Schwinger-Dyson equations (3.15) can be written as[7]

$$\begin{cases} \rho(\omega) & = \frac{\sigma(\omega)}{(\omega+\pi\sigma^H(\omega))^2+(\pi\sigma(\omega))^2} \ , \\ \sigma(\omega) & = \mathcal{J}^2 \left(\frac{2\cosh(\beta\omega/2)}{q} \tilde{\rho}^{*(q-1)}(\omega) + s^2 \frac{2\cosh(\beta\omega/2)}{\tilde{q}} \tilde{\rho}^{*(\tilde{q}-1)}(\omega) \right) \ , \end{cases} \tag{3.47}$$

where σ^H is the Hilbert transform,

$$\sigma^H(\omega) = -\frac{1}{\pi} \mathcal{P} \int \mathrm{d}\nu \frac{\sigma(\nu)}{\omega - \nu} \ , \tag{3.48}$$

with $\mathcal{P}$ denoting the Cauchy principal value. The spectral function $\tilde{\rho}(\omega)$ is given by $\tilde{\rho}(\omega) \equiv \rho(\omega)/\cosh(\beta\omega/2)$, while $\tilde{\rho}^{*(n)}(\omega)$ denotes the n-fold convolution defined by

$$\tilde{\rho}^{*(n)}(\omega) = \int \left[\prod_{i=1}^{n-1} \mathrm{d}\mu_i \right] \tilde{\rho}(\omega - \sum_{i=1}^{n-1} \mu_i) \prod_{i=1}^{n-1} \tilde{\rho}(\mu_i) \ . \tag{3.49}$$

The equations (3.47) are then solved numerically on a discretised frequency grid. The size and spacing of the grid needed depends on how quickly the spectral function $\rho(\omega)$ decays, which in turn depends the values of q and the inverse temperature $\beta\mathcal{J}$. For our purposes we typically used a grid

[7] Our $\rho(\omega)$ and $\sigma(\omega)$ are $\rho^-(\omega)$ and $\sigma^-(\omega)$, respectively, in the conventions of [98].

spanning from $\omega = -30$ to $\omega = 30$ in steps of $\Delta\omega = 0.01$.

The numerical procedure begins with an ansatz for $\rho(\omega)$ which we take to be $\rho(\omega) \sim 1/(\omega^2+0.1)$. At each step in the iteration $\sigma(\omega)$ is computed from $\rho(\omega)$ using the second equation of (3.47) and then $\sigma^H(\omega)$ is computed from (3.48). Finally, $\rho(\omega)$ is updated by a proportion of the error in the first equation of (3.47),

$$\rho_{j+1}(\omega) = \rho_j(\omega) + \eta \left(\frac{\sigma_j(\omega)}{(\omega + \pi\sigma_j^H(\omega))^2 + (\pi\sigma_j(\omega))^2} - \rho_j(\omega) \right) , \tag{3.50}$$

where the weight η is initially set to 0.5. After each iteration we keep track of the difference

$$\rho_{\text{diff}} = \sum_{\omega} |\rho_{j+1}(\omega) - \rho_i(\omega)| . \tag{3.51}$$

If the difference increases we drop the value of the weighting parameter η by half. We terminate the procedure when $\rho_{\text{diff}} < 10^{-8}$. The n-fold convolution (3.49) can be carried out extremely efficiently in `Mathematica` using the built-in `ListConvolve` function. Due to the appearance of diverging factors of $\cosh(\beta\omega/2)$, a further trick is needed to avoid large numbers causing numerical instabilities when $\beta\mathcal{J} \gtrsim 10$. The trick involves expanding out the factors of $\cosh(\beta\omega/2)$ multiplying the convolutions in the second equation of (3.47) in such a way that the resulting equation consists of convolutions only involving $\rho(\omega)$ and $\rho(\omega)\tanh(\beta\omega/2)$. For example, if $q = 4$ we would write the factor of $\cosh(\beta\omega/2)$ as

$$\cosh(\beta\omega/2) = \cosh\left(\beta\left(\omega - \mu_1 - \mu_2\right)/2 + \beta\mu_1/2 + \beta\mu_2/2\right) , \tag{3.52}$$

and then expand the three terms in the argument of the RHS using the addition formula. This results in four terms involving products of hyperbolic cosines and hyperbolic sines, that simplify with the hyperbolic cosines in the denominator of the convolution $\tilde{\rho}^{*(3)}(\omega)$. This trick can be trivially extended to any value of q. The procedure converges in the order of seconds on a standard laptop.

In figure 4 we plot numerical computations of $\rho(\omega)$ and $\sigma(\omega)$ for the single SYK model with $q = 6$ at inverse temperatures of $\beta\mathcal{J} = 10, 100$. We note that as $\beta\mathcal{J}$ increases the spectral functions become more sharply peaked around the origin, making it more difficult to compute

them accurately. Using $\rho(\omega)$ computed with this method we were able to compute the Lyapunov and Krylov exponents for inverse temperatures of up to $\beta\mathcal{J} \sim 125$.

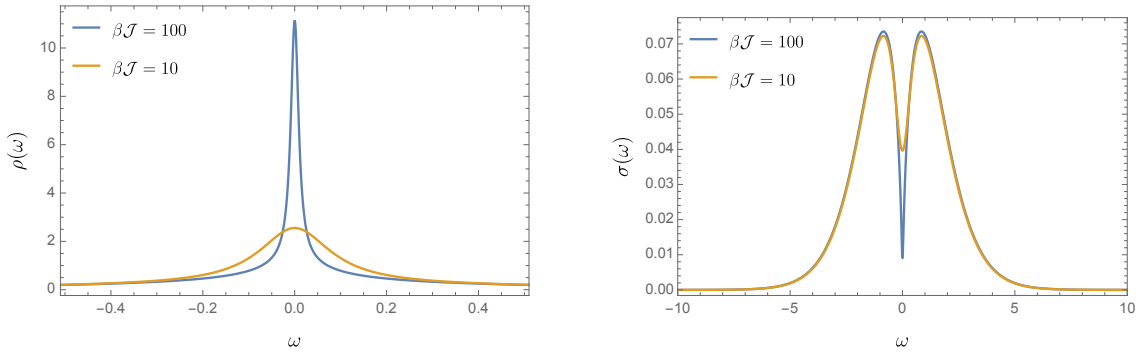

(a) $\rho(\omega)$ (b) $\sigma(\omega)$

Fig. 4: Spectral functions computed for the single SYK model with $q = 6$ at inverse temperatures $\beta\mathcal{J} = 10, 100$. For large inverse temperatures the spectral functions are more sharply peaked around the origin.

4 Single deformation and RG flows

4.1 Introduction

Given the description of a theory at a conformally invariant fixed point, one is naturally led to examine deformations causing the theory to flow toward a novel phase in the infrared. Sufficiently close to the fixed point, one can quantify the deformations by the set of primary operators which are relevant with respect to the original fixed point. The richer the space of relevant operators, the more elaborate the landscape of renormalisation group (RG) flows away from the underlying fixed point, and the more ample the opportunity to design particular infrared behaviour.

A useful strategy to gain insight into RG flows is to study the theory at finite temperature and use this as the energy scale of the problem [53, 100–103]. In this part of the thesis we will take this approach to analyse the effect of a relevant deformation causing a flow away from the near-fixed point of the SYK model [29, 31, 40]. The structure of the flow will be revealed through the detailed dependence of thermal correlations and thermodynamic quantities on the strength of the relevant term. The presence of additional fixed points and other properties of the flow are revealed through such physical quantities.

The essential motivation behind this work is to develop a new direction in the study of holographic renormalisation [104, 105] by identifying tractable renormalisation group flows for strongly coupled theories at large N. From the perspective of the gravitational description, the renormalisation group flow manifests itself in a geometry that flows away from the asymptotically AdS boundary describing the fixed point. The basic challenge is that strongly coupled fixed points with tractable renormalisation group flows are hard to come across. Although relevant deformations of SYK have not been studied extensively in the literature, there are exceptions [46, 49, 50, 52, 53]. Moreover, there have been a host of interesting variations of SYK including entangling a pair of SYK theories to each other [106, 107], endowing SYK type models with internal global symmetries [108–111], non-Hermitian SYK Hamiltonians modelling open quantum systems [112, 113], models of SYK chains and higher-dimensional analogues [38, 114, 115], and supersymmetric extensions [116, 117].

In what follows we employ a variety of analytical and numerical techniques to analyse deformed SYK models of the form (2.47). Concrete evidence is provided that for sufficiently small s, the deformation can be viewed as a relevant deformation by a specific conformal operator of the near-

fixed point describing the low energy physics of the undeformed SYK model. Previous work [53] has established this in the large q limit with $q/\tilde{q} = 2$. Here, we establish this phenomenon at both large and finite q, $\tilde{q}$. Moreover, the effect is seen for several values for $\mathfrak{n} \equiv q/\tilde{q}$. The flow is shown to end at a near-fixed point in the deep infrared, where the theory is captured by an SYK theory governed by $H_{\tilde{q}}$. Interestingly, the Schwarzian sector of the theory in the deep infrared resides entirely within the strongly coupled sector of the theory. From a holographic point of view, this can be viewed as a soft mode emerging in the interior of a bulk asymptotically AdS_2 spacetime.

4.2 Thermodynamics of the deformed SYK

In this section we analyse the deformed models (2.47) for general values of $\mathfrak{n} = q/\tilde{q}$, both at finite and large q. An emphasis is placed on the deep IR behaviour of the deformed model, given by $\beta\mathcal{J} \gg 1/s^2$. When $\mathfrak{n} \neq 2$, we must resort to a combination of analytical and numerical techniques to compute thermodynamic quantities. We begin by analysing the large q limit. We compute the large q entropy at low temperatures, from which we can numerically extract the coefficient, denoted by $\bar{\aleph}(s, \mathfrak{n})$, of the linear-in-temperature part of the entropy, for various values of $\mathfrak{n}$. We conjecture that a similar structure for the entropy holds for finite values of q and check it against numerical data for $\mathfrak{n} = 2, 3, 4$, and different finite values of q, finding good agreement. We also provide evidence for the existence of models with two near-conformal regimes at both large and finite q, characterised by two linear-in-temperature regimes for the entropy. Finally, we uncover a novel analytically tractable window for $\mathfrak{n} = 1 + \varepsilon$, with ε small.

4.2.1 Large q

We start by computing $\bar{\aleph}(s, \mathfrak{n})$ numerically for general $\mathfrak{n}$, in the large q limit. To do so, we need to solve equation (2.50), with boundary conditions $g(0) = g(\beta) = 0$. Given a numerical solution $g(\tau)$, we can compute the free energy following equation (2.53). The entropy then can be obtained using (2.37). Instead of computing the thermodynamic derivative numerically we use that $\beta\partial_\beta = \mathcal{J}\partial_\mathcal{J}$ [31] to compute the entropy directly as

$$\frac{S}{N} = S_0^{\text{free}} + \frac{\beta}{8\mathfrak{n}^2\tilde{q}^2}\int_0^\beta d\tau \left[\frac{1}{2}\left(\partial_\tau g(\tau)\right)^2 - \mathcal{J}^2\left(2\mathfrak{n}^2 s^2 e^{g(\tau)/\mathfrak{n}} + 2e^{g(\tau)}\right)\right] . \tag{4.1}$$

In the deep IR, it is more convenient to parameterise formulae in terms of $\tilde{q}$ instead of q, as $H_{\tilde{q}}$ is the dominating term in the Hamiltonian in this regime. Our numerical results confirm that at low enough temperatures, $\beta\mathcal{J} \gg 1/s^2$, the entropy is linear in the temperature, taking the form

$$\frac{S}{N} = \left(S_0^{\text{free}} + S_0(s,\mathfrak{n})\right) + \bar{\aleph}(s,\mathfrak{n})\frac{\pi^2}{\tilde{q}^2}\frac{1}{s\beta\mathcal{J}} + \cdots , \tag{4.2}$$

where $\bar{\aleph}(s,\mathfrak{n})$ can in general depend on s and $\mathfrak{n}$, but is independent of $\beta\mathcal{J}$. The zero temperature entropy is shifted by a factor $S_0(s,\mathfrak{n})$ that may also generally depend on s and $\mathfrak{n}$.

Zero temperature entropy. We can find $\tilde{q}^2 S_0(s,\mathfrak{n})$ numerically by performing a linear fit of $\tilde{q}^2\beta\mathcal{J}\left(S/N - S_0^{\text{free}}\right)$ as a function of $\beta\mathcal{J}$ for large values of $\beta\mathcal{J}$. In figure 5, we show results for $s^2 = 0.1, 1, 4$ with $1 \leq \mathfrak{n} \leq 3$, using values of $\beta\mathcal{J}$ between 2000 and 3000 for the linear fit. We find that for $\mathfrak{n} \geq 2$, the shift in the zero temperature entropy is given by $\tilde{q}^2 S_0(s,\mathfrak{n}) = -\pi^2/4$, the same as that of a single SYK model with Hamiltonian $sH_{\tilde{q}}$. As shown in figure 5, there are deviations from the single SYK result within the interval $1 < \mathfrak{n} < 2$, but they vanish as $\mathfrak{n} \to 2$. The s dependence of the entropy at vanishing temperature, as well as the transition at $\mathfrak{n} = 2$, and their potential holographic interpretation, merit a deeper understanding perhaps along the lines of [118]. We will return to this in future work.

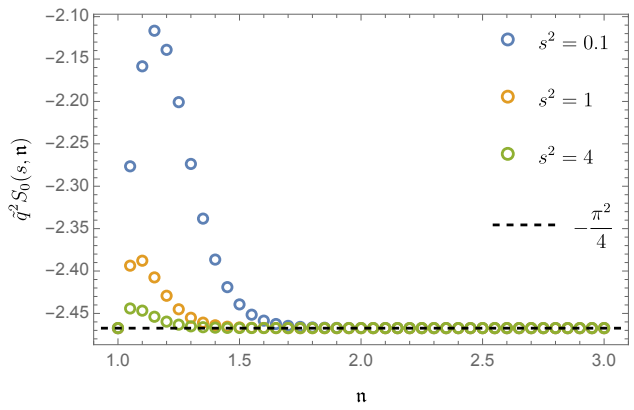

Fig. 5: The zero temperature entropy $\tilde{q}^2 S_0(s,\mathfrak{n})$ as a function of $\mathfrak{n}$, for $s^2 = 0.1, 1, 4$. The circles are numerical computations for different values of s^2, while the dashed black line indicates the analytic value of $\tilde{q}^2 S_0$ for a single SYK model $sH_{\tilde{q}}$.

The deep IR phase at large q. We numerically compute the entropy $\tilde{q}(S/N - S_0^{\text{free}})$ at a single

low temperature point.[8] Subtracting the previously obtained values for $\tilde{q}^2 S_0(s,\mathfrak{n})$ from this, the leading contribution to the difference is a term that is proportional to $(\beta\mathcal{J})^{-1}$, from which we can numerically extract $\bar{\aleph}(s,\mathfrak{n})$ in (4.2). For $\mathfrak{n}=2$, there is an analytic answer for $\bar{\aleph}$ given by (2.58). We use this as a consistency check of our numerical procedure. In figure 6, we show agreement between our numerical algorithm and the analytic result for $\mathfrak{n}=2$.

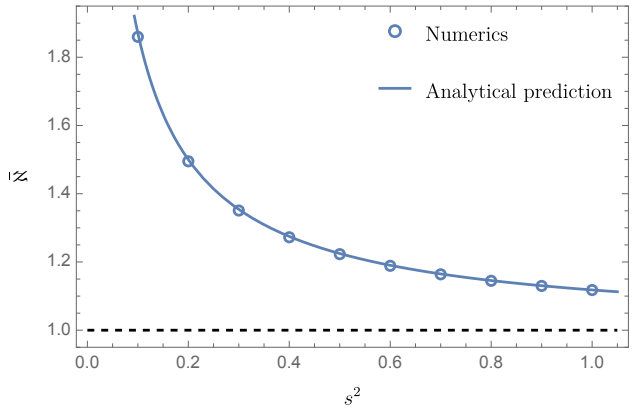

Fig. 6: $\bar{\aleph}$ as a function of s^2 for the deformed SYK model in the large q limit with $\mathfrak{n}=2$. The circles are numerical computations while the blue solid curve shows the analytic result in (2.58), for comparison. At large s, we expect the numerics to tend towards the black dashed line at $\bar{\aleph}=1$.

For $\mathfrak{n}\neq 2$, there are no known analytic solutions. However, we do expect a certain behaviour of $\bar{\aleph}(s,\mathfrak{n})$ in a variety of limits. Namely,

1. For $s\to\infty$ and fixed $\mathfrak{n}$, we expect the leading entropy to be that of a single SYK model with Hamiltonian $sH_{\tilde{q}}$ and so, $\bar{\aleph}(s\to\infty,\mathfrak{n})\to 1$ in this limit.

2. At fixed s but $\mathfrak{n}\to\infty$, we also expect $\bar{\aleph}(s,\mathfrak{n}\to\infty)\to 1$. To see this, note that $\mathfrak{n}\to\infty$ implies $q\to\infty$ with $\tilde{q}$ finite. The contribution to the free energy from H_q is given by $2^{q-1}q^{-2}G^q$, see (2.48). Given that $|G(\tau)|\leq 1/2$, if we take q to infinity this contribution is negligible and only the terms with $\tilde{q}$ will contribute. Thus, $\bar{\aleph}(s,\mathfrak{n}\to\infty)\to 1$.

3. When $\mathfrak{n}=1$, the theory is equivalent to a single SYK with Hamiltonian $\sqrt{1+s^2}H_q$. We therefore expect that

$$\bar{\aleph}(s,\mathfrak{n}=1)=\frac{s}{\sqrt{1+s^2}}\ . \tag{4.3}$$

[8] In figures 6 and 7 we present numerical results for $\beta\mathcal{J}=3000$. We have also performed this procedure for other values of $\beta\mathcal{J}$ between 2000 and 3000 allowing us to test the postulated β-dependence of (4.2).

4. Finally, as discussed, when $\mathfrak{n} = 2$, we know analytically that

$$\bar{\aleph}(s, \mathfrak{n} = 2) = \frac{\sqrt{1 + 4s^2}}{2s} \,. \tag{4.4}$$

In figure 7 we plot numerical values of $\bar{\aleph}(s, \mathfrak{n})$ as a function of $\mathfrak{n}$ for different values of s^2. We see that the numerical results behave as expected in the limits mentioned above. When $\mathfrak{n} = 1$ and $\mathfrak{n} = 2$, the numerical values agree with the analytically known values. We also observe that as s^2 grows deviations from $\bar{\aleph}(s, \mathfrak{n}) = 1$ decrease for all values of $\mathfrak{n}$, consistent with the expectation that when s becomes large $\bar{\aleph}(s, \mathfrak{n}) \to 1$. Furthermore, as $\mathfrak{n}$ becomes large we see that $\bar{\aleph}(s, \mathfrak{n}) \to 1$, as expected.

We also notice an interesting behaviour of $\bar{\aleph}(s, \mathfrak{n})$ between $\mathfrak{n} = 1$ and $\mathfrak{n} = 2$, characterised by a peak whose position depends on s. Following the analytic arguments on section 4.3.1, we expect the peak to move towards $\mathfrak{n} = 3/2$, as s becomes smaller. Though we were unable to find a general analytic form for $\bar{\aleph}(s, \mathfrak{n})$, the numerical results suggest that, at least at small s and $\mathfrak{n} \geq 2$, the empirical formula

$$\bar{\aleph}(s, \mathfrak{n}) \approx \frac{a(\mathfrak{n})}{s^{4/\mathfrak{n}^2}} \,, \tag{4.5}$$

holds with $1/2 \leq a(\mathfrak{n}) \leq 1$. More details on this are provided in appendix C.

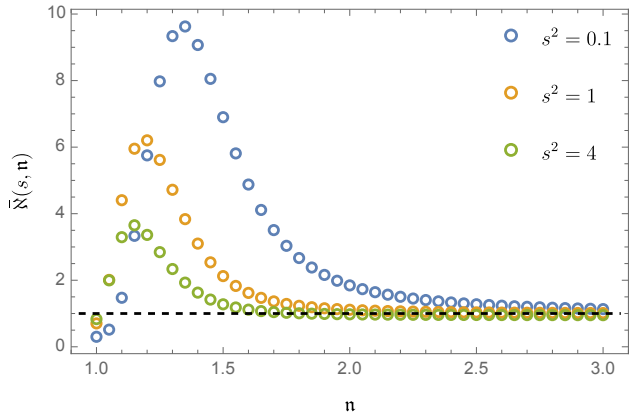

Fig. 7: $\bar{\aleph}(s, \mathfrak{n})$ as a function of $\mathfrak{n}$ for $s^2 = 0.1, 1, 4$. The circles are numerical computations. For large $\mathfrak{n}$, $\bar{\aleph}(s, \mathfrak{n})$ tends towards the expected value of $\bar{\aleph}(s, \mathfrak{n}) = 1$ shown in a dashed black line.

The intermediate IR phase at large q. For large values of q and $\mathfrak{n} \geq 2$, the RG flow at small enough s develops two near-fixed points. At finite temperature this is revealed by the presence of two linear-in-temperature regimes for the entropy. We find that, just as in the $\mathfrak{n} = 2$ case, the

entropy in the intermediate IR regime is given by (2.55). An example of this behaviour, for $\mathfrak{n} = 3$, is given in figure 8.

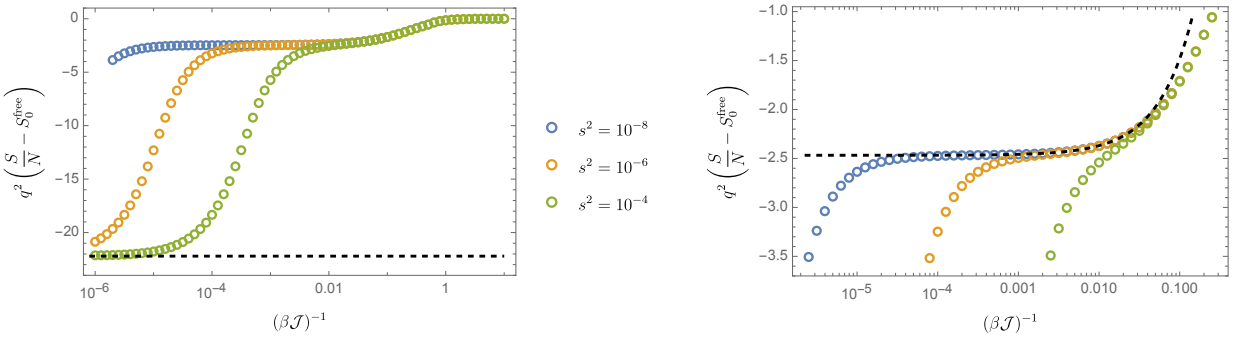

(a) $\mathfrak{n} = 3$, full RG flow

(b) $\mathfrak{n} = 3$, intermediate IR

Fig. 8: The entropy as a function of temperature (in logarithmic scale) for the deformed SYK model at large N and large q with $\mathfrak{n} = 3$. In 8(a) we plot the full RG flow accessible to our numerics. The dashed line gives the expected zero temperature entropy (see figure 5, noting that in this case $q = 3\tilde{q}$). In 8(b) we zoom into the intermediate IR regime. The dashed line gives the expected analytic form (2.55).

In sections 4.2.2 and 4.3.3 we provide evidence for the existence of a near-fixed point at finite q. Moreover, in section 4.3.3 we present evidence of the intermediate fixed point for $1 < \mathfrak{n} < 2$ at large q. A systematic analysis of the behaviour in the proximity of the two near-fixed points is discussed in section 4.3.

4.2.2 Finite q

Given the results in the large q limit, we now analyse the case of finite q. This is numerically more involved than the previous case, as the Schwinger-Dyson equations no longer reduce to an ordinary differential equation. Instead, we need to solve the Schwinger-Dyson equations (2.49) numerically. This set of equations is amenable to numerical computations using a recursive algorithm and the fast Fourier transform. In section 3.2 we outline the details of this procedure, which is analogous to the one described in appendix G of [31] for the single SYK model. The simplest deformed model at finite q has $q = 4$ and $\tilde{q} = 2$, which is first studied in [46]. In the present work, we extend this analysis to include smaller values of s^2, allowing us to observe two different near-conformal regimes. We also present results for a more general class of models with different values of q and $\tilde{q}$.

The deep IR phase at finite q. We start by focussing on the form of the entropy in the deep

IR limit. We have numerical access to this regime provided s is not very small. For a single SYK model with $\tilde{q}$ and coupling $s\mathcal{J}$, the entropy in the limit $\beta\mathcal{J} \gg 1/s$ is given by

$$\frac{S}{N} = \left(S_0^{\text{free}} - \int_0^{1/\tilde{q}} dx\, \pi \left(\frac{1}{2} - x\right) \tan \pi x \right) + \frac{4\pi^2 \alpha(\tilde{q})}{s\beta\mathcal{J}} + \cdots \,, \tag{4.6}$$

where $\alpha(\tilde{q})$ is the same (numerical) coefficient that appeared in the Schwarzian action in (2.35) (see appendix B for more detail).

Moving to the case of the deformed Hamiltonian, we first discuss the case of $\mathfrak{n} = 2$. In section 4.2.1, we found that for $\mathfrak{n} \geq 2$ the zero temperature entropy of the deformed model was the same as that of a single SYK. Assuming this is the case even at finite q, we propose that the entropy in the deformed theory should be generalised to

$$\frac{S}{N} = \left(S_0^{\text{free}} - \int_0^{1/\tilde{q}} dx\, \pi \left(\frac{1}{2} - x\right) \tan \pi x \right) + \bar{\aleph}\, \frac{4\pi^2 \alpha(\tilde{q})}{s\beta\mathcal{J}} + \cdots \,. \tag{4.7}$$

Namely, the zero temperature entropy remains the same and the linear-in-temperature term gets an extra coefficient of $\bar{\aleph}$ – as defined in (2.58) – with respect to the single SYK theory. We numerically find that for large s and low temperatures, $(S/N - S_0^{\text{free}})$ approaches the predicted value of -0.346 obtained from setting $\tilde{q} = 2$ in (4.7) (see for example figure 11).

To test the linear-in-temperature coefficient, we compute the entropy at a single low temperature point and subtract the zero temperature entropy. In figure 9, we show the numerical results for the coefficient and compare to the analytic prediction, as in (4.7), for different values of q and $\tilde{q}$, with fixed $\mathfrak{n} = 2$. To compute the predicted coefficient, we use values of $\alpha(\tilde{q})$ obtained from the Padé approximation as described in appendix B and the analytic value of $\bar{\aleph}$ for $\mathfrak{n} = 2$ in the large q limit. We find good agreement, suggesting the possibility of using large q (analytical) results to extract finite q information.

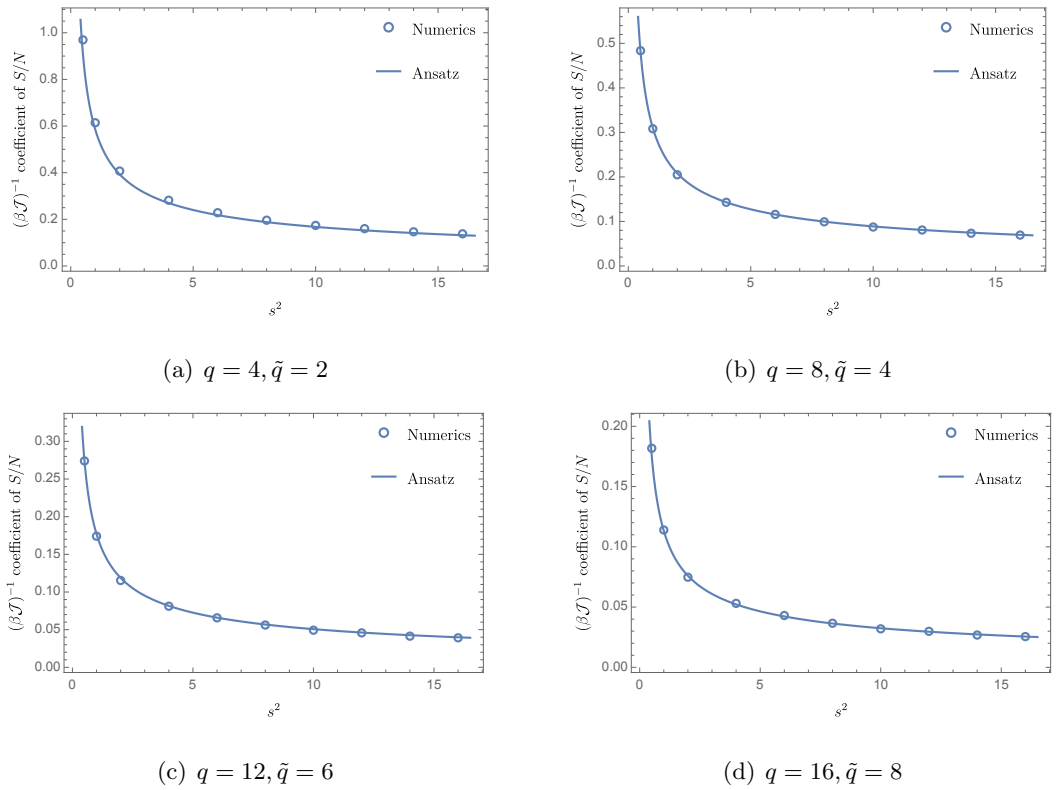

(a) $q = 4, \tilde{q} = 2$

(b) $q = 8, \tilde{q} = 4$

(c) $q = 12, \tilde{q} = 6$

(d) $q = 16, \tilde{q} = 8$

Fig. 9: The linear-in-temperature coefficient of the entropy as a function of s^2, in the deformed SYK with $\mathfrak{n} = 2$ for finite q and $\tilde{q}$. The circles correspond to numerical computations while the blue solid curve corresponds to (4.7), conjectured from the large q limit behaviour.

The results for $\mathfrak{n} = 2$ hint towards the possibility of generalising the form of the low temperature entropy even away from the $\mathfrak{n} = 2$ point. In fact, following the results at large q, we propose that the only change in the form of the entropy (4.7) for $\mathfrak{n} > 2$ is to take $\bar{\aleph} \to \bar{\aleph}(s, \mathfrak{n})$, where $\bar{\aleph}(s, \mathfrak{n})$ is the coefficient obtained numerically in the large q limit, see figure 7. Note that for $1 < \mathfrak{n} < 2$ we would also expect a change in the zero temperature entropy, as is seen at large q. The proposal, then, is that, at finite q, for $\mathfrak{n} \geq 2$, the low temperature entropy takes the form,

$$\frac{S}{N} = \left(S_0^{\text{free}} - \int_0^{1/\tilde{q}} dx\, \pi \left(\frac{1}{2} - x \right) \tan \pi x \right) + \bar{\aleph}(s, \mathfrak{n}) \frac{4\pi^2 \alpha(\tilde{q})}{s\beta\mathcal{J}} \,. \tag{4.8}$$

We test this conjecture for $\mathfrak{n} = 3$ and $\mathfrak{n} = 4$ by numerically computing the entropy for $q = 12$, $\tilde{q} = 4$ and $q = 16$, $\tilde{q} = 4$ respectively. As before we use a single low temperature point and subtract the zero temperature entropy to isolate the linear-in-temperature coefficient. To compute the predicted linear-in-temperature coefficient, as in (4.8), we again use values of $\alpha(\tilde{q})$ from the Padé approximant

described in appendix B but now use values of $\bar{\aleph}(s,\mathfrak{n})$ obtained numerically at large q. The results are shown in figure 10, providing strong evidence for (4.8).

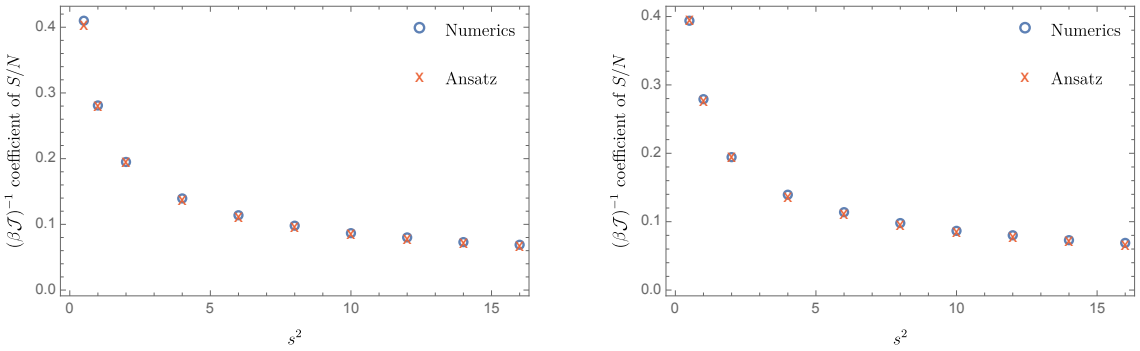

(a) $q = 12, \tilde{q} = 4$ (b) $q = 16, \tilde{q} = 4$

Fig. 10: The linear-in-temperature coefficient of the entropy as a function of s^2, in the deformed SYK for $\mathfrak{n} = 3, 4$ with finite q and $\tilde{q}$. The circles correspond to numerical computations while the crosses correspond to (4.8) with the value of $\bar{\aleph}(s,\mathfrak{n})$ obtained numerically in the large $q, \tilde{q}$ limit.

The intermediate IR phase at finite q. We now provide evidence that even at finite q, the RG flow at small enough s develops two near-conformal regimes. We consider the cases of $\mathfrak{n} = 2$ with $q = 4$ and $\tilde{q} = 2$ and $\mathfrak{n} = 3$, with $q = 6$ and $\tilde{q} = 2$. In figure 11, we plot entropy as a function of $(\beta\mathcal{J})^{-1}$ for different values of the coupling s^2, from $s^2 = 1$ to $s^2 = 10^{-6}$, for both models. In each case, at large temperatures, all the curves approximate the entropy of the free fermions. As we move towards the IR, and similar to what happens at large q, there are two clearly different behaviours depending on the value of s^2. When $s^2 \sim 1$, the entropy goes directly into the deep IR phase. When $s^2 \ll 1$, there is a different intermediate IR phase appearing with a linear-in-temperature regime. It is natural to suspect that at even lower temperatures, these theories will also end up flowing into the deep IR phase. However, the numerical techniques employed are only powerful enough to reach $(\beta\mathcal{J})^{-1} \gtrsim 10^{-3}$. This does not permit us to compute a full RG flow exhibiting both the intermediate and the deep IR phase. Implementing an algorithm based on spectral methods might provide an efficient way of reaching even lower temperatures of order at least $(\beta\mathcal{J})^{-1} \sim 10^{-4}$ (see section 3.2) [85]. We leave such an approach for future work.

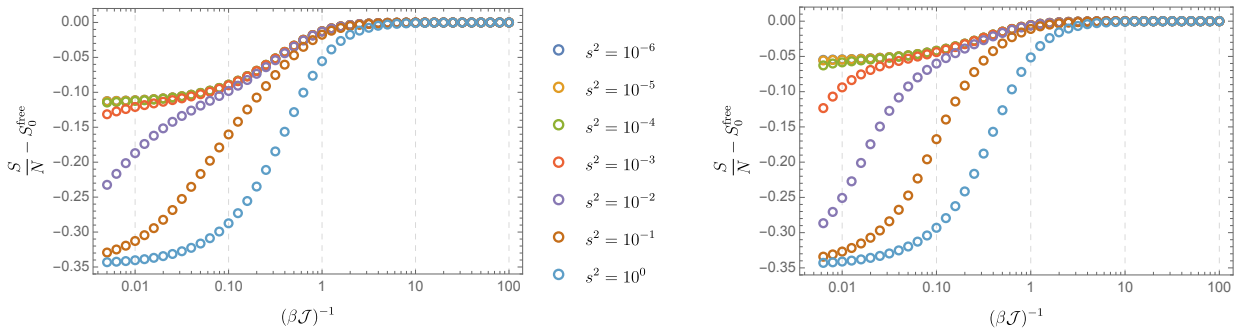

(a) $q = 4, \tilde{q} = 2$ (b) $q = 6, \tilde{q} = 2$

Fig. 11: The entropy as a function of temperature (in logarithmic scale) for the deformed SYK model at large N and finite q. Different colours correspond to different values of s^2. Circles correspond to numerical computations.

4.2.3 Large q with $\mathfrak{n} = 1 + \varepsilon$

To finish this section we discuss a novel analytically tractable RG flow at large q, for $\mathfrak{n} = 1 + \varepsilon$, with ε a small positive number.

We first discuss the leading order solution $g_0(\tau)$ with $\mathfrak{n} = 1$. At the level of the effective action (2.48), the deformed model with $\mathfrak{n} = 1$ is equivalent to a single SYK model with random couplings averaged over a Gaussian distribution with a variance proportional to $\mathcal{J}^2(1 + s^2)$. In fact, at large q, the differential equation (2.50) for $\mathfrak{n} = 1$, becomes

$$\partial_\tau^2 g_0(\tau) = 2\mathcal{J}^2(1 + s^2)e^{g_0(\tau)} \,, \tag{4.9}$$

which after imposing thermal boundary conditions, $g_0(0) = g_0(\beta) = 0$, is solved by

$$e^{g_0(\tau)} = \frac{\cos^2 \nu}{\cos^2\left(2\nu\left(\frac{1}{2} - \frac{\tau}{\beta}\right)\right)} \,, \qquad \beta\mathcal{J} = \frac{2\nu}{\sqrt{1 + s^2}\cos\nu} \,. \tag{4.10}$$

We now consider $\mathfrak{n} = 1 + \varepsilon$, perturbatively in ε. We can expand $g(\tau)$ as

$$g(\tau) = g_0(\tau) + \varepsilon g_1(\tau) + \mathcal{O}(\varepsilon^2). \tag{4.11}$$

Substituting this into the differential equation (2.50), we find, at leading order in ε, a differential

equation for $g_1(\tau)$

$$\partial_\tau^2 g_1(\tau) = 2e^{g_0(\tau)}\mathcal{J}^2\left((1-g_0(\tau))s^2 + g_1(\tau)\left(1+s^2\right)\right) \ . \tag{4.12}$$

It is straightforward to show that

$$g_1(\tau) = \frac{s^2}{1+s^2} g_0(\tau)\,, \tag{4.13}$$

is the solution to (4.12) with boundary conditions $g_1(0) = g_1(\beta) = 0$. To see this, note that if we plug this expression for $g_1(\tau)$ in (4.12), we get that

$$\partial_\tau^2 g_0(\tau) = 2\mathcal{J}^2(1+s^2)e^{g_0(\tau)} \ , \tag{4.14}$$

which is exactly (4.9), so it is satisfied by $g_0(\tau)$. Next, we consider the corrections to the free energy coming from this deformation. Expanding (2.53) to leading order in ε we obtain

$$\left.\frac{\beta F}{N}\right|_{\mathfrak{n}=1+\varepsilon} = -S_0^{\text{free}} + \frac{\nu(\nu-2\tan\nu)}{\tilde{q}^2} - \frac{2\nu(\nu-2\tan\nu)}{1+s^2}\frac{\varepsilon}{\tilde{q}^2} + \mathcal{O}(\varepsilon^2) \ . \tag{4.15}$$

Using (2.37) we find the entropy to leading order in ε is given by

$$\left.\frac{S}{N}\right|_{\mathfrak{n}=1+\varepsilon} = S_0^{\text{free}} - \frac{\nu^2}{\tilde{q}^2} + \frac{2\nu^2}{1+s^2}\frac{\varepsilon}{\tilde{q}^2} + \mathcal{O}(\varepsilon^2) \ . \tag{4.16}$$

This can be used to find the entropy as a function of temperature for the full RG flow. Though we do not observe an intermediate IR at this order in ε, we are able to access some interesting features of the deep IR. Expanding (4.16) in powers of $(\beta\mathcal{J})^{-1}$ we find the correction to the entropy,

$$\left.\frac{S}{N}\right|_{\mathfrak{n}=1+\varepsilon} = \left.\frac{S}{N}\right|_{\mathfrak{n}=1} + \left(\frac{\pi^2}{2\left(1+s^2\right)} - \frac{2\pi^2}{\left(1+s^2\right)^{3/2}}\frac{1}{\beta\mathcal{J}} + \mathcal{O}\left(\beta\mathcal{J}\right)^{-2}\right)\frac{\varepsilon}{\tilde{q}^2} + \mathcal{O}(\varepsilon^2) \ , \tag{4.17}$$

where the entropy at low temperatures for $\mathfrak{n}=1$ is given by equation (2.45) with $\mathcal{J} \to \sqrt{1+s^2}\mathcal{J}$ and $q \to \tilde{q}$. Equation (4.17) provides two predictions that can be tested against numerical computations. We study these next.

Zero temperature entropy. Note that the correction to the zero temperature entropy at large

$\tilde{q}$ is given by

$$\lim_{\beta\mathcal{J}\to\infty} \frac{\tilde{q}^2 S(\beta\mathcal{J})}{N}\bigg|_{\mathfrak{n}=1+\varepsilon} - \frac{\tilde{q}^2 S(\beta\mathcal{J})}{N}\bigg|_{\mathfrak{n}=1} = \frac{\pi^2}{2(1+s^2)}\varepsilon + \mathcal{O}(\varepsilon^2) \ . \tag{4.18}$$

We can numerically compute the large $q, \tilde{q}$ entropy for $\mathfrak{n} = 1$ and for $\mathfrak{n} = 1 + \varepsilon$ at large $\beta\mathcal{J}$ for small values of ε and compare with the analytic prediction. We show the results for $s^2 = 0.1, 1, 4$ at $\beta\mathcal{J} = 2000$ in figure 12, showing agreement between the analytical predictions and the numerical computations.

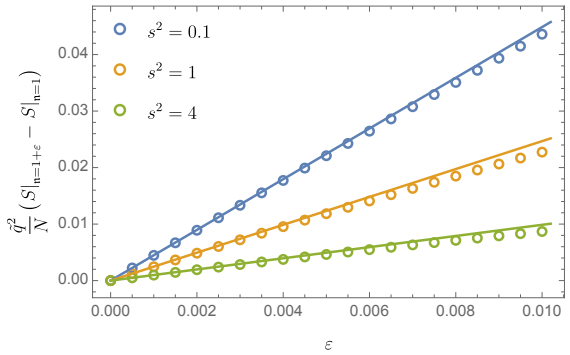

Fig. 12: The difference in the zero temperature entropy between the large $q, \tilde{q}$ model with $\mathfrak{n} = 1 + \varepsilon$ and $\mathfrak{n} = 1$, as function of small ε, for different values of s^2. The circles correspond to numerical computations at $\beta\mathcal{J} = 2000$, while the solid lines are the analytic prediction from (4.18). For small enough ε, both overlap.

Linear-in-temperature entropy. We can also find analytically the correction to the linear-in-temperature term in the entropy, and from this the correction $\bar{\aleph}(s, \mathfrak{n})$ near $\mathfrak{n} = 1$. From (4.17), we find

$$\bar{\aleph}(s, 1+\varepsilon) - \bar{\aleph}(s, 1) = -\varepsilon \frac{2s}{(1+s^2)^{3/2}} + \mathcal{O}(\varepsilon^2) \ , \tag{4.19}$$

where as $\bar{\aleph}(s, 1)$ is given by (4.3). Note that the expected value of $\bar{\aleph}(s, \mathfrak{n})$ is lower than the value for $\mathfrak{n} = 1$. In figure 13, we test the predicted correction in (4.19) against numerical computations for $s^2 = 0.1$ and small values of ε, finding excellent agreement.

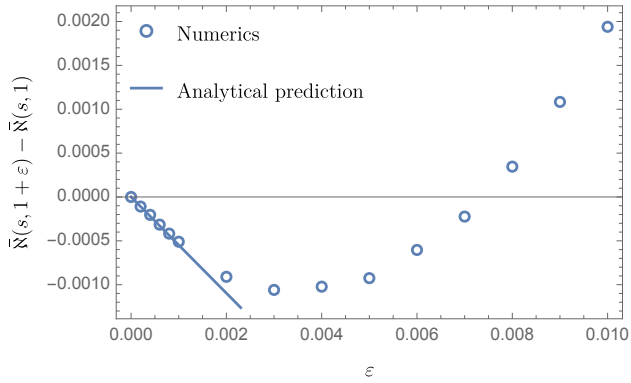

Fig. 13: Difference in the values of $\bar{\aleph}(s,\mathfrak{n})$ between $\mathfrak{n}=1+\varepsilon$ and $\mathfrak{n}=1$, as a function of small values of ε, with $s^2=0.1$. The circles correspond to numerical computations, while the solid blue line is the analytic result from (4.19). Note that they match at small ε, showing that $\bar{\aleph}(s,\mathfrak{n})$ initially decreases as $\mathfrak{n}$ moves away from $\mathfrak{n}=1$. For larger ε, $\bar{\aleph}(s,\mathfrak{n})$ starts increasing again, which agrees with the results shown in figure 7. We do not see the initial decrease in $\bar{\aleph}(s,\mathfrak{n})$ in figure 7 since the lowest ε considered there is $\varepsilon=0.05$, much larger than the values shown in this plot.

4.3 Conformal perturbation theory

In this section we explore thermodynamic contributions to the free energy and entropy of the deformed SYK near each fixed point. We argue that the leading terms in the entropy expansions (2.57) and (2.55) can be understood as perturbations to the conformal actions of the single SYK models $sH_{\tilde{q}}$ and H_q, respectively. In particular, we will argue that in both cases, the leading irrelevant correction to the free energy, which is proportional to the temperature, stems from a Schwarzian action. Moreover, in the intermediate IR regime, the leading relevant correction away from the intermediate fixed point can be understood from a relevant conformal operator in conformal perturbation theory.

4.3.1 Schwarzian for the deep IR

In section 4.2.2 numerical evidence was presented indicating that the entropy, S, for the finite q deformed model in the deep IR takes the low temperature expansion

$$\frac{S}{N}=\text{const}+\bar{\aleph}(s,\mathfrak{n})\frac{4\pi^2\alpha(\tilde{q})}{s\beta\mathcal{J}}+\cdots\ . \tag{4.20}$$

The linear-in-temperature part in S is modified from that of an undeformed SYK model with Hamiltonian $sH_{\tilde{q}}$ by $\bar{\aleph}(s,\mathfrak{n})$.

We would like to understand the linear-in-temperature part in S as coming from the leading correction to a conformal piece of the action associated with the SYK Hamiltonian $sH_{\tilde{q}}$ [81]. More explicitly, by taking $\Sigma \to \Sigma + \partial_\tau$, we can re-write the $G\Sigma$-action (2.48) as $I = \tilde{I}_{\rm CFT} + \tilde{I}_{\rm UV}$ where

$$\tilde{I}_{\rm CFT} = -\frac{1}{2}\log\det(-\Sigma) + \frac{1}{2}\int_0^\beta\int_0^\beta d\tau_1 d\tau_2 \left(\Sigma G - s^2\mathcal{J}^2\frac{2^{\tilde{q}-1}}{\tilde{q}^2}G^{\tilde{q}}\right) , \tag{4.21}$$

$$\tilde{I}_{\rm UV} = \frac{1}{2}\int_0^\beta\int_0^\beta d\tau_1 d\tau_2 \left(\delta(\tau_1-\tau_2)\partial_{\tau_2}G - \mathcal{J}^2\frac{2^{q-1}}{q^2}G^q\right) . \tag{4.22}$$

The CFT action (4.21) is the same as the action (2.32) discussed in section 2.3 upon making the replacements $\mathcal{J} \to s\mathcal{J}$ and $q \to \tilde{q}$. The UV action, $\tilde{I}_{\rm UV}$, has an additional term as compared to that of the undeformed SYK model. Note that so far all we have done is to rewrite (2.48). We rewrite it in this way because we would like to view $\tilde{I}_{\rm UV}$ as a perturbation to $\tilde{I}_{\rm CFT}$ and will be interested in computing its leading effect.

We have a continuous family of saddle solutions of $\tilde{I}_{\rm CFT}$ written in terms of reparameterisations, $\phi(\tau)$, of the circle to itself with a single unit of winding

$$G_\phi(\tau_1,\tau_2) = \phi'(\tau_1)^\Delta\, b\,\mathrm{sgn}(\tau_1-\tau_2)\left(\frac{\pi}{\beta s\mathcal{J}\sin\left(\frac{\pi(\phi(\tau_1)-\phi(\tau_2))}{\beta}\right)}\right)^{2\Delta}\phi'(\tau_2)^\Delta , \qquad \Delta \equiv 1/\tilde{q} , \tag{4.23}$$

where the constant b is given by (2.34).

We now argue that the leading correction to $\tilde{I}_{\rm CFT}$ due to the effect of $\tilde{I}_{\rm UV}$ takes the form of a Schwarzian action and gives a linear-in-temperature contribution to the specific heat. The argument we make is analogous to the one used for the single SYK [40, 81].[9] For an alternative treatment of the Schwarzian action and near-conformal perturbations see [119, 120]. It will be convenient to rewrite the reparameterisation modes $\phi(\tau)$ in terms of modes on the line $f(\tau)$, defined by

$$f(\tau) = \tan\left(\frac{\pi\phi(\tau)}{\beta}\right) . \tag{4.24}$$

After this transformation we find our solutions (4.23) are parameterised as

$$G_f(\tau_1,\tau_2) = \frac{b}{(s\mathcal{J})^{2\Delta}}\frac{f'(\tau_1)^\Delta f'(\tau_2)^\Delta}{|f(\tau_1)-f(\tau_2)|^{2\Delta}} . \tag{4.25}$$

[9] In appendix D we show that this argument gives the correct low temperature entropy in the integrable case of a single SYK model with $q = 2$.

We will want to use (4.25) in $\tilde{I}_{\rm UV}$, so that we only pick out contributions to the path integral along the conformal saddle solutions. We expand $G_f(\tau_1,\tau_2)$ around $(\tau_1,\tau_2)=(\tau_+,\tau_+)$, where $\tau_+\equiv(\tau_1+\tau_2)/2$, giving a series in powers of $\tau_{12}\equiv\tau_1-\tau_2$,

$$G_f(\tau_1,\tau_2)=\frac{1}{(s\mathcal{J})^{2\Delta}|\tau_{12}|^{2\Delta}}\left(1+\frac{\Delta}{6}\tau_{12}^2\,\mathrm{Sch}(f(\tau_+),\tau_+)+\mathcal{O}(\tau_{12}^3)\right)\ , \tag{4.26}$$

where the Schwarzian derivative is defined by

$$\mathrm{Sch}(f(\tau_+),\tau_+)\equiv\frac{f'''(\tau_+)}{f'(\tau_+)}-\frac{3}{2}\left(\frac{f''(\tau_+)}{f'(\tau_+)}\right)^2=\frac{1}{2}\left(\left(\frac{2\pi}{\beta}\right)^2\phi'(\tau_+)^2-\left(\frac{\phi''(\tau_+)}{\phi'(\tau_+)}\right)^2\right)\ . \tag{4.27}$$

We now substitute the expansion (4.26) into $\tilde{I}_{UV}$ while changing the integration variables from (τ_1,τ_2) to (τ_+,τ_{12}). Due to the periodicity of our fields in β we can take the new region of integration as $0\le\tau_{12}<\beta$ and $0\le\tau_+<\beta$. We then carry out the integral over τ_{12} by taking a cutoff at short time scales beyond $\tau_{12}=\varepsilon/s\mathcal{J}$, where ε is a small positive number (the range of integration is taken to be $\varepsilon/s\mathcal{J}\le\tau_{12}<\beta-\varepsilon/s\mathcal{J}$). Assuming $\mathfrak{n}\equiv q/\tilde{q}\neq 3/2$, we find a term proportional to the Schwarzian action in terms of the cutoff ε

$$\tilde{I}_{\rm Sch}=\left[\left(\frac{b\mathfrak{n}(\mathfrak{n}-q)\varepsilon^{1-2\Delta}}{6q^2}\right)\frac{1}{s\mathcal{J}}-\left(\frac{\mathfrak{n}}{2\mathfrak{n}-3}\frac{(2b)^q\varepsilon^{3-2\mathfrak{n}}}{24q^2s^2}\right)\frac{1}{s\mathcal{J}}\right]\int_0^\beta d\tau_+\ \mathrm{Sch}(f(\tau_+),\tau_+)\ . \tag{4.28}$$

Here, we have kept only terms in the coefficient of the Schwarzian that are constant in β as these contribute to the linear-in-temperature specific heat when the Schwarzian is evaluated on shell.

The first term in the Schwarzian coefficient (4.28) stems from the kinetic term in $I_{\rm UV}$, while the second from the non-kinetic term in $I_{\rm UV}$. Notice that in the large q limit the cutoff dependence of the first term goes like ε whilst that of the second term goes like $\varepsilon^{3-2\mathfrak{n}}$. This suggests that for $\mathfrak{n}$ close to 1 both terms are important as we take the cutoff $\varepsilon\to 0$. For larger values of $\mathfrak{n}$, the second term dominates.[10] For the sake of concreteness, let us focus on the case $\mathfrak{n}=2$. Equation (4.28) becomes

$$\tilde{I}_{\rm Sch}=\left[\left(\frac{b(2-q)\varepsilon^{1-2\Delta}}{3q^2}\right)\frac{1}{s\mathcal{J}}-\left(\frac{(2b)^q}{12q^2s^2\varepsilon}\right)\frac{1}{s\mathcal{J}}\right]\int_0^\beta d\tau_+\ \mathrm{Sch}(f(\tau_+),\tau_+)\ . \tag{4.29}$$

[10] Since the coefficient of the Schwarzian governs the linear-in-temperature specific heat, this competition of factors could perhaps underlie the transition we see in the value of $\bar{\aleph}(s,\mathfrak{n})$ for small values of $\mathfrak{n}$ in figure 7.

The non-kinetic term goes like $1/\varepsilon$ and so provides the most significant correction to the conformal part of the action. The reparametrisation symmetry is broken by choosing the saddle of the Schwarzian which occurs when $\phi(\tau) = \tau$. Substituting this into (4.29) we find the linear-in-temperature contribution to the entropy to leading order in ε

$$\frac{S_{\text{Sch}}}{N} = \frac{(2b)^q}{6q^2 s^2 \varepsilon}\left(\frac{2\pi^2}{s\beta\mathcal{J}}\right) . \tag{4.30}$$

The takeaway message of this analysis is that due to the dominance of the second term (4.29) the correction to the conformal action comes from the strongly coupled phase of the theory rather than the weakly coupled UV regime which is customary for the undeformed SYK model. Holographically, for those deformed SYK models having both an intermediate and deep IR near-fixed point, we anticipate the emergence of the Schwarzian mode in the interior of an asymptotically AdS_2 spacetime flowing to a distinct infrared AdS_2 region.

4.3.2 Schwarzian for the intermediate IR

We now proceed to consider the conformal fixed point associated to H_q with a small perturbation near the fixed point. By taking $\Sigma \to \Sigma + \partial_\tau$ in (2.48) we can then write $I = I_{\text{CFT}} + I_{\text{pert}}$ where

$$I_{\text{CFT}} = -\frac{1}{2}\log\det(-\Sigma) + \frac{1}{2}\int_0^\beta\int_0^\beta d\tau_1 d\tau_2 \left(\Sigma G - \mathcal{J}^2\frac{2^{q-1}}{q^2}G^q\right) , \tag{4.31}$$

$$I_{\text{pert}} = \frac{1}{2}\int_0^\beta\int_0^\beta d\tau_1 d\tau_2 \left(\delta(\tau_1-\tau_2)\partial_{\tau_2}G - s^2\mathcal{J}^2\frac{2^{\tilde{q}-1}}{\tilde{q}^2}G^{\tilde{q}}\right) . \tag{4.32}$$

As in the previous section, we make an expansion of the saddle solution to I_{CFT} in powers of τ_{12}, written in terms of soft modes $f(\tau_+)$,

$$G_f(\tau_1,\tau_2) = \frac{1}{\mathcal{J}^{2\Delta}|\tau_{12}|^{2\Delta}}\left(1 + \frac{\Delta}{6}\tau_{12}^2\,\text{Sch}(f(\tau_+),\tau_+) + \mathcal{O}(\tau_{12}^3)\right) , \tag{4.33}$$

where now $\Delta = 1/q$. Substituting this into $I_{\text{pert.}}$, we change variables to (τ_{12},τ_+) and carry out the τ_{12} integral with a short time scale cutoff $\varepsilon/\mathcal{J}$. Keeping only terms constant in β (since these are the terms that contribute to the linear-in-temperature part of the entropy when the Schwarzian is

evaluated on shell). Again focusing on $\mathfrak{n} = 2$ for the sake of concreteness, we find

$$I_{\text{Sch}} = \left[\left(\frac{b(1-q)\varepsilon^{1-2\Delta}}{6q^2}\right)\frac{1}{\mathcal{J}}\right]\int_0^\beta d\tau_+ \,\text{Sch}(f(\tau_+),\tau_+) \,. \tag{4.34}$$

The coefficient of the Schwarzian is seen to come purely from the kinetic term in (4.32), mimicking the behaviour of the underformed SYK model with Hamiltonian H_q. Accordingly, the linear-in-temperature term in the entropy expansions (2.55) and (2.45) are found to be the same, and do not depend on s.

4.3.3 Relevant conformal perturbation theory

We would now like to test the hypothesis that the leading infrared correction away from conformality of the intermediate IR phase can be studied using conformal perturbation theory. The starting point [85,121] is to view the deformed SYK model near the intermediate fixed point as a conformal field theory perturbed by a series of relevant primary operators $O_h(\tau)$ of weight $h \in (0,1)$.[11] More explicitly,

$$I = I_{\text{CFT}} + \sum_{h\in\text{rel.}} g_h \int_0^\beta d\tau\, O_h(\tau) \,, \tag{4.35}$$

where h denotes the conformal weight of the given operator. We note here that the spectrum of conformal operators discussed in [31,37,85,108,121], does not contain any relevant operators with $h \in (0,1)$. They are in fact all irrelevant and are encoded in the operator product expansion of the fusion of two fermionic operators. Motivated by the structure of the Hamiltonian deformation (2.47), here we will focus instead on the following microscopic operator

$$O_h(\tau) \equiv \mathcal{N}_h\, i^{\frac{\tilde{q}}{2}} \sum_{1\le i_1<\cdots<i_{\tilde{q}}\le N} J_{i_1 i_2\cdots i_{\tilde{q}}}\psi_{i_1}\psi_{i_2}\cdots\psi_{i_{\tilde{q}}} \,. \tag{4.36}$$

This operator is to be understood in an averaged sense since it depends on the couplings $J_{i_1 i_2\cdots i_{\tilde{q}}}$ which are averaged over.[12] The operator $O_h(\tau)$ involves a product of $\tilde{q}$ fermions. In the undeformed model each fermion has scaling dimension $\Delta_\psi = 1/q$, so the naive estimate of the total weight of the

[11] Since in one dimension we can conformally map the line to the circle, we can employ conformal perturbation theory methods on the circle.

[12] This is somewhat in the spirit of [122]. It is interesting that in contrast to operators associated to large black holes, which are highly irrelevant, $O_h(\tau)$ is a complicated operator that is relevant. Perhaps, given its averaged nature, one can associate an entropy different from that of the horizon to its effect on the bulk spacetime.

operator (4.36) is $h = 1/\mathfrak{n}$ up to small corrections, which is within the relevant window $h \in (0,1)$. We fix the value of $\mathcal{N}_h$ implicitly by our choice of normalisation for the conformal two-point function averaged over the couplings

$$\langle O_h(\tau_1) O_h(\tau_2)\rangle_\beta = N\left(\frac{\pi}{\beta\mathcal{J}\sin\left(\frac{\pi\tau_{12}}{\beta}\right)}\right)^{2h} . \tag{4.37}$$

The action $I_{\rm CFT}$ in (4.35) governs the intermediate IR fixed point. According to conformal perturbation theory we find the following free energy

$$\beta F = \beta F_{\rm CFT} + g_h\int_0^\beta d\tau\langle O_h\rangle_\beta - \frac{g_h^2}{2}\int_0^\beta\int_0^\beta d\tau_1 d\tau_2\langle O_h(\tau_1) O_h(\tau_2)\rangle_\beta + \cdots . \tag{4.38}$$

Here O_h is the relevant operator (4.36), and again it is understood that we are averaging over the couplings. The one-point function of the O_h vanishes under the assumption of conformal invariance of the vacuum. Using the conformal form of the two-point function (4.37), the second order correction is given by [85, 103, 121]

$$-\frac{\beta\delta^2 F_h}{N} = \frac{\pi^{2h-\frac{1}{2}}\Gamma\left(\frac{1}{2}-h\right)}{2\Gamma(1-h)}\frac{g_h^2}{\mathcal{J}^2(\beta\mathcal{J})^{2h-2}} . \tag{4.39}$$

We will now provide evidence that the above correction indeed gives the leading correction to the intermediate CFT as we flow towards the IR. First, we consider the large q limit with $\mathfrak{n}=2$, where we have the analytical form of the correction. We then consider general $\mathfrak{n}$ in the large q limit and at finite q, where we compare to numerics.

Case I: $\mathfrak{n}=2$. The intermediate IR CFT free energy is known analytically [53] at large q with $q/\tilde{q}=2$. Concretely, in the regime $1 \ll \beta\mathcal{J} \ll 1/s^2$, the free energy of the deformed model can be written as

$$-\frac{\beta F}{N} = \left[\frac{1}{q^2}\beta\mathcal{J} + \left(S_0^{\rm free} - \frac{\pi^2}{4q^2}\right) + \frac{\pi^2}{2q^2}\frac{1}{\beta\mathcal{J}} + \cdots\right] + \left[\frac{2s^2}{q^2}\beta\mathcal{J}\log\left(\frac{2\beta\mathcal{J}}{\pi}\right) + \cdots\right] , \tag{4.40}$$

where the terms in the first square bracket are derivable from $I_{\rm CFT}$ given by (4.31) accompanied by the leading irrelevant operators [85, 121], and they grow with increasing temperature. The terms

in the second square bracket stem from the corrections due to relevant operators.

We will now argue that the leading relevant correction to the free energy arises from a relevant operator of weight $h = 1/2$. Given that expression (4.39) diverges when we take $h = 1/2$, we are led to a divergent contribution to the free energy which requires regularisation. As a simple regularisation scheme, we take $h = 1/2 - h_\varepsilon$ for some small number $h_\varepsilon > 0$, such that

$$-\frac{\beta\delta^2 F_{h=1/2-h_\varepsilon}}{N} = \frac{\Gamma(h_\varepsilon)^2 (g_{1/2}^2/\mathcal{J}^2)}{4\Gamma(2h_\varepsilon)} \beta\mathcal{J} \left(\frac{2\beta\mathcal{J}}{\pi}\right)^{2h_\varepsilon} . \tag{4.41}$$

Expanding in small h_ε gives

$$-\frac{\beta\delta^2 F_{h=1/2}}{N} = \frac{g_{1/2}^2}{2h_\varepsilon \mathcal{J}^2}\beta\mathcal{J} + \frac{g_{1/2}^2}{\mathcal{J}^2}\beta\mathcal{J}\log\left(\frac{2\beta\mathcal{J}}{\pi}\right) + \mathcal{O}(h_\varepsilon) . \tag{4.42}$$

Consequently, the divergent term only affects the zero point energy whose contribution to the free energy is independent of β. The remaining h_ε-independent terms agree with (4.40) provided we take

$$g_{1/2}^2 \to \frac{2s^2\mathcal{J}^2}{q^2} \quad \text{as} \quad q \to \infty . \tag{4.43}$$

This provides evidence that for $\mathfrak{n} = 2$, and in the large q limit, we can view O_h in (4.36) as a relevant conformal primary of conformal dimension $h = \tilde{q}/q = 1/2$. We now consider the case of general $\mathfrak{n}$.

Case II: General $\mathfrak{n}$. For general $\mathfrak{n}$ we do not have access to an analytic form of the free energy near the intermediate IR fixed point. Nonetheless, we can test the prediction from conformal perturbation theory against numerical results. To do so, we compute the entropy of the model numerically in the large q limit with $q = \mathfrak{n}\tilde{q}$ as described in section 4.2.1. Taking $h = 1/\mathfrak{n}$ in (4.39) and using the formula $S = (1 - \beta\partial_\beta)(-\beta F)$ we find that the correction to the entropy due to the relevant perturbation is given by

$$\frac{\delta^2 S_{h=1/\mathfrak{n}}}{N} = \left(1 - \left(2 - \frac{2}{\mathfrak{n}}\right)\right) \frac{\pi^{\frac{2}{\mathfrak{n}}-\frac{1}{2}}\Gamma\left(\frac{1}{2}-\frac{1}{\mathfrak{n}}\right)(g_{1/\mathfrak{n}}^2/\mathcal{J}^2)}{2\Gamma\left(1-\frac{1}{\mathfrak{n}}\right)} (\beta\mathcal{J})^{2-\frac{2}{\mathfrak{n}}} . \tag{4.44}$$

From this it follows that the entropy near the intermediate IR fixed point, as predicted by conformal

perturbation theory, can be expressed as

$$q^2\left(\frac{S}{N}-S_0^{\text{free}}\right)=\left[-\frac{\pi^2}{4}+\frac{\pi^2}{\beta\mathcal{J}}+\cdots\right]+\left[q^2\frac{\delta^2 S_{h=1/\mathfrak{n}}}{N}+\cdots\right]\ . \tag{4.45}$$

The terms in the first square bracket are derivable from I_{CFT} and the irrelevant operators whilst the terms in the second square bracket are proposed to come from the relevant deformation. In figure 14 we plot numerical results for the entropy in the intermediate IR phase against the analytic prediction (4.45), as well as the linear-in-temperature curve without the correction from the relevant perturbation. We show plots for $s^2=10^{-6}$ and $s^2=10^{-8}$, both with curves for $\mathfrak{n}=3,4,5,6$ and 10. Provided

$$g_{1/\mathfrak{n}}^2\to\frac{\mathfrak{n}^2 s^2\mathcal{J}^2}{2q^2}\quad\text{as}\quad q\to\infty\ , \tag{4.46}$$

there is strong agreement with the numerics.

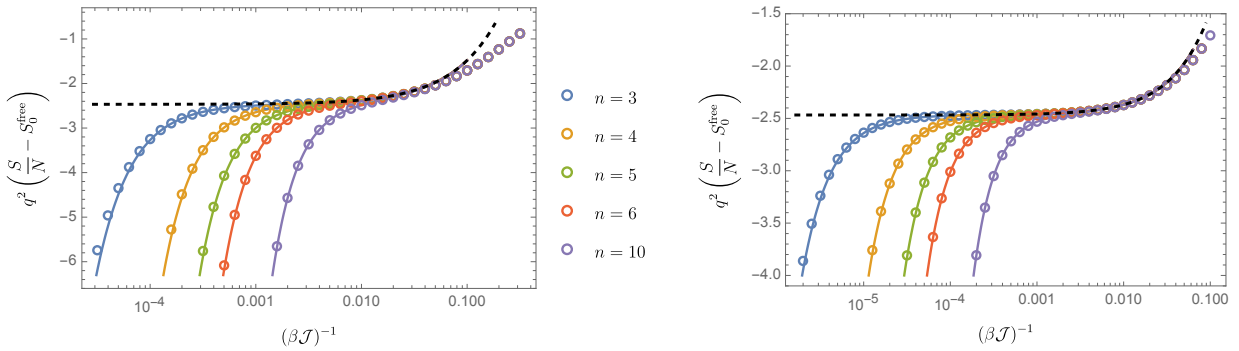

(a) $s^2=10^{-6}$ (b) $s^2=10^{-8}$

Fig. 14: Entropy as a function of temperature (in logarithmic scale) for the intermediate IR phase in the large N and q expansion. The circles give numerical results. The solid lines give the analytical prediction (4.45) with both the leading irrelevant and relevant corrections. The dashed line gives the analytical prediction (4.45) with only the leading irrelevant correction.

We can also study higher order corrections from conformal perturbation theory. By dimensional analysis the k^{th} order correction is found to be of the form

$$\frac{\delta^k S_{h=1/\mathfrak{n}}}{N}\propto s^k(\beta\mathcal{J})^{k-\frac{k}{\mathfrak{n}}},\qquad k\geq 2\ . \tag{4.47}$$

To find the sub-leading relevant correction we subtract the prediction (4.45), up to and including the leading relevant correction, from the numerically calculated entropy and perform a numerical fit.

For the values of $\mathfrak{n}$ we have tested we find the sub-leading relevant correction to be proportional to $s^4(\beta\mathcal{J})^{4-\frac{4}{\mathfrak{n}}}$. We also find evidence, as discussed below, that this is true even at finite q. The absence of a term proportional to $s^3(\beta\mathcal{J})^{3-\frac{3}{\mathfrak{n}}}$ leads us to believe that the conformal three-point function is sub-leading in the large N expansion, as is seen to be the case for the conformal three-point functions discussed in [123].

Finally, it is also interesting to note that we also find an intermediate IR regime for values of $\mathfrak{n}$ such that $1 < \mathfrak{n} < 2$, whose behaviour is in agreement with (4.45). In figure 15 we plot the intermediate IR regime for $\mathfrak{n} = 1.3$ and various values of s^2, again seeing excellent agreement with the prediction from conformal perturbation theory. From our analysis in section 4.2.1 we would also expect the zero temperature entropy of such flows to have a non-trivial s dependence, giving them an additional richness compared to the case $\mathfrak{n} \geq 2$.

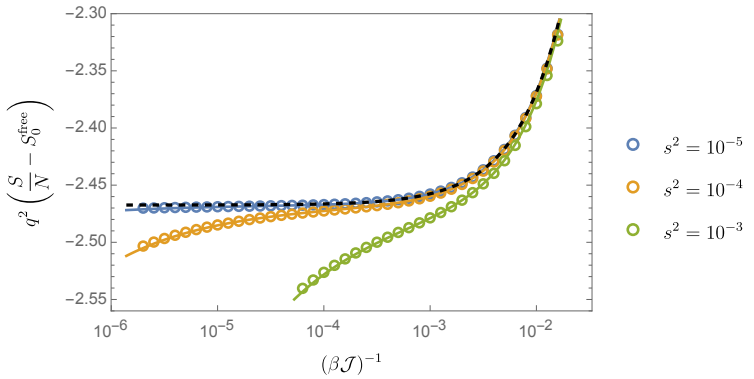

Fig. 15: Entropy as a function of temperature (in logarithmic scale) for $\mathfrak{n} = 1.3$ and $s^2 = 10^{-5}, 10^{-4}, 10^{-3}$ in the intermediate IR phase in the large N and q expansion. The circles give numerical results. The solid lines give the analytical prediction (4.45) with both the leading irrelevant and relevant corrections. The dashed line gives the analytical prediction (4.45) with only the leading irrelevant correction.

Case III: Finite q. We now test whether the perturbative correction (4.44) still applies at finite $q, \tilde{q}$ and large N. In this case, the predicted entropy near the intermediate IR fixed point is given by

$$\frac{S}{N} - S_0^{\text{free}} = \left[-\int_0^{1/q} dx\, \pi \left(\frac{1}{2} - x\right) \tan \pi x + \frac{4\pi^2 \alpha(q)}{\beta\mathcal{J}} + \cdots \right] + \left[\frac{\delta^2 S_{h=1/\mathfrak{n}}}{N} + \cdots \right] , \tag{4.48}$$

and the coupling constant of our conformal operator takes the form

$$g^2_{1/\mathfrak{n}} = \gamma(q,\tilde{q}) s^2 \mathcal{J}^2 \,, \tag{4.49}$$

where $\gamma(q,\tilde{q})$ is an unknown function which, from (4.46), we know tends to $1/(2\tilde{q}^2)$ in the large $\tilde{q}$ limit. The value of $\gamma(q,\tilde{q})$ can be found by fitting the prediction (4.48) to numerically determined values for the entropy in the intermediate IR phase. In figure 16 we plot numerical results against the prediction (4.48) and (4.49) with values for $\gamma(q,\tilde{q})$ shown in Table 1. We show plots with $s^2 = 10^{-4}$ and $s^2 = 10^{-3}$.

q	$\tilde{q}$	$\gamma(q,\tilde{q})$
4	2	0.098
6	2	0.111
8	2	0.116
8	4	0.028

Table 1: Numerical values for $\gamma(q,\tilde{q})$ in (4.49) found by fitting the prediction (4.48) to numerically determined values for the entropy in the intermediate IR phase.

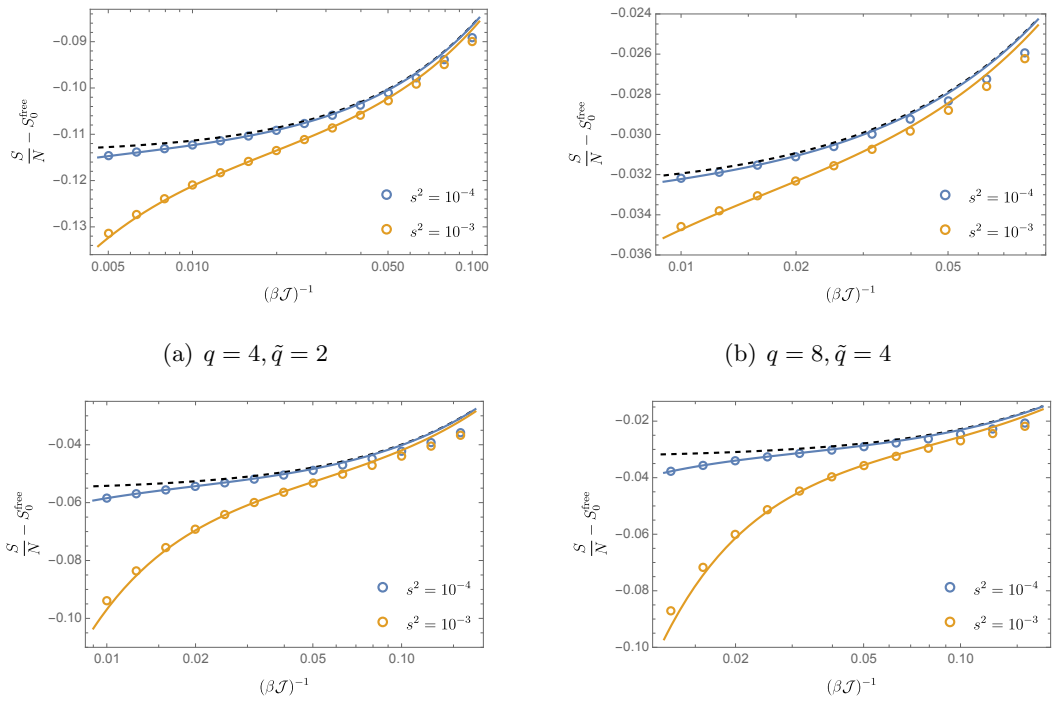

(a) $q = 4, \tilde{q} = 2$

(b) $q = 8, \tilde{q} = 4$

(c) $q = 6, \tilde{q} = 2$

(d) $q = 8, \tilde{q} = 2$

Fig. 16: Entropy as a function of temperature (in logarithmic scale) for the intermediate IR phase at finite q in the large N expansion. The circles give numerical results. The solid lines give the analytical prediction (4.48) and (4.49) with values for $\gamma(q, \tilde{q})$ shown in Table 1. The dashed line gives the analytical prediction (4.48) with only the leading irrelevant correction.

As for the large q limit, we can also find the sub-leading relevant correction by performing a numerical fit. In all cases considered, we again find that the sub-leading relevant correction is proportional to $s^4(\beta\mathcal{J})^{4-\frac{4}{\mathfrak{n}}}$.

4.4 Geometrisation of an RG flow

The goal of this section has been to explore RG flows at strong coupling, and in particular at finite temperature, for deformations of SYK models. We have identified a class of models permitting a robust treatment by means of both numerical and analytic methods. Given the holographic character of SYK models, our analysis opens up an interesting chapter in the story of holographic renormalisation [104,105], which has so far been explored mostly from the bulk perspective. We have identified models exhibiting RG flows between two near-fixed points and provided an interpretation in terms of conformal perturbation theory. The general character of the models is a sum of two

ordinary SYK Hamiltonians (2.47), but with differing numbers of interacting fermions. As for the ordinary SYK model, the flows we study preserve a rich thermodynamic structure and exhibit an extensive entropy all the way into the deep infrared/small temperature regime.

Our analysis is performed entirely from the perspective of the microphysical theory. From a holographic perspective, it is interesting to assess what features the putative holographic dual will exhibit. In the vicinity of each near-fixed point, it is natural to postulate that the bulk theory will mimic that of an ordinary SYK, whose thermodynamic features in the large N limit are captured by a JT gravity theory governed by the classical Euclidean action

$$S_E = -S_0 - \frac{1}{2\kappa}\int_{\mathcal{M}} d^2x\sqrt{g}\left(\phi R + U(\phi)\right) - \frac{1}{\kappa}\int_{\partial\mathcal{M}}\sqrt{h}\phi K \ , \tag{4.50}$$

with dilaton potential $U(\phi) = -2\alpha\phi$ with α real and positive. For $\alpha = -1$, one finds that the two-dimensional metric g_{ij} is Euclidean AdS_2 at the classical level. At finite temperature, $\mathcal{M}$ is taken to have a disk topology with S^1 boundary $\partial\mathcal{M}$, and we have the metric on the Poincaré disk. The thermodynamic properties of asymptotically AdS_2 geometries follow readily from the form of $U(\phi)$. The specific heat C_U and temperature, for instance, are given by [71, 124, 125]

$$C_U = \frac{2\pi}{\kappa}\frac{U(\phi_h)}{\partial_\phi U(\phi_h)} \ , \qquad \beta = \frac{4\pi}{|U(\phi_h)|} \ , \tag{4.51}$$

where ϕ_h is the value of the dilaton field ϕ at the Euclidean horizon. It follows that the near-fixed point exhibits a specific heat linear in the temperature.

For two near-fixed points, the ratio of the specific heats fixes the ratio, $\mathcal{R} \equiv \alpha_{\mathrm{UV}}/\alpha_{\mathrm{IR}}$, of the slopes for the two linear regimes of $U(\phi)$. For the models we have studied, we find $\mathcal{R} > 1$. This is in line with an increasing number of degrees of freedom as we go to higher temperatures and can be viewed as a consequence of unitarity and thermal equilibrium. At large enough temperatures, the geometry is a pure AdS_2 and there is boundary soft mode governed by the Schwarzian action. This is the bulk dual of the Schwarzian associated to the intermediate near-fixed point discussed in section 4.3.2. As we decrease the temperature, we flow to the interior of the geometry and an additional AdS_2 region emerges, corresponding to the near-fixed point in the deep infrared.

Continuity of the thermodynamic quantities along the RG flow, throughout which the theory remains in the strongly coupled phase, suggests that the geometric picture continues to hold between

the two near-fixed points. For this to occur, one can invoke [53] a more general dilaton potential $U(\phi)$, as studied for example in [71, 124–126] with linear behaviour at the two endpoints. The classical geometry will be asymptotically, but not isometrically, Euclidean AdS_2. The presence of a macroscopic entropy in the deep infrared/low temperature regime of the flow leads us to postulate that the dual geometry retains a horizon. In section 4.3 we argued that the RG flow is triggered by a relevant operator of weight $\Delta_{\text{rel}} = \tilde{q}/q < 1$. Thus, the bulk theory should have a corresponding field associated to the relevant operator. Moreover, associated to the near-fixed point in the deep infrared is the presence of a soft mode residing at the boundary of the near-AdS_2 geometry in the deep finite interior region, governed by the Schwarzian action. It is interesting that this soft mode resides entirely within the geometric description.[13] We depict this phenomenon in figure 17. The appearance of a worldline theory in the midst of a gravitating spacetime is a phenomenon worth pursuing in more detail.

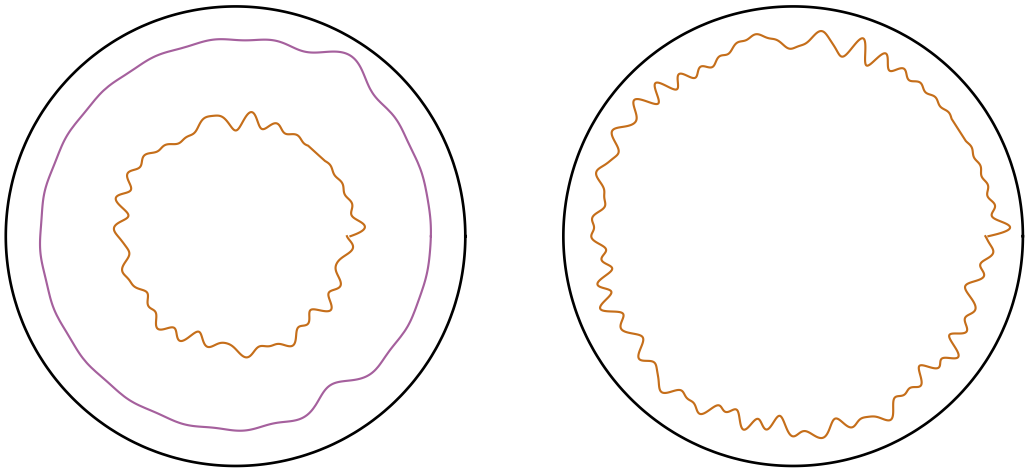

(a) $\beta\mathcal{J} \gtrsim (\beta\mathcal{J})_*$ (b) $\beta\mathcal{J} \lesssim (\beta\mathcal{J})_*$

Fig. 17: Pictorial representation of the two Schwarzian soft modes appearing inside Euclidean AdS_2. (a) For $\beta\mathcal{J}$ larger that some critical $(\beta\mathcal{J})_*$ there is a Schwarzian soft mode appearing in the deep interior of AdS_2. (b) For $1 \ll \beta\mathcal{J} \lesssim (\beta\mathcal{J})_*$, there is a Schwarzian soft mode residing closer to the AdS boundary. In the large q model with $\mathfrak{n} = 2$, $(\beta\mathcal{J})_* \sim s^{-2}$, with $s \ll 1$.

[13] A similar emergence of a soft mode in the interior of an interpolating geometry was also discussed for the centaur geometries studied in [72, 127, 128].

5 Multiple deformations and non-Hermitian models

5.1 Introduction

In this section we shall be interested in extending our discussion of SYK flows to a larger class of deformations given by concatenating multiple SYK Hamiltonians,

$$H_{\text{def}} = H_q + \sum_{i=1}^{k} s_i H_{\tilde{q}_i} \ , \tag{5.1}$$

where $q > \tilde{q}_1 > \tilde{q}_2 > \ldots > \tilde{q}_k$ and the coupling constants $s_i \in \mathbb{C}$ are tunable dimensionless parameters. The term $\sum_{i=1}^{k} s_i H_{\tilde{q}_i}$ can be viewed as a relevant deformation of the model H_q that induces an RG flow and modifies the thermodynamic behaviour of the model in the infrared.

While unitarity constrains $s \in \mathbb{R}$, we also extended our consideration to the more general case of $s \in \mathbb{C}$. This extension is rooted in the holographic interpretation of the deformed SYK models. Here, the IR thermodynamics are described by a dilaton gravity theory governed by the Euclidean action

$$I_E = -\frac{1}{2\kappa}\int_{\mathcal{M}} d^2x\sqrt{g}\left(\phi R + U(\phi)\right) - \frac{1}{\kappa}\int_{\partial\mathcal{M}} \sqrt{h}\phi K \ , \tag{5.2}$$

where $U(\phi)$ is the dilaton potential. By choosing an appropriate dilaton potential it is possible construct geometries that flow from an AdS_2 boundary to a dS_2 interior [53, 56, 127], providing the possibility for a holographic interpretation of (a portion of) the de Sitter static patch. Dilaton gravity theories with a dS interior entail a dilaton potential transitioning from a $+\phi$ dependence for large values of ϕ to a $-\phi$ dependence at small values of ϕ.

A no-go argument. In the SYK dual, this manifests as an entropy flow $S\left(\beta^{-1}\right)$, transitioning from a positive linear dependence on the temperature β^{-1}, to a negative linear one. For the thermal state, $\partial S/\partial(\beta^{-1}) = \beta^3(\Delta E)^2$, where $(\Delta E)^2$ signifies the energy variance in the ensemble. Consequently, a negative entropy slope proves unattainable for a Hermitian Hamiltonian.

We are thus left with two options: either working with a state other than the thermal one, or considering non-Hermitian physics. Non-Hermitian Hamiltonians defined by considering $s \in \mathbb{I}$ are able to yield negative entropy gradients in two scenarios:

- For a single deformation $H_{\text{def}} = H_q + sH_{\tilde{q}}$ in the large q limit, with $q/\tilde{q} = 2$, another regime of linear-in-temperature entropy is seen in the deep infrared ($\beta\mathcal{J} \gg 1/s^2$). Moreover, the gradient of the entropy in this regime scales as $1/s^2$. Naively, an imaginary s produces a negative linear-in-temperature entropy. This was suggested in [53].

- Perturbatively around the intermediate fixed point of H_q.

In this part of the thesis, we consider the latter case. In this case, considering the thermal state remains pertinent since we are perturbing near the intermediate conformal fixed point which we know to be described by unitary physics. Conformal perturbation theory reveals the role of imaginary s. In particular, the leading relevant correction to the entropy predicted by conformal perturbation theory is proportional to s^2. This results in imaginary values of s giving positive corrections to the entropy as we flow away from the fixed point, which can lead to a negative slope in $S(\beta^{-1})$.

5.2 Entropy flow from conformal perturbation theory

5.2.1 Large N for multiple deformations

Generalising the large N effective theory from a single deformation to multiple deformations is simple, and we now state the key formulae. In terms of G and Σ the large N action reads

$$I = -\frac{1}{2}\log\det\left(\delta(\tau_1-\tau_2)\partial_{\tau_2} - \Sigma\right) + \frac{1}{2}\int_0^\beta d\tau_1 d\tau_2 \left(\Sigma G - \mathcal{J}^2\left(\frac{2^{q-1}}{q^2}G^q + \sum_{i=1}^k s_i^2 \frac{2^{\tilde{q}_i-1}}{\tilde{q}_i^2}G^{\tilde{q}_i}\right)\right) , \tag{5.3}$$

from which we find the Schwinger-Dyson equations

$$\begin{cases} G = (\partial_\tau - \Sigma)^{-1} , \\ \Sigma = \mathcal{J}^2\left(\frac{2^{q-1}}{q}G^{q-1} + \sum_{i=1}^k s_i^2 \frac{2^{\tilde{q}_i-1}}{\tilde{q}_i}G^{\tilde{q}_i-1}\right) . \end{cases} \tag{5.4}$$

In the large q limit, the Schwinger-Dyson equations (5.4) become a single ordinary differential equation for $g(\tau)$, namely

$$\partial_\tau^2 g(\tau) = 2\mathcal{J}^2 e^{g(\tau)} + 2\mathcal{J}^2 \sum_{i=1}^k \mathfrak{n}_i s_i^2 e^{g(\tau)/\mathfrak{n}_i} , \tag{5.5}$$

where $\mathfrak{n}_i := q_i/\tilde{q}_i$ and the equation is has thermal boundary conditions, $g(0) = g(\beta) = 0$. The entropy can be computed from the large q action [52, 53]

$$\frac{S}{N} = S_0^{\text{free}} + \frac{\beta}{8q^2}\int_0^\beta d\tau \left[\frac{1}{2}\left(\partial_\tau g(\tau)\right)^2 - \mathcal{J}^2\left(\sum_{i=1}^k 2\mathfrak{n}_i^2 s_i^2 e^{g(\tau)/\mathfrak{n}_i} + 2e^{g(\tau)}\right)\right] , \tag{5.6}$$

where $S_0^{\text{free}} \equiv \log 2/2$.

5.2.2 Conformal perturbation theory: thermodyamics

We now generalise our discussion of relevant conformal perturbation theory in section 4.3.3 to flows with multiple and possibly non-Hermitian deformations. As before we describe the deformed SYK model near the intermediate fixed point by the action (4.35), where

$$I_{\text{CFT}} = -\frac{1}{2}\log\det(-\Sigma) + \frac{1}{2}\int_0^\beta\int_0^\beta d\tau_1 d\tau_2 \left(\Sigma G - \mathcal{J}^2\frac{2^{q-1}}{q^2}G^q\right) . \tag{5.7}$$

For multiple deformations we now have a relevant operator $O_{h_i}(\tau)$ of weight $h_i = 1/\mathfrak{n}_i$ for each Hamiltonian term $H_{\tilde{q}_i}$ in (5.1). Following the same steps as in section 4.3.3, we find that the leading relevant correction to the entropy due to the relevant perturbation is given by

$$\frac{\delta^2 S}{N} = \sum_{i=1}^k \left(\frac{2}{\mathfrak{n}_i} - 1\right)\frac{\pi^{\frac{2}{\mathfrak{n}_i}-\frac{1}{2}}\Gamma\left(\frac{1}{2}-\frac{1}{\mathfrak{n}_i}\right)}{2\Gamma\left(1-\frac{1}{\mathfrak{n}_i}\right)}\frac{g^2_{1/\mathfrak{n}_i}}{\mathcal{J}^2}\left(\beta\mathcal{J}\right)^{2-\frac{2}{\mathfrak{n}_i}} , \tag{5.8}$$

where $g^2_{1/\mathfrak{n}_i}$ is given by (4.46) at large q and (4.49) at finite q. The entropy of the model in the neighbourhood of the near-conformal fixed point is therefore well described by

$$\left.\frac{S}{N}\right|_{H_{\text{def}}} = \left.\frac{S}{N}\right|_{H_q} + \frac{\delta^2 S}{N} + \cdots , \tag{5.9}$$

where the dots signify further relevant corrections. We also recall that one can also expand the entropy of the undeformed SYK as [31, 40]

$$\left.\frac{S}{N}\right|_{H_q} = S_0^{\text{free}} - \int_0^{1/q} dx\, \pi\left(\frac{1}{2}-x\right)\tan\pi x + \frac{4\pi^2\alpha(q)}{\beta\mathcal{J}} + \cdots , \tag{5.10}$$

where $\alpha(q)$ is the coefficient of the Schwarzian action and must be computed numerically. The dots signify further irrelevant corrections that can also be found by conformal perturbation theory [37, 85, 121]. In figure 18 we compare the predictions of conformal perturbation theory with multiple deformations to numerics. Specifically, we deform the Hamiltonian H_8 by $(10^{-3/2})H_2$, $(10^{-1}i)H_4$ and $(10^{-3/2})H_2 + (10^{-1}i)H_4$ and plot the numerical computation of the entropy against the prediction (5.9) and (5.10).

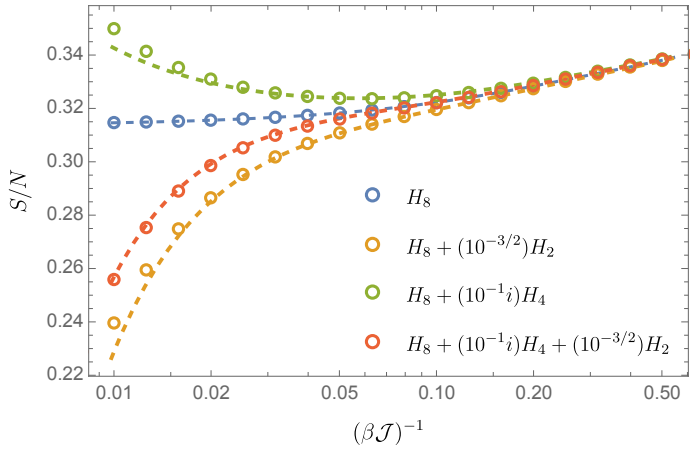

Fig. 18: Entropy as a function of temperature (in logarithmic scale) in the vicinity of the intermediate fixed point at finite q in the large N limit. The circles give numerical results from solving the Schwinger-Dyson equations (5.4). The dashed lines give the analytical prediction (5.9) with the leading relevant correction (5.8).

Note in particular that for the model $H_{\text{def}} = H_8 + (10^{-3/2}i)H_4$, the slope of the entropy turns from positive to negative as we decrease the temperature. Such a turning of the entropy slope is generally possible when allow imaginary couplings, $s_i \in \mathbb{I}$. To see this note that

$$\left(\frac{2}{\mathfrak{n}_i} - 1\right) \frac{\pi^{\frac{2}{\mathfrak{n}_i}-\frac{1}{2}} \Gamma\left(\frac{1}{2} - \frac{1}{\mathfrak{n}_i}\right)}{2\Gamma\left(1 - \frac{1}{\mathfrak{n}_i}\right) \mathcal{J}^2} < 0 \quad \text{for} \quad \mathfrak{n}_i > 1 \ , \tag{5.11}$$

and so the sign of each term in the correction (5.8) is determined by the sign of $g^2_{1/\mathfrak{n}_i}$. From (4.46) and (4.49) we see that $g^2_{1/\mathfrak{n}_i} > 0$ for $s_i \in \mathbb{R}$, but $g^2_{1/\mathfrak{n}_i} < 0$ for $s_i \in \mathbb{I}$. Thus imaginary values of s_i will give positive corrections to the entropy which in turn can lead to a negative slope in $S(\beta^{-1})$. We shall explore such models further in the following sections.

5.2.3 Conformal perturbation theory: two-point function

We can also use conformal perturbation theory to study relevant corrections to the two-point function near the intermediate fixed point. Using (4.35) the two-point function in this regime can be computed as

$$G(\tau) = \frac{1}{Z}\int [D\psi]\frac{\psi_i(\tau)\psi_i(0)}{N}e^{-I_{\text{CFT}}}e^{-\sum_{i=1}^{k} g_{h_i}\int_0^\beta d\tau' O_{h_i}(\tau')} . \tag{5.12}$$

Expanding the second exponential we find that the first two relevant corrections to the two-point function are given by

$$\begin{aligned} G(\tau) = G_{\text{CFT}}(\tau) \quad &- \quad \sum_{i=1}^{k} g_{h_i}\int_0^\beta d\tau \frac{\langle\psi_i(\tau)\psi_i(0)O_{h_i}(\tau)\rangle_\beta}{N} \\ &+ \quad \sum_{i=1}^{k}\frac{g_{h_i}^2}{2}\int_0^\beta d\tau_3 d\tau_4 \frac{\langle\psi_i(\tau)\psi_i(0)O_{h_i}(\tau_3)O_{h_i}(\tau_4)\rangle_\beta}{N}, \end{aligned} \tag{5.13}$$

where the three-point and four-point functions in the above expression are conformal. We will now focus on the case were we deform by a single SYK; that is $H_{\text{def}} = H_q + sH_{\tilde{q}}$, where $\tilde{q} < q$ and $s \in \mathbb{C}$. Recall that at the intermediate conformal fixed point the fermions have scaling dimension $\Delta_\psi = 1/q$ and the relevant operator O_h has scaling dimension $h = 1/\mathfrak{n}$. Using this and the general form of conformal three and four-point functions, without computing the integrals we can observe that the first and second order corrections to $G(\tau)$ have the form

$$\delta^1 G \propto g_h \frac{1}{(\beta\mathcal{J})^{h+\frac{2}{q}-1}} f_1(\tau/\beta), \tag{5.14}$$

$$\delta^2 G \propto g_h^2 \frac{1}{(\beta\mathcal{J})^{2h+\frac{2}{q}-2}} f_2(\tau/\beta) , \tag{5.15}$$

where f_1, f_2 are functions of τ/β whose exact form we will not need. We can test the β dependence of these corrections in the following way. We first numerically compute the two-point function for both the undeformed and deformed SYK models at $\tau = k\beta$ for some fixed constant $k \in (0,1)$. We do this over a range of temperatures near the intermediate fixed point. We then compare the difference between the two and check that it is consistent with the corrections. Numerics show that the leading non-vanishing correction to $G(\tau)$ near the intermediate fixed point takes the form (5.15) and hence we conclude that the three-point function is subleading. Moreover recall that $g_h^2 \propto s^2$

and so the leading correction to the two-point function is proportional to s^2. This means that the correction will have opposite signs depending on whether s is taken to be purely real, or purely imaginary. By looking at numerics we find that

$$\begin{cases} G(\tau) & \leq G_{\text{single}}(\tau) \quad \text{for} \quad s \in \mathbb{R} \,, \\ G(\tau) & \geq G_{\text{single}}(\tau) \quad \text{for} \quad s \in \mathbb{I} \,, \end{cases} \tag{5.16}$$

where $G_{\text{single}}(\tau)$ denotes the two-point function for the undeformed SYK. As an example, in figure 19 we show log-log plots for the difference between the two-point functions for $H_{\text{single}} = H_6$ and $H_{\text{def}} = H_6 + sH_2$, across a range of temperatures in the vicinity of the intermediate fixed point at fixed time $\tau = \beta/2$. Plots are shown for $s = 10^{-3/2}$ and $s = 10^{-3/2}i$. In agreement with (5.15) (and the fact that (5.14) vanishes) we find for both plots a straight line with slope $2h + 2/q - 2$. Figure 20 compares the full two-point functions at fixed temperature $(\beta\mathcal{J})^{-1} = 0.01$. All figures also show agreement with (5.16). Numerics were also performed for other values for the parameters $(q, \tilde{q}, s, \tau)$, and all cases checked are consistent with these conclusions.

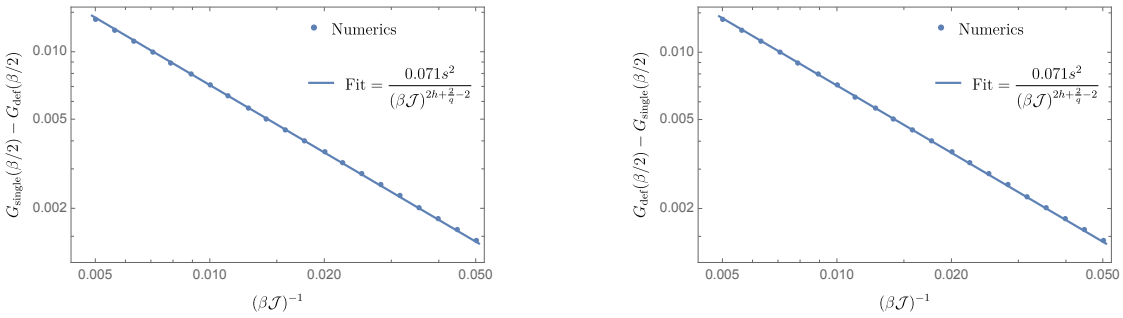

(a) $H_{\text{def}} = H_6 + 10^{-3/2}H_2$ (b) $H_{\text{def}} = H_6 + (10^{-3/2}i)H_2$

Fig. 19: The difference between the two-point function of the undeformed SYK model H_6 and deformed SYK $H_6 + sH_2$ at fixed time $\tau = \beta/2$ and over a range of temperatures near the intermediate fixed point. For plot (a) $s = 10^{-3/2}$ whilst for plot (b) $s = 10^{-3/2}i$.

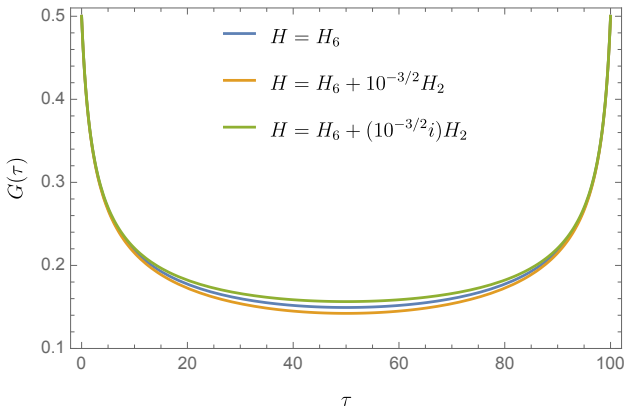

Fig. 20: The two-point functions at finite temperature, with $\beta\mathcal{J} = 100$, for the undeformed SYK model H_6 (blue line) and deformed models $H_6 + 10^{-3/2} H_2$ (orange line) and $H_6 + (10^{-3/2} i) H_2$ (green line).

5.3 Entropy flows at finite N

So far the entropy flows have only been shown to leading order in the large N limit of the theory. We would like to also see evidence for them at finite N. At finite N the SYK model is solvable by exact diagonalisation procedures for values of N up to $N \sim 34$. Thermodynamics results at large N should be comparable to finite N calculations for $N \gg \beta\mathcal{J}$. Since even the intermediate fixed point in the large N limit occurs at temperatures for which $\beta\mathcal{J} \gg 1$ direct comparisons of the entropy flows to finite N results would require values of N far beyond current numerical capabilities. However, it was shown in [41] that, for the undeformed SYK, the regime of linear-in-temperature entropy characterising the (single) near fixed point can be matched to an extrapolation of finite N results with $N \leq 32$. We carry out a similar extrapolation, detailed below, for our deformed models with a single deformation. We find that not only are we able to access the linear-in-temperature regime of the intermediate fixed point, but we are also able to match the leading relevant correction away from the fixed point. Thus we find finite N evidence of the flow from the intermediate IR fixed point towards the deep IR fixed point found in the large N limit. As done for the undeformed SYK model in [41], at finite N, we compute the entropy numerically by exact diagonalisation of the Hamiltonian. For more details on the specrta of such models see appendix E. We then compute the average entropy for each N by averaging over a number of realisations of the couplings. Finally, we extrapolate to infinite N by fitting to a polynomial in $1/N$ up to $\mathcal{O}(N^{-2})$ and taking the constant term as the result. In figure 21 we compare extrapolations from finite N with large N numerics from solving the Schwinger Dyson equations (5.4) for the models

$H = H_4$, $H = H_4 + 0.1\,H_2$ and $H = H_4 + 0.1i\,H_2$. The extrapolations show excellent agreement with the large N solution for $\beta\mathcal{J} > 10^{-1}$. For temperatures below this the extrapolations start to deviate significantly. There are likely multiple sources contributing to this error. Firstly at low temperatures, handling both small and large numbers poses numerical precision challenges in computing the entropy. Secondly, the extrapolations are up to $N = 30$; it is likely that larger N is necessary to improve accuracy at smaller temperatures. Related to this, with relatively few values of N used, the extrapolations are fit to curves up to $\mathcal{O}(N^{-2})$, neglecting higher-order terms to prevent overfitting. However, it's possible that including such terms may be necessary at lower temperatures for accurate extrapolation. Finally, more averaging may be needed to improve the accuracy of the extrapolations. Nonetheless, in both cases the extrapolations capture the leading relevant correction away from the near-conformal fixed point of the undeformed SYK, H_4, providing finite N evidence of the flow away from the intermediate fixed point.

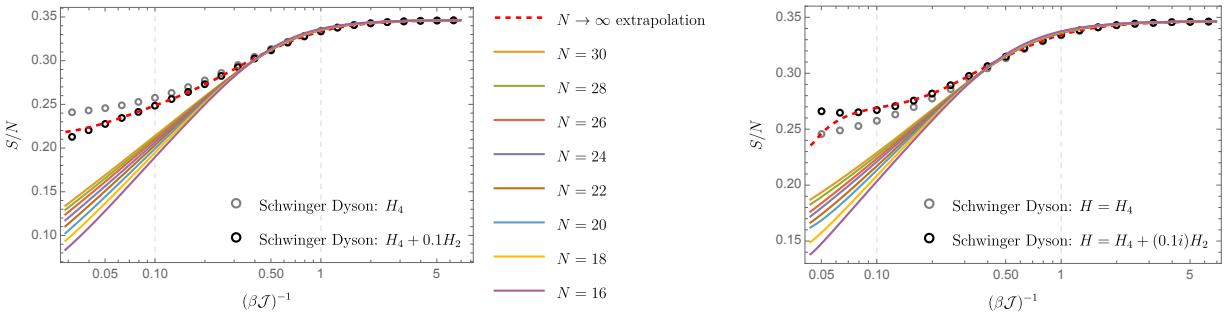

(a) $H_{\text{def}} = H_4 + 0.1H_2$ (b) $H_{\text{def}} = H_4 + (0.1i)H_2$

Fig. 21: Extrapolations of the averaged entropy S/N from finite N curves. In each case even values of N from $N = 16$ to $N = 30$ were used with $2^{20-(N/2)}$ realisations averaged over. Extrapolations (red dashed lines) are compared to large N numerics from solving Schwinger Dyson equations (circles).

5.4 A model with linear-in-temperature entropy and negative slope

Working in the large N and large q limits, we now present a model of the type (5.1), whose entropy as a function of temperature exhibits a region of negative slope that is approximately linear. Such a model is achieved by tuning the model parameters $(\mathfrak{n}_i, s_i)$ using conformal perturbation theory as a guide. In particular we know that the correction to the flow away from the near-conformal fixed point of H_q at large q is described by (5.8) and (4.46). Using linear regression we fit regressors belonging to set of functions $\{(\beta\mathcal{J})^{2-\frac{2}{\mathfrak{n}}} : \mathfrak{n} \in \mathbb{Z}, \mathfrak{n} > 1\}$ to a straight line with negative slope. Once

an appropriate fit is found we can read off the parameters s_i from the regression coefficients which, along with the $\mathfrak{n}_i$ of the chosen regressors, describe a model that gives rise to such a correction term. We can then compute the entropy for such a model by numerically solving the equation (5.5) and plugging this into (5.6). In figure 22 we plot numerics for the entropy as a function of temperature for such a model around the near-conformal fixed point, along with the prediction from conformal perturbation theory. In table 2 we state the parameters used.

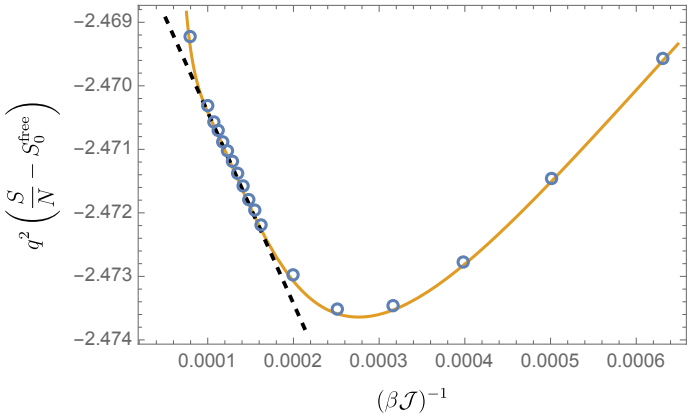

Fig. 22: Entropy as a function of temperature in the vicinity of the intermediate fixed point for the large q deformed SYK with model parameters given in table 2. Circles give numerics from solving the large q Schwinger-Dyson equation (5.5) whilst the orange line shows the prediction from conformal perturbation theory (5.9). The black dashed line shows the function used to fit the regressors and hence define the model. Such a model is seen to have a region of approximately linear-in-temperature entropy with negative slope.

i	$\mathfrak{n}_i$	s_i^2
1	20/7	3.36385×10^{-7}
2	4	2.4819×10^{-7}
3	5	9.76218×10^{-8}
4	20/3	-3.44481×10^{-8}
5	10	-4.53241×10^{-8}
6	20	8.36213×10^{-9}
7	200	-1.70624×10^{-11}

Table 2: Model parameters for the large q deformed SYK model whose entropy is shown in figure 22.

5.5 Holographic spacetimes

5.5.1 Thermodynamic considerations

We first briefly review how to construct the bulk holographic spacetime of the deformed SYK models from their thermodynamics. We recall from section 2.5 that in general the gravitational part of the bulk theory is described by a dilaton gravity theory with Euclidean action

$$S_E = -\frac{1}{2\kappa}\int_{\mathcal{M}} d^2x\sqrt{g}\left(\phi R + U(\phi)\right) - \frac{1}{\kappa}\int_{\partial\mathcal{M}}\sqrt{h}\phi K \ , \tag{5.17}$$

where $\mathcal{M}$ is taken to be a disk topology with boundary $\partial\mathcal{M} = S^1$. A purely topological term can also always be added to the theory which sets the zero temperature entropy of the theory. This theory permits general black hole solutions of the form

$$ds^2 = f(r)dt^2 + \frac{dr^2}{f(r)}, \quad f(r) = \frac{1}{\tilde{\phi}}\int_{r_h}^{r} dr' U(\phi(r')) \ , \quad \phi(r) = \tilde{\phi} r \ , \tag{5.18}$$

where r_h is the position of the horizon. The low energy sector of the undeformed SYK model is thought to correspond to JT gravity, where the dilation potential has the form $U(\phi) = 2\phi$ and the corresponding metric for the theory is that of AdS_2. The duality manifests itself in the IR limit of SYK model, where the physics is described by the same Schwarzian action that governs the theory of the JT gravity. At the level of the thermodynamics this corresponds to both theories having a linear-in-temperature entropy with positive slope.

By adding a relevant deformation to the SYK model of the form (5.1) we expect to deform the interior of the bulk AdS_2 geometry [53]. To understand how the bulk interior gets deformed it is useful to note that the dilaton potential can be obtained directly from the thermodynamics of the dilaton theory. In particular, from (2.76), we have that

$$T = \frac{\left|U\left(\frac{\kappa}{2\pi}(S - S_0)\right)\right|}{4\pi\tilde{\phi}}, \tag{5.19}$$

where T is the temperature of the theory, S is the entropy and S_0 is the zero temperature entropy. Thus, if we have access to $S(T)$ for our deformed SYK model, we can invert this function to find the dilaton potential for the holographic bulk. In particular, a deformed SYK model where $S(T)$ has a regime with a negative linear slope, the corresponding dilaton potential will contain a portion

of a negative linear slope. The deformed SYK model described in section 5.4 is proposed to be describe such a situation.

5.5.2 Two-point correlation functions: heavy fields

We would now like to explore the correspondence between the deformed SYK models and their proposed dual dilaton-gravity theories beyond the level of thermodynamics. To do so we shall first borrow our intuition from the worldline formalism where one can compute the two-point function of a free massive scalar as a path integral

$$G(X,Y) = \int d\mathcal{P} e^{-mL[\mathcal{P}]} \approx \sum_{g \in \text{geodesics}} e^{-mL_g} \ , \tag{5.20}$$

where $\mathcal{P}$ denotes a path between the points X and Y and $L[\mathcal{P}]$ the length of the path. The final approximation assumes the mass is large allowing us to take a saddle point approximation, reducing the integral to a sum over geodesic between X and Y. In the case of spacetimes that are asymptotically AdS, the two-point function between points on the spacetime boundary can be related to the two-point function of operators in the holographic dual.

To check this statement holds in our case, we would like to first evaluate how the lengths of geodesics anchored at the boundary of AdS_2 are affected by a small deformation of the dilaton potential. Consider,

$$U(\phi) = 2\phi + \delta U(\phi) \ , \tag{5.21}$$

where $\delta U(\phi)$ is a smooth function of ϕ. In our comparison we would like to keep the temperature of the deformed and undeformed geometries fixed. From (2.76), we see that to keep the temperature fixed after deforming the dilaton potential we must shift the position of the horizon. In particular, the shifted horizon r_h' can be expressed in terms of the original horizon r_h as

$$|2\tilde{\phi} r_h' + \delta U(\tilde{\phi} r_h')| = |2\tilde{\phi} r_h| \ . \tag{5.22}$$

For our argument we will avoid this subtlety by setting $\delta U(\tilde{\phi} r_h') = 0$, so that $r_h' = r_h$. We can do this for example by taking $\delta U(\phi)$ to have compact support in some region $[r_1^*, r_2^*]$ for $r_2^* > r_1^* > \tilde{\phi} r_h$.

The blackening factor resulting from such a dilaton potential is given by

$$f(r) = r^2 - r_h^2 + g(r) \ , \qquad g(r) = \frac{1}{\tilde{\phi}} \int_{r_h}^{r} dr' \, \delta U(\tilde{\phi} r') \ , \tag{5.23}$$

where we note that this is consistent with the horizon being at $r = r_h$, since $g(r_h) = 0$. As a further simplification, we focus on geodesics which correspond to straight lines through the centre of the deformed Poincaré disc, connecting opposite sides of the thermal circle, see figure 23. We provide further details on how to compute the geodesics in appendix F.

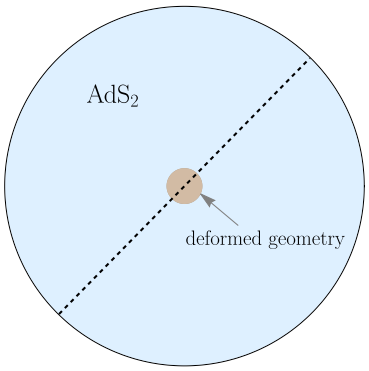

Fig. 23: The brown shaded region depicts the deformed region of the geometry that is supported on $r_1^* \leq r \leq r_2^*$. The blue shaded region depicts the pure AdS$_2$ geometry for $r_2^* \leq r \leq R_b$. The dashed line depicts the geodesic under consideration.

The length of such a geodesic is given by

$$L = \int ds = 2 \int_{r_h}^{R_b} \frac{1}{\sqrt{r^2 - r_h^2 + g(r)}} \, dr \ , \tag{5.24}$$

where we regularise the length by anchoring the geodesic to a boundary circle of finite radius R_b. We will consider two cases corresponding to $\delta U(\phi) \leq 0$ and $\delta U(\phi) \geq 0$. The case where $\delta U(\phi) \leq 0$ corresponds to a bending downward of the dilaton potential as we reduce ϕ past r_2^*, thus mimicking a deformed SYK with real s in the vicinity of the intermediate fixed point. The case where $\delta U(\phi) \geq 0$ corresponds to a bending upward of the dilaton potential and thus mimics the deformed SYK with imaginary s near the intermediate fixed point. Note that beyond the aforementioned constraints, the exact form of the dilaton potential does not matter for our argument, and in particular we can choose it to match the thermodynamics of the corresponding SYK model we are trying to describe. What is important for us to note is that in the case that $\delta U(\phi) \leq 0$ we have that $g(r) \leq 0$ for all r

and similarly in the case $\delta U(\phi) \geq 0$ we have that $g(r) \geq 0$ for all r. From (5.24) we see that this means that

$$\begin{cases} L \geq L_{\text{AdS}_2} & \text{for} \quad \delta U(\phi) \leq 0 \ , \\ L \leq L_{\text{AdS}_2} & \text{for} \quad \delta U(\phi) \geq 0 \ , \end{cases} \tag{5.25}$$

where L_{AdS_2} corresponds to the case $g = 0$. To relate this result to the SYK model we use (5.20). From this we would expect the two-point function of the deformed SYK to obey the following inequalities

$$\begin{cases} G(\beta/2) \sim e^{-mL} \leq e^{-mL_{\text{AdS}_2}} \sim G_{\text{single}}(\beta/2); \ s \in \mathbb{R} \ , \\ G(\beta/2) \sim e^{-mL} \geq e^{-mL_{\text{AdS}_2}} \sim G_{\text{single}}(\beta/2); \ s \in \mathbb{I} \ , \end{cases} \tag{5.26}$$

which is consistent with (5.16).

5.5.3 Two-point correlation functions: light fields

We can also check whether our expectation from (5.16) is consistent with what we find for the bulk two-point functions of light fields. In [53], it is shown that for a two-dimensional metric in Euclidean signature of the form

$$ds^2 = e^{2\gamma(z)}(d\tau^2 + dz^2) \ , \tag{5.27}$$

the boundary two-point function for light fields in frequency space can be written as a perturbative expansion in the mass of the field, taking the form

$$G(\omega) = -\left(|\omega| + m^2 \int_{z_c}^{\infty} dy \ e^{2\gamma(y)} e^{-2|\omega|(y-z_c)} + \cdots\right) \ . \tag{5.28}$$

For thermal spacetimes the only modification to this formula is that ω should take discrete values. It is easy to apply (5.28) to both the AdS_2 black hole and for the deformed geometry (5.23) by re-writing these metrics in the conformal frame. One can then show that we have the following inequality valid for $\delta U(\phi) \geq 0$

$$|G(\omega_n)| \geq |G_{\text{AdS}_2}(\omega_n)| \ , \tag{5.29}$$

where in (5.29) G is the boundary two-point function for the deformed AdS_2 geometry and G_{AdS_2} is that of pure AdS_2 space. Applying Parseval's identity to this we find

$$\begin{aligned} &\delta U(\phi) \geq 0 \Rightarrow \sum_{n\in\mathbb{Z}} |G(\omega_n)|^2 \geq \sum_{n\in\mathbb{Z}} |G_{\mathrm{AdS}_2}(\omega_n)|^2 \\ &\Rightarrow \int_0^\beta d\tau\ |G(\tau)|^2 \geq \int_0^\beta d\tau\ |G_{\mathrm{AdS}_2}(\tau)|^2\ . \end{aligned} \tag{5.30}$$

We can also make an analogous argument to conclude

$$\delta U(\phi) \leq 0 \Rightarrow \int_0^\beta d\tau\ |G(\tau)|^2 \leq \int_0^\beta d\tau\ |G_{\mathrm{AdS}_2}(\tau)|^2\ . \tag{5.31}$$

This is again consistent with our expectations from the boundary theory. More details of the computation can be found in appendix G.

6 Krylov complexity and chaos in deformed SYK models

6.1 Introduction

In this section we will explore the relation between the Lyapunov exponent λ_L and the Krylov exponent λ_K in the SYK model and its deformations. In most cases, the SYK model develops a chaotic behaviour in its strongly-coupled phase, but it can nevertheless be solved in different limits using different numerical and analytical techniques at any temperature. In fact, the SYK model is maximally chaotic at low temperatures in the sense of (1.5). The Lyapunov exponent [31, 129], the spectral form factor [41] and operator size distribution [43] were among the first ideas explored regarding the chaotic nature of the SYK model.

We will focus on the large N limit of the SYK model and its deformations, where the model is dominated by a saddle-point approximation of its partition function. When one further takes the large q limit, it has been shown that the Krylov exponent satisfies $\lambda_L = \lambda_K$, both at infinite and finite temperature [26]. Thus the lower bound on λ_K in eq. (1.5) is saturated, fuelling the hope that Krylov complexity provides a computational advantage to diagnose chaos in quantum systems. We will see in this section however that this is only the case when the SYK model is not deformed. As a first step, we extend the previous result to the next order in the large q expansion, as well as to finite q and conclude that the tight upper bound on the Lyapunov exponent remains robust in these models at all temperatures. When $q = 2$, the interaction term in the Hamiltonian becomes a random mass term, which is known to be integrable. In this case, we show that the Lanczos coefficients saturate both at finite and infinite temperature, which gives $\lambda_K = 0$.

We then turn our attention to deformed SYK models of the form (2.47) [46–55]. These deformed models can have non-trivial behaviour in the infrared, including the possibility of transitions between different regions of near-maximal chaos or transitions between near-maximally chaotic and integrable behaviour. In both cases, both the Lyapunov and the Krylov exponent can be computed and compared. We find strong evidence analysing different kinds of deformed SYK models, both analytically and numerically, that while the Lyapunov exponent can have non-monotonic behaviour as a function of the inverse temperature, the Krylov exponent can only behave monotonically. So, for instance, if an initially chaotic system becomes integrable (or the Lyapunov exponent becomes very small) at large inverse temperatures, λ_K will not provide a good diagnostic of this transition.

In fact, in some of the models we studied, the Lyapunov exponent decays to zero at large inverse temperatures, while the Krylov exponent saturates to its maximal value. We conjecture that, when it is well-defined, the monotonicity of the Krylov exponent may be a generic feature of unitary quantum systems.

6.2 Computation of Krylov exponent

6.2.1 Krylov exponent from moments

In what follows, we will compute λ_K, in different quantum systems where λ_L can also be computed, to gain insight into how tight is the bound, especially in systems where the behaviour of λ_L is not necessarily monotonic, and could even go to zero. For a brief review of quantum chaos and Krylov complexity and the definitions we use for $\lambda_{L,K}$, we refer the reader back to sections 2.1 and 2.2 respectively. We now describe two methods to compute λ_K, one based on the explicit calculation of the Lanczos coefficients and the other based on analytic properties of the Wightman two-point function.

Performing the algorithm (2.15) can be numerically challenging. Instead, if we know the Wightman autocorrelation function, $C(t)$, defined by

$$C(t) = (\mathcal{O}(t)|\mathcal{O}(0))^W_\beta \ , \tag{6.1}$$

the Lanczos coefficients can be computed using a recursive algorithm [130]. The first step is to analytically continue to imaginary time and perform a Taylor expansion to find the moments, μ_{2n},

$$C(-i\tau) = \sum_{n=0}^{\infty} \mu_{2n} \frac{\tau^{2n}}{(2n)!} \ , \tag{6.2}$$

where the odd coefficients vanish since we have assumed that $\mathcal{O}$ is Hermitian. The moments are therefore related to expectation values of powers of the Liouvillian $\mu_{2n} := (\mathcal{O}|\mathcal{L}^{2n}|\mathcal{O}) = \frac{d^{2n}}{d\tau^{2n}} C(-i\tau)|_{\tau=0}$ and so products of the Lanczos coefficients are given by determinants of minors of the Hankel matrix of moments: $b_1^{2n}....b_n^2 = \det(\mu_{i+j})_{0\leq i,j\leq n}$.[14] Therefore, after obtaining the

[14] In this expression we fixed a small typo in equation (A4) of [26], see *e.g.,* (2.10) of [68].

moments the following recursive algorithm can be used to obtain the Lanczos coefficients, b_n:

$$\begin{cases} \text{Goal}: \quad b_n = \sqrt{M_{2n}^{(n)}} \ , \\ \text{Recursive step}: \quad M_{2k}^{(n)} = \frac{M_{2k}^{(n-1)}}{b_{n-1}^2} - \frac{M_{2k-2}^{(n-2)}}{b_{n-2}^2} \ , \\ \text{Stopping conditions}: \quad M_{2k}^{0} = \mu_{2k} \ , \ M_{2k}^{(-1)} = 0 \ , \ b_{-1} = b_0 = 1 \ . \end{cases} \tag{6.3}$$

Once sufficiently many Lanczos coefficients are obtained in this way, the Krylov exponent, λ_K can be found by computing the slope of the coefficients, see however footnote 3.

In what follows we will study the Krylov complexity for the SYK model and its deformations with respect to a single fermion operator $\mathcal{O} = \sqrt{2}\psi_1$. In the large N, limit the autocorrelation function $\langle \psi_i(\tau)\psi_i(0)\rangle$ is independent of i [83] and therefore

$$C(-i\tau) = 2G(\tau + \beta/2) \ , \tag{6.4}$$

where $G(\tau) \equiv G(\tau, 0)$ was defined in (2.26). The moments used as a starting point for the algorithm (6.3) are computed as follows

$$\mu_{2n} = \frac{d^{2n}}{d\tau^{2n}} \left(2G(\tau + \beta/2)\right)|_{\tau=0} \ . \tag{6.5}$$

6.2.2 Krylov exponent from pole of autocorrelation function

If the Lanczos coefficients b_n have a linear asymptotic growth of the form (2.19), then the asymptotic slope α can be extracted from the location of the first pole of the autocorrelation function in Euclidean time [26, 61, 79, 131]. This can be seen by relating the moments μ_{2n} to the Lanczos coefficients b_n. Assuming (2.19) the moments have the following asymptotic form [26],

$$\mu_{2n} = \left(\frac{4n\alpha}{e\pi}\right)^{2n} e^{o(n)} \ . \tag{6.6}$$

Using (6.6), one can then apply the root test to (6.2) to see that the radius of convergence and hence the location of the first pole, which we denote by τ_*, is given by

$$\tau_* = \frac{\pi}{2\alpha} \ . \tag{6.7}$$

From this one can compute the Krylov exponent using the relation

$$\lambda_K = \frac{\pi}{\tau_*} \,. \tag{6.8}$$

For the SYK and its deformations, from (6.4) we see that τ_* is the first pole of $G(\tau + \beta/2)$.

6.3 Krylov complexity of a single SYK model

6.3.1 The integrable $q = 2$ model

Consider the single SYK Hamiltonian (2.24). When $q = 2$, the interaction term becomes just a random mass term for the fermions, and the model is known to be integrable. We thus expect the Lanczos coefficients to grow sub-linearly with n, for large enough n. At infinite temperature, this was already demonstrated in [26]. Here we consider the theory at finite inverse temperature β. For $q = 2$, the thermal two-point function is known analytically [31],

$$G(\tau) = \int_0^\pi \frac{\mathrm{d}\theta}{\pi} \cos^2\theta \frac{\cosh[(\frac{\tau}{\beta} - \frac{1}{2})2\beta\mathcal{J}\sin\theta]}{\cosh(\beta\mathcal{J}\sin\theta)} \,. \tag{6.9}$$

We can use the two methods described in sections 6.2.1 and 6.2.2 to compute the Krylov exponent. Using the first method, we computed the first ~ 25 Lanczos coefficients, for a range of different temperatures. The results are shown in figure 24. We see that $b_n/\mathcal{J}$ initially grows with n but then reaches a plateau around the value of 1. As we increase $\beta\mathcal{J}$ the value of n at which the plateau is reached increases approximately linearly with $\beta\mathcal{J}$, as can be seen from figure 25.

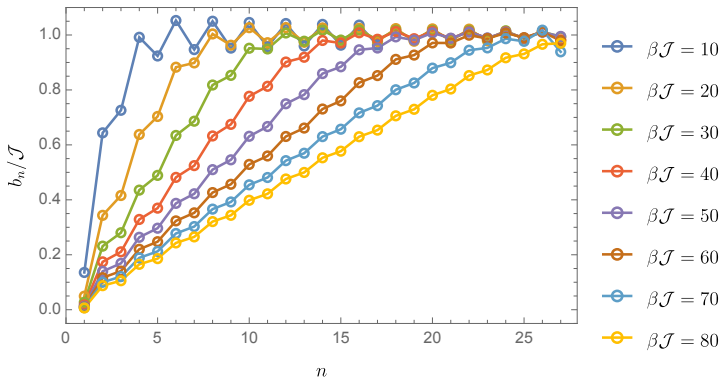

Fig. 24: Lanczos coefficients b_n for the single SYK with $q = 2$ for different values of $\beta\mathcal{J}$.

This means that at sufficiently low temperatures, the number of Lanczos coefficients required to see the saturation can go beyond computational control. One might be fooled to think that the system becomes chaotic at low temperatures, since the available Lanczos coefficients seem to behave linearly with n. However, this is not the case. To verify this, it is useful to use the second method, which directly gives the asymptotic behaviour of the slope of the Lanczos coefficients. Since we have the analytic form of the autocorrelation function this is not hard to compute. We need to find the location of the pole in Euclidean time that is closest to the origin in (6.9).

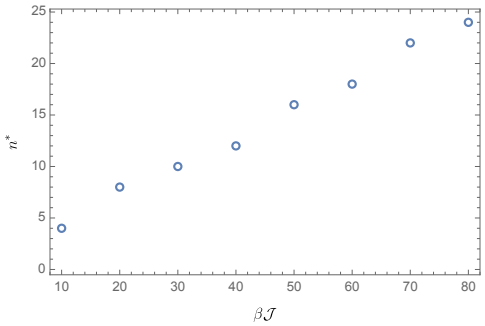

Fig. 25: The saturation point n^* as a function of $\beta\mathcal{J}$. The saturation point is defined as the first n such that $|b_n/\mathcal{J} - 1| \leq 0.1$.

At any temperature, the only divergence of the two-point function is at $\tau_* \to \infty$. From (6.8), this trivially gives that the slope of the Lanczos coefficients is zero and so, as expected, $\lambda_K = 0$ at any temperature for the single SYK with $q = 2$.

This behaviour of the Lanczos coefficients provides a sharp distinction from that of chaotic many body systems, for which the Lanczos coefficients are expected to grow indefinitely according to the operator growth hypothesis (2.19).

Finally, let us remark that in [132], it was found that at *finite* but large N, with $q = 4$, the Lanczos coefficients do in fact reach a plateau. In this case however, this is not due to the system being integrable but rather that the Hilbert space is finite. In particular they show that the value of this plateau grows linearly with N suggesting that they would not get saturation in the large N limit.

6.3.2 Large q and $1/q$ corrections

Now we turn to the discussion of chaotic SYK models. The first example analysed in the context of Krylov complexity was the large q model, as it is possible to get analytic expressions for the

autocorrelation function, see (2.42).

It was shown that both at finite and infinite temperature, the resulting Lanczos coefficients display the expected linear growth [26]. Using the moments method, the Lanczos coefficients at infinite temperature take the form

$$b_n/\mathcal{J} = \begin{cases} \sqrt{2/q} + O(1/q)\,, & n = 1\,, \\ \sqrt{n(n-1)} + O(1/q)\,, & n > 1\,. \end{cases} \tag{6.10}$$

At finite temperature, we have that

$$b_n/\mathcal{J} = \begin{cases} \frac{2\nu}{\beta\mathcal{J}}\sqrt{2/q} + O(1/q)\,, & n = 1\,, \\ \frac{2\nu}{\beta\mathcal{J}}\sqrt{n(n-1)} + O(1/q)\,, & n > 1\,. \end{cases} \tag{6.11}$$

By considering the asymptotic form of the coefficients for large n, it follows that

$$\lambda_K = \frac{4\nu}{\beta}\,. \tag{6.12}$$

This value for the Krylov exponent can also be verified by looking at the pole of the autocorrelation function (2.42), with the Euclidean time shifted to compute the Wightman correlator, see (6.4). In fact, one finds that

$$\tau_* = \frac{\beta\pi}{4\nu} \longrightarrow \lambda_K = \frac{4\nu}{\beta}\,. \tag{6.13}$$

It is easy to find the low-temperature behaviour of λ_K by using the expansion of ν in (2.44),

$$\lambda_K = \frac{2\pi}{\beta}\left(1 - \frac{2}{\beta\mathcal{J}} + \frac{4}{(\beta\mathcal{J})^2} - \frac{24+\pi^2}{3(\beta\mathcal{J})^3} + \cdots\right)\,. \tag{6.14}$$

We see that the Krylov exponent, in the strict large q limit, provides a far better bound for the Lyapunov exponent than the chaos bound (2.8). Indeed, the Krylov exponent saturates the left inequality in (1.5),

$$\lambda_L = \lambda_K \leq \frac{2\pi}{\beta}\,, \tag{6.15}$$

yielding an optimal bound for the Lyapunov exponent, while the chaos bound (2.8) is only reached, in this case, in the zero temperature limit.

Corrections in $1/q$. It is natural to ask if the tight bound (6.15) holds beyond the large q-limit. To answer this question, we consider the next-to-leading contributions in $1/q$ to the thermal autocorrelation function, which were computed in [90]. We will consider the full finite q result numerically in the next section.

We expand the autocorrelation function as follows,

$$G(\tau) = \frac{1}{2}\left(1 + \frac{g(\tau)}{q} + \frac{h(\tau)}{q^2} + O(1/q^3)\right) \ , \tag{6.16}$$

where the leading order $g(\tau)$ is given in (2.42) while $h(\tau)$ is found to be [90]

$$\begin{aligned} h(\tau) = \frac{1}{2}g^2(\tau) - 2\ell(\tau) - 4\left(\tan\left(\nu - \frac{2\nu\tau}{\beta}\right)\int_{\beta/2}^{\tau}\left(-\frac{2\nu}{\beta}\right)\ell(y)\,dy + 1\right) \\ + 4\frac{1 + \left(\nu - \frac{2\nu\tau}{\beta}\right)\tan\left(\nu - \frac{2\nu\tau}{\beta}\right)}{1 + \nu\tan\nu}\left(\tan\nu\int_{\beta/2}^{0}\left(-\frac{2\nu}{\beta}\right)\ell(y)\,dy + 1\right), \end{aligned} \tag{6.17}$$

with $\ell(\tau) \equiv g(\tau) - e^{-g(\tau)}\mathrm{Li}_2(1 - e^{g(\tau)})$ and

$$\int_{\beta/2}^{0}\left(-\frac{2\nu}{\beta}\right)\ell(y)\,dy = -\frac{\nu^2}{6\cos^2\nu}(2\nu + 3\sin 2\nu) \ . \tag{6.18}$$

Here ν is the same as in the large q SYK, given implicitly as a function of the inverse temperature in equation (2.42).

As before, we evaluate the moments and Lanczos coefficients from $G(\tau)$, which now includes a correction at order $1/q$. Note that when evaluating the moments, the integral $\int_{\beta/2}^{\tau}\left(-\frac{2\nu}{\beta}\right)\ell(y)\,dy$ does not need to be computed since the moments μ_{2n} for $n > 1$ are extracted by taking τ-derivatives and for the case of μ_0 the integral vanishes at $\tau = \beta/2$. Figure 26(a) shows the first 15 Lanczos coefficients at large q and infinite temperature including the $1/q$ corrections for different values of q.

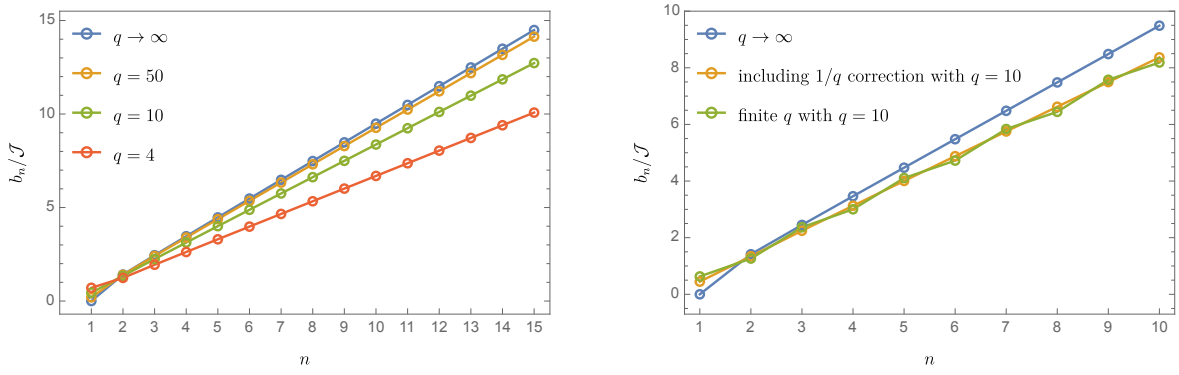

(a) (b)

Fig. 26: Lanczos coefficients as a function of n, computed perturbatively in the large q expansion including the $1/q$ correction at infinite temperature. In (a) we plot different values of q while in (b) we compare to the finite $q = 10$ result.

Note that the Lanczos coefficients at infinite temperature and large q (including the next-order correction) differ significantly from those found in [133]. We do not observe a super-linear growth and sub-linear growth in the even and odd Lanczos coefficients, respectively. In fact we find a linear dependence and do not observe any staggering.

We can compare our large q results with numerical results obtained at finite q (see section 6.3.3). For $q = 10$ at infinite temperature, the results are shown in figure 26(b), finding good agreement between the large q expansion and the finite q numerical result. In figure 27 we compare the large q Krylov exponent (computed from the slope of the Lanczos sequence) at infinite temperature to the finite q results for different values of q, again finding good agreement for $q \gtrsim 10$. Note that in both cases, in order to get this agreement, it was essential to also include the $1/q$-correction. This shows that, at least at infinite temperature, the results obtained in the large q expansion for the Lanczos coefficients are reasonable and a good approximation to the finite q results.

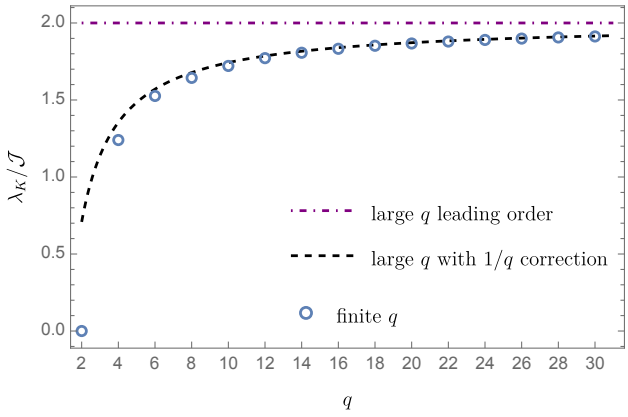

Fig. 27: Comparison of the Krylov exponent at infinite temperature between the large q result with $1/q$-correction and finite q results for different values of q. The dashed-dotted purple line at $\lambda_K/\mathcal{J} = 2$ denotes the value of the Krylov exponent to leading order in the large q expansion.

Next, we move away from infinite temperature. In fact, using the expansion in ν, we can obtain analytic results for the first Lanczos coefficients at small $\beta\mathcal{J}$. The first five Lanczos coefficients as $\beta\mathcal{J} \to 0$ are given by,

$$\begin{cases} b_1/\mathcal{J} &= \left(\sqrt{2} - \frac{(\beta\mathcal{J})^2}{4\sqrt{2}} + O\left(\beta\mathcal{J}\right)^3\right) \frac{1}{\sqrt{q}} \ , \\ b_2/\mathcal{J} &= \left(\sqrt{2} - \frac{(\beta\mathcal{J})^2}{4\sqrt{2}} + O\left(\beta\mathcal{J}\right)^3\right) + \left(-\frac{1}{\sqrt{2}} + \frac{5(\beta\mathcal{J})^2}{8\sqrt{2}} + O\left(\beta\mathcal{J}\right)^3\right) \frac{1}{q} \ , \\ b_3/\mathcal{J} &= \left(\sqrt{6} - \frac{\sqrt{3}(\beta\mathcal{J})^2}{4\sqrt{2}} + O\left(\beta\mathcal{J}\right)^3\right) + \left(-\frac{5}{\sqrt{6}} - \frac{13(\beta\mathcal{J})^2}{8\sqrt{6}} + O\left(\beta\mathcal{J}\right)^3\right) \frac{1}{q} \ , \\ b_4/\mathcal{J} &= \left(2\sqrt{3} - \frac{\sqrt{3}(\beta\mathcal{J})^2}{4} + O\left(\beta\mathcal{J}\right)^3\right) + \left(-\frac{35}{6\sqrt{3}} + \frac{85(\beta\mathcal{J})^2}{48\sqrt{3}} + O\left(\beta\mathcal{J}\right)^3\right) \frac{1}{q} \ , \\ b_5/\mathcal{J} &= \left(2\sqrt{5} - \frac{\sqrt{5}(\beta\mathcal{J})^2}{4} + O\left(\beta\mathcal{J}\right)^3\right) + \left(-\frac{377}{36\sqrt{5}} - \frac{883(\beta\mathcal{J})^2}{288\sqrt{5}} + O\left(\beta\mathcal{J}\right)^3\right) \frac{1}{q} \ . \end{cases} \tag{6.19}$$

Note that this is a double expansion, first in $1/q$, and then in $\beta\mathcal{J}$, that seems reliable for small $\beta\mathcal{J}$.

We can also perform an expansion for large $\beta\mathcal{J}$, where we expect both the Lyapunov and the

Krylov exponent to saturate the chaos bound. Perturbatively, for large $\beta\mathcal{J}$, they are given by,

$$\begin{cases} b_1/\mathcal{J} &= \left(\frac{\sqrt{2}\pi}{\beta\mathcal{J}} + O\left(\frac{1}{\beta\mathcal{J}}\right)^2\right)\frac{1}{\sqrt{q}}\,, \\ b_2/\mathcal{J} &= \left(\frac{\sqrt{2}\pi}{\beta\mathcal{J}} + O\left(\frac{1}{\beta\mathcal{J}}\right)^2\right) + \left(\frac{\sqrt{2}\pi}{\beta\mathcal{J}} + O\left(\frac{1}{\beta\mathcal{J}}\right)^2\right)\frac{1}{q}\,, \\ b_3/\mathcal{J} &= \left(\frac{\sqrt{6}\pi}{\beta\mathcal{J}} + O\left(\frac{1}{\beta\mathcal{J}}\right)^2\right) + \left(\frac{\sqrt{3}\pi}{\sqrt{2}\beta\mathcal{J}} + O\left(\frac{1}{\beta\mathcal{J}}\right)^2\right)\frac{1}{q}\,, \\ b_4/\mathcal{J} &= \left(\frac{\sqrt{12}\pi}{\beta\mathcal{J}} + O\left(\frac{1}{\beta\mathcal{J}}\right)^2\right) + \left(\frac{2\pi}{\sqrt{3}\beta\mathcal{J}} + O\left(\frac{1}{\beta\mathcal{J}}\right)^2\right)\frac{1}{q}\,, \\ b_5/\mathcal{J} &= \left(\frac{\sqrt{20}\pi}{\beta\mathcal{J}} + O\left(\frac{1}{\beta\mathcal{J}}\right)^2\right) + \left(\frac{\sqrt{5}\pi}{2\beta\mathcal{J}} + O\left(\frac{1}{\beta\mathcal{J}}\right)^2\right)\frac{1}{q}\,. \end{cases} \tag{6.20}$$

The first 10 Lanczos coefficients up to order $1/q$ are shown for different temperatures in figure 28, where we also compare to numerical finite temperature results at finite q (see section 6.3.3), again finding good agreement.

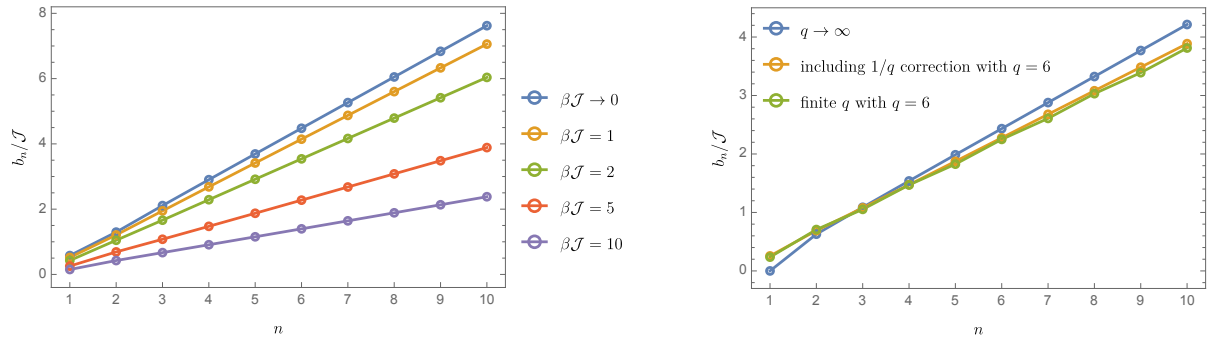

(a) (b)

Fig. 28: Lanczos coefficients as a function of n, computed perturbatively in the large q expansion including the $1/q$ correction with $q = 6$ at finite temperature. In (a) we plot different values of $\beta\mathcal{J}$ while in (b) we compare to the finite $q = 6$ result at $\beta\mathcal{J} = 5$.

6.3.3 Finite q

The final analysis we perform for a single SYK model is for finite $q \geq 4$ and finite temperatures. The aim is to find whether the conjectured bound (1.5) holds and how tight it is. For $q \geq 4$ the autocorrelation function can only be obtained numerically. In order to get to the regime of very low temperatures where the maximal chaos bound is almost saturated, we need high numerical precision in our calculations. We find that it is necessary to get to at least $\beta\mathcal{J} \sim 100$, to be close to maximal chaos.

To find the Lanczos coefficients, one could proceed by solving the Schwinger-Dyson equations (2.29) numerically and then taking numerical derivatives. This method however quickly accumulates errors. The reason is that at very low temperatures, $G(\tau)$ becomes very flat near $\tau \sim \beta/2$, which is the point at which derivatives need to be evaluated to compute the moments (6.5) at finite temperature. Then, in order to get higher-n Lanczos coefficients it is necessary to take further and further derivatives, whose values become smaller and smaller, and even small numerical errors become important.

Instead, it is more convenient to work in frequency space and numerically compute the spectral function $\rho(\omega)$ defined by

$$\rho(\omega) = \frac{G^{>}(\omega)}{2\pi}(1 + e^{-\beta\omega}) \ , \quad G^{>}(t) \equiv \frac{1}{N}\sum_i \langle \psi_i(t)\psi_i(0)\rangle_\beta = G(it + \varepsilon) \ , \tag{6.21}$$

using the procedure introduced in [98]. See appendix 3.5 for details. From $\rho(\omega)$ we can find $G(\tau + \beta/2)$ by the following relation [31]

$$G(\tau + \beta/2) = \int d\omega \ e^{-\omega(\tau + \frac{\beta}{2})} \frac{\rho(\omega)}{1 + e^{-\beta\omega}} \ . \tag{6.22}$$

Taking derivatives, we find that

$$\mu_{2n} = \frac{d^{2n}}{d\tau^{2n}} \left(2G(\tau + \beta/2)\right)|_{\tau=0} = \int d\omega \ \omega^{2n} e^{-\frac{\omega\beta}{2}} \frac{2\rho(\omega)}{1 + e^{-\beta\omega}} \ . \tag{6.23}$$

We compute the moments μ_{2n} by numerically evaluating the integral in (6.23) and then obtain the Lanczos coefficients using the algorithm (6.3). With this method we are able to reliably compute up to ~ 40 Lanczos coefficients, with inverse temperatures as large as $\beta\mathcal{J} \sim 100$. Using this procedure, all these numerical computations can be done in the order of minutes on a standard laptop.

The first thing we note is that the Lanczos coefficients for $q = 4$, unlike those of $q = 2$, do not saturate for large values of n and finite inverse temperature. The comparison between the results in section 6.3.1 and the Lanczos coefficients for the $q = 4$ model at finite temperature can be found in figure 29.

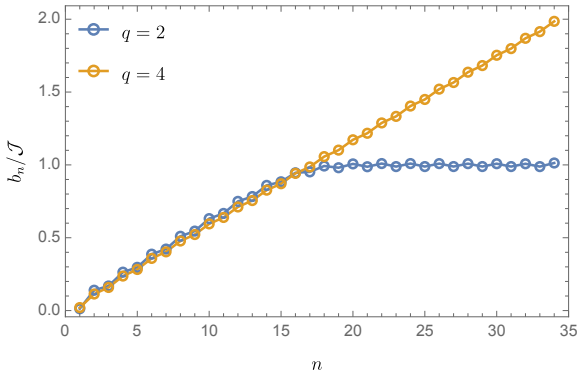

Fig. 29: First 35 Lanczos coefficients for the single $q = 4$ (yellow) and $q = 2$ (blue) SYK model at $\beta\mathcal{J} = 50$. While the coefficients saturate for the $q = 2$ model, they keep growing linearly for the $q = 4$ one.

Note also that the even and the odd coefficients are staggered, but both sets grow linearly for large values of n with equal slope and the staggering is a very small effect. To find λ_K, we calculate the slope from the largest 3 odd coefficients computed. We perform the same analysis for different values of $\beta\mathcal{J}$ to get the Krylov exponent λ_K as a function of $\beta\mathcal{J}$.

In figure 30 we show the result of this computation both for $q = 6$ and $q = 4$. We also plot their corresponding Lyapunov exponents, that we also computed numerically following the procedure described in appendix 3.4. For comparison, we also include the analytic expression for the Lyapunov exponent computed in the conformal (low temperature) limit and its leading correction (2.46). Finally, we also include the analytic curve for the Krylov exponent at large q which is known to be the same as the Lyapunov exponent and given by (6.12).

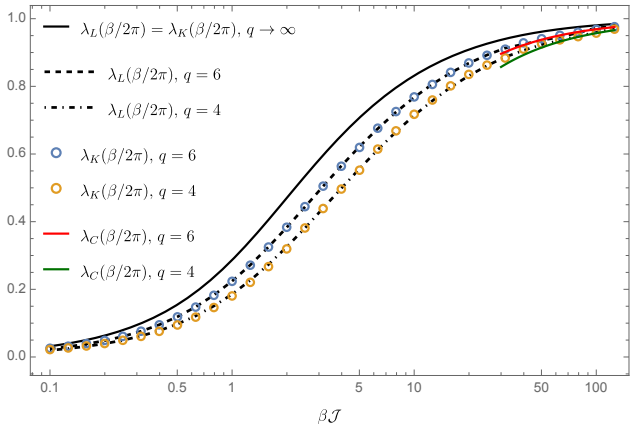

Fig. 30: Krylov and Lyapunov exponent as a function of $\beta\mathcal{J}$ in the single SYK model. The dots are numerical computations of λ_K for $q = 4$ and $q = 6$. The dashed-dotted and dashed curves are the respective Lyapunov exponents, computed numerically. The solid curves are analytical computations of the exponent in the large q limit (black), and analytic results at low temperatures for the Lyapunov exponent for $q = 4$ (green) and $q = 6$ (red). To the precision achieved, we find that $\lambda_K \simeq \lambda_L$, which was previously found to be equal analytically at large q.

As can be seen in figure 30, the computation of the Krylov exponent matches (at least to numerical accuracy) the one for the Lyapunov exponent, both for $q = 4$ and $q = 6$. This provides clear evidence that for the undeformed SYK model, $\lambda_K \simeq \lambda_L$ for all temperatures, not just at large q but at finite q as well. This also shows that in these models λ_K is a tight bound for the Lyapunov exponent, in general better than the chaos bound, that is only reached at very low temperatures.

6.4 Krylov complexity of deformed SYK models

In this part of the thesis, we will study deformed SYK models in which the total Hamiltonian is the sum of two SYK Hamiltonians with different number of fermions q and $\tilde{q}$ in each interaction term, see section 2.4. At finite temperature, these Hamiltonians generate interesting renormalisation group (RG) flows [54]. As a consequence, the Lyapunov exponent does not behave monotonically as a function of $\beta\mathcal{J}$. We are interested in comparing the behaviour of the Krylov exponent λ_K along the RG flow to that of the Lyapunov exponent λ_L.

When $\tilde{q} \neq 2$, the thermal RG flow interpolates two regions of nearly maximal chaos. Between these regions, the Lyapunov exponent decreases and then increases again when approaching the second maximally chaotic region. We refer to these models as chaos-to-chaos RG flows and we study them in section 6.4.1, both at infinite and finite $q, \tilde{q}$.

When $\tilde{q} = 2$, the intermediate near fixed point is still near-maximally chaotic, but the deforma-

tion consists of an integrable Hamiltonian. The Lyapunov exponent decreases at sufficiently large $\beta\mathcal{J}$. We refer to this case as chaos-to-integrable RG flow, and we study it both at finite and infinite q in section 6.4.2.

6.4.1 Chaos-to-chaos RG flows

6.4.1.1 Large $q, \tilde{q}$

The simplest model that presents non-monotonic behaviour of the Lyapunov exponent is the deformed SYK model with Hamiltonian (2.47) and $\tilde{q} = q/2$, in the large q limit. The two-point correlator of this model is known analytically for any value of $\beta\mathcal{J}$ and s, see (2.51), (2.52) [52–54]. If $s \ll 1$, the infrared of the theory is known to have two regions where the Lyapunov exponent is nearly maximal, see (2.59). In between these two regions, the Lyapunov exponent is sub-maximal, but it can nevertheless be computed numerically [52], see details in appendix 3.4. Since we have an analytic expression for the two-point function, we can compute λ_K using both methods described in sections 6.2.1 and 6.2.2.

We start by computing the asymptotic slope of the Lanczos coefficients by looking at the pole of the Wightman autocorrelation function. It is straightforward to verify that the pole τ_* of $G(\tau+\beta/2)$ in (2.51) is given by,

$$\tau_* = \frac{\beta \cos^{-1}\left(-\frac{s^2(\beta\mathcal{J})^2}{\sqrt{(\beta\mathcal{J})^2\nu^2+s^4(\beta\mathcal{J})^4}}\right)}{2\nu} , \tag{6.24}$$

where ν is implicitly given as a function of $\beta\mathcal{J}$ and s in (2.52). This immediately gives,

$$\lambda_K = \frac{2\pi\nu}{\beta \cos^{-1}\left(-\frac{s^2(\beta\mathcal{J})^2}{\sqrt{(\beta\mathcal{J})^2\nu^2+s^4(\beta\mathcal{J})^4}}\right)} , \tag{6.25}$$

that reproduces the single SYK large q result (6.12) when $s \to 0$. We emphasise again that this result is valid for any value of $\beta\mathcal{J}$ and s. If $s \ll 1$, we can further expand ν analytically at low temperatures close to each of the near fixed points, see (2.54) and (2.56). This gives,

$$\lambda_K = \begin{cases} \frac{2\pi}{\beta}\left(1 - \frac{2}{\beta\mathcal{J}} + \frac{4}{(\beta\mathcal{J})^2} - \frac{24+\pi^2}{3(\beta\mathcal{J})^3} + \frac{2(\beta\mathcal{J})^2 s^2}{(\beta\mathcal{J})^3} + \cdots\right) , & \text{Intermediate IR} , \\ \frac{2\pi}{\beta}\left(1 - \frac{\sqrt{4s^2+1}-1}{\beta\mathcal{J}s^2} + \frac{2+4s^2-2\sqrt{4s^2+1}}{(\beta\mathcal{J})^2 s^4} + \cdots\right) , & \text{Deep IR} , \end{cases} \tag{6.26}$$

where we observe *for the first time* an SYK-like model where the Krylov exponent λ_K does not provide a tight bound for the Lyapunov exponent λ_L. Comparing to (2.59), we see that nevertheless, the conjectured bound (1.5) still holds around the fixed points, where the expansion is valid. Note that the first four terms in the intermediate IR expansion, are exactly the ones of a single SYK, see (6.14), so the first correction that depends on s will be very suppressed. Furthermore, the corrections away from maximal chaos in the deep IR are extremely small for small s.

In order to have an independent calculation of the Krylov exponent, we also compute the slope of the Lanczos coefficients using the moment method (6.3). We indeed verify that the slope is linear and the Lanczos coefficients do not stagger for the values of n that are computationally available, which validates the use of the pole method above. The full plot of the Krylov exponent as a function of $\beta\mathcal{J}$ for different values of s can be found in figure 31. We include the computation of λ_K using both methods, as well as the result of the Lyapunov exponent, computed numerically, as described in appendix 3.4.

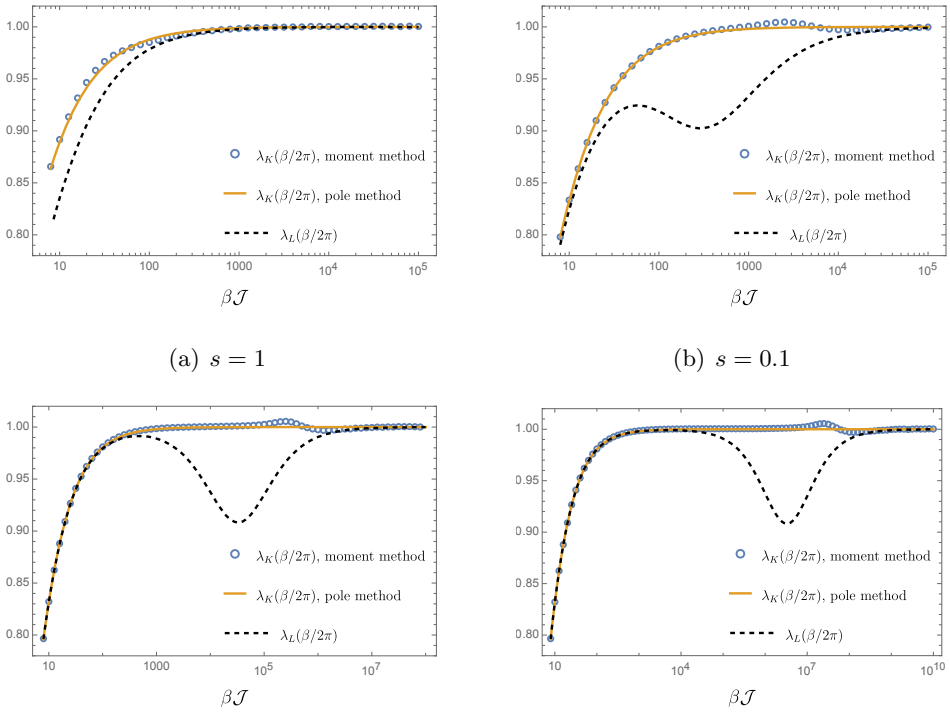

(a) $s = 1$ (b) $s = 0.1$

(c) $s = 0.01$ (d) $s = 0.001$

Fig. 31: Krylov and Lyapunov exponents as a function of $\beta\mathcal{J}$ for the deformed model (2.47) in the large q limit with $q = 2\tilde{q}$. The Krylov exponent is computed in two ways: the blue dots are computed using the moments method described in section 6.2.1 whilst the solid orange lines are computed from the pole of the autocorrelation function. The black dashed lines show the Lyapunov exponent, which is computed numerically. Plots are shown for different values of s. Unlike the Lyapunov exponent, the Krylov exponent grows monotonically and does not detect the region of sub-maximal chaos between the near maximally chaotic regions.

The first aspect to notice is that both methods agree to good precision, except for a small bump that can be seen in the computation using the moments method for inverse temperatures slightly larger than $\beta\mathcal{J} \sim s^{-2}$. If physical, this bump would not violate the left inequality in (1.5), but it would violate the right one. Moreover, it would mean that the two methods of computing the Krylov exponent are not equivalent. However, we checked that this bump is not physical. In particular, it is an artifact of the numerical procedure to compute the moments at large Lanczos coefficient index n, and we verified that the size of the bump decreases with n. See appendix H.[15]

Secondly, we observe that the Krylov exponent is always larger than or equal to the Lyapunov exponent, so that the bound between the two still holds for all the values of $\beta\mathcal{J}$ and s explored. The difference with the single SYK is that now the bound $\lambda_L \leq \lambda_K$ is not tight anymore in the infrared.

[15] We are grateful to Xiangyu Cao and Pratik Nandy for discussions on this point.

In fact, while the Lyapunov exponent exhibits non-monotonic behaviour and sub-maximal chaos in between the near-maximally chaotic regions, the Krylov exponent is monotonic in $\beta\mathcal{J}$. This can be clearly seen from figure 32, where we plot $\beta\partial_\beta\left(\lambda_{K,L}(\beta/2\pi)\right)$ and observe that $\beta\partial_\beta\left(\lambda_K(\beta/2\pi)\right) \geq 0$.

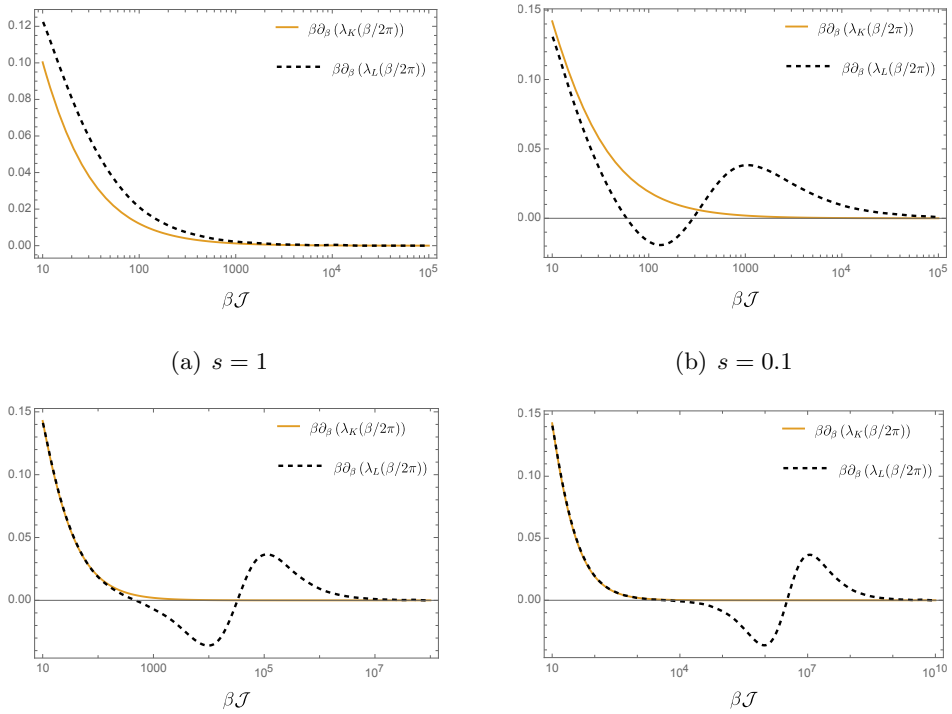

(a) $s = 1$ (b) $s = 0.1$

(c) $s = 0.01$ (d) $s = 0.001$

Fig. 32: Derivatives of Krylov and Lyapunov exponents as a function of $\beta\mathcal{J}$ for the deformed SYK in the large q limit with $q = 2\tilde{q}$. We observe that in all cases $\beta\partial_\beta\left(\lambda_K(\beta/2\pi)\right) \geq 0$, whilst this is not the case for the Lyapunov exponent.

In passing, we note that if instead of looking at the asymptotic growth of the Lanczos coefficients at large n, we focus on the approximately linear slope of the first few coefficients, we surprisingly find a non-monotonic behaviour that resembles closely the one of the Lyapunov exponent. We refer the reader to appendix I for plots substantiating the relation. It would be interesting to understand the physical reason for this feature, if any, in future work. It would also be interesting to understand how the various features presented in this section depend on $\mathfrak{n} = q/\tilde{q}$ and we leave this for future work.

6.4.1.2 Finite $q, \tilde{q}$

Next, we move to the study of deformed SYK models at finite q and $\tilde{q}$. The numerical methods used in section 6.3.3 to compute the Krylov and the Lyapunov exponent, can be readily adapted to the deformed Hamiltonians (2.47).

To compute the Krylov exponent, we will be using the moments method, as in the single SYK at finite q. In contrast to the analytic control of the large q models, in the current case, numerical errors pose a challenge to a reliable computation of the autocorrelation function (and its moments) at very low temperatures. Using the techniques described in appendices 3.4 and 3.5, we managed to reliably compute the Krylov and Lyapunov exponents along the RG flow for inverse temperatures as high as $\beta\mathcal{J} \sim 100$. As we will see, this will not allow us to observe the full RG flow in the deep infrared, but will be enough to observe the main chaotic features of the flow for values of $s \sim 0.1$.

If we want to consider models that are maximally chaotic in the deep infrared, then $\tilde{q}$ has to be at least 4, which also means that $q \geq 6$. Reaching large values of $\beta\mathcal{J}$ is even more challenging in this case, since the spectral function $\rho(\omega)$ becomes sharply peaked at lower values of $\beta\mathcal{J}$ as we increase q, see appendix 3.5. Nevertheless, we managed to compute both the Krylov and the Lyapunov exponents up to $\beta\mathcal{J} = 100$ for $s = 0.2$. The result can be seen in figure 33. From the results at large q, we expect that the Lyapunov exponent will initially grow for small $\beta\mathcal{J}$. At some intermediate region, this growth will stop, the Lyapunov exponent will decrease and eventually it will go back to near maximal chaos at very large $\beta\mathcal{J}$. At the computationally available inverse temperatures, we managed to clearly observe the slowdown of the growth of the Lyapunov exponent, see the dashed-dotted purple curve in figure 33. On the other hand, the Krylov exponent of the flow SYK follows closely the Krylov exponent of the single SYK with $q = 6$ at all available inverse temperatures, until it saturates to the value of the near-conformal Lyapunov exponent result of a single $q = 6$ SYK model (2.46).

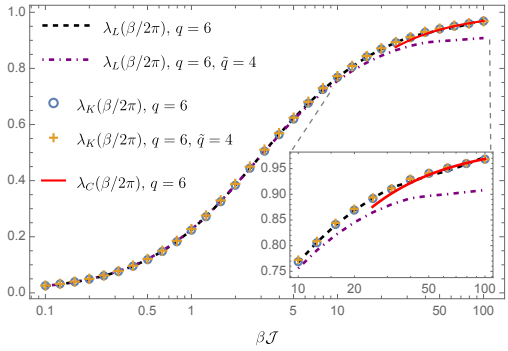

Fig. 33: The Krylov exponent λ_K and the Lyapunov exponent λ_L as a function of $\beta\mathcal{J}$ for the deformed SYK model with $q = 6$, $\tilde{q} = 4$ and $s = 0.2$. We added the analogous computations for the single SYK model with $q = 6$ (together with the analytic expansion for the Lyapunov exponent at large $\beta\mathcal{J}$) as a reference (red). In the caption, we zoom into the region of large $\beta\mathcal{J}$, to clearly distinguish the behaviour of λ_K from λ_L.

Once again, paralleling the large q results, the Krylov exponent shows a monotonic behaviour and is not able to follow the slowdown of the Lyapunov exponent. This does not violate either of the bounds in (1.5), but shows that the Krylov exponent does not provide a tight bound for chaotic-to-chaotic thermal RG flows in SYK. We therefore suspect that it cannot distinguish the different regimes of chaos-to-chaos RG flows.

6.4.2 Chaos-to-integrable RG flows

6.4.2.1 Finite q and $\tilde{q} = 2$

We now consider the deformed SYK model with $\tilde{q} = 2$ and finite $q \geq 4$. For $q = 4$, the Lyapunov exponent has been numerically computed before showing an initial increase at low temperatures, with a later decrease at even lower temperatures [46]. It is a subject of debate whether the Lyapunov exponent (in the large N limit) actually becomes zero at finite temperature or if this is only achieved in the strict zero temperature limit [46–48].

In order to compute the Krylov exponent, we first compute the Lanczos coefficients for fixed values of $\beta\mathcal{J}$ and s, using the numerical moments method. As an example, we show the first ~ 40 Lanczos coefficients for $\beta\mathcal{J} = 80$ and $s = 0.2$ in figure 34. We compare them with the Lanczos coefficients of the single SYK with $q = 2$, see section 6.3.1, and we clearly see that the saturation present in the $q = 2$ model is not present in the deformed SYK model. Moreover, the Lanczos coefficients seem to closely follow those of the single SYK with q fermions, both for $q = 6$ and $q = 4$, so it seems unlikely that the Krylov exponent will decrease (when taking larger values of the

Lanczos index n) for this choice of parameters.

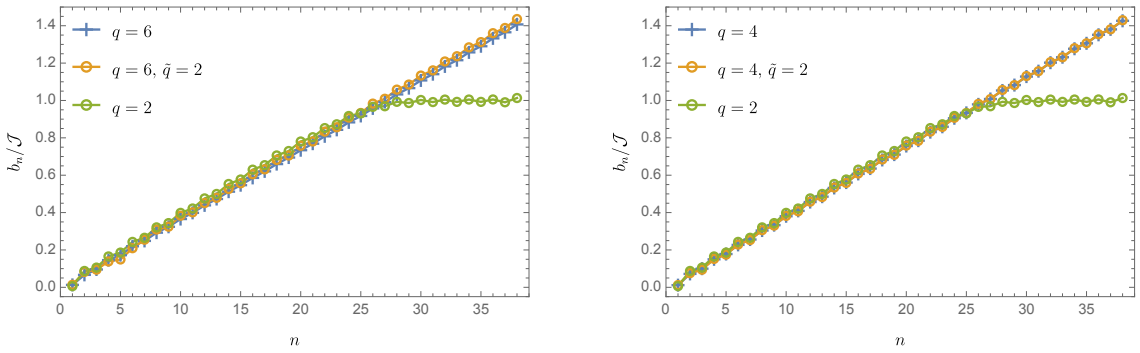

(a) $q = 6,\ \tilde{q} = 2$ (b) $q = 4,\ \tilde{q} = 2$

Fig. 34: First 38 Lanczos coefficients for the deformed SYK Hamiltonian with $s = 0.2$ and $\beta\mathcal{J} = 80$. For reference, we also include the first Lanczos coefficients for the single $q = 2$ SYK (which saturate at large n) and those of the single q model with $q = 6$ in plot (a) and $q = 4$ in plot (b).

We show the full behaviour of the Krylov exponent as a function of $\beta\mathcal{J}$ for fixed $s = 0.2$ in figure 35, both for $q = 6$ and $q = 4$ to $\tilde{q} = 2$ flows, along with their corresponding Lyapunov exponents, computed using techniques in appendix 3.4 . In the range of temperatures numerically available, we can clearly see a pronounced decrease of the Lyapunov exponent, which becomes even more evident in the $q = 6$ case. In contrast, the Krylov exponent does not depart from the Krylov exponent of the single q SYK model, that we also plot for reference. In particular, while the bound (1.5) is still obeyed at all temperatures, we do not observe a decrease in the Krylov exponent, that monotonically increases towards the maximal chaos bound at very low temperatures. See also figure 36, where we plot $\beta\partial_\beta(\lambda_K\beta/2\pi)$. This is consistent with the behaviour found for λ_K in the other examples considered so far, both in the single SYK and in the chaos-to-chaos RG flows.

Before going to a large q example of chaos-to-integrable flows, let us make a brief comment on the behaviour of the Lyapunov exponent at low temperatures. In [47], it was reported that for the $q = 4$ to $\tilde{q} = 2$ SYK flow, the decay of the Lyapunov exponent at large inverse temperatures for large s follows a power-law behaviour, $\lambda_L(\beta/2\pi) \sim (\beta\mathcal{J})^{-1}$. From 35(a), it seems that the $q = 6$ model with small s also exhibits a power-law behaviour. In this regime, we observe that the tail at large $\beta\mathcal{J}$ seems to go as $\lambda_L(\beta/2\pi) \sim (\beta\mathcal{J})^{-2}$, which suggests that, as in [47], at large N the Lyapunov exponent λ_L reaches zero only at infinite $\beta\mathcal{J}$. The precise low-temperature behaviour seems to depend both on q and s. It would be interesting to understand this dependence better.

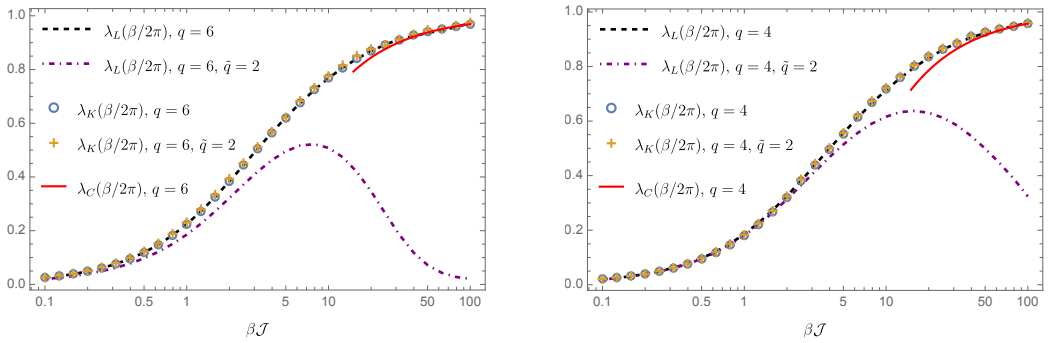

(a) $q=6,\ \tilde{q}=2$ (b) $q=4,\ \tilde{q}=2$

Fig. 35: The Krylov exponent λ_K and the Lyapunov exponent λ_L as a function of $\beta\mathcal{J}$ for the deformed SYK model with $s=0.2$. We added the analogous computations for the single SYK model (together with its analytical prediction at large $\beta\mathcal{J}$) as a reference. At low temperatures $\lambda_L \leq \lambda_K$, but the bound is not tight.

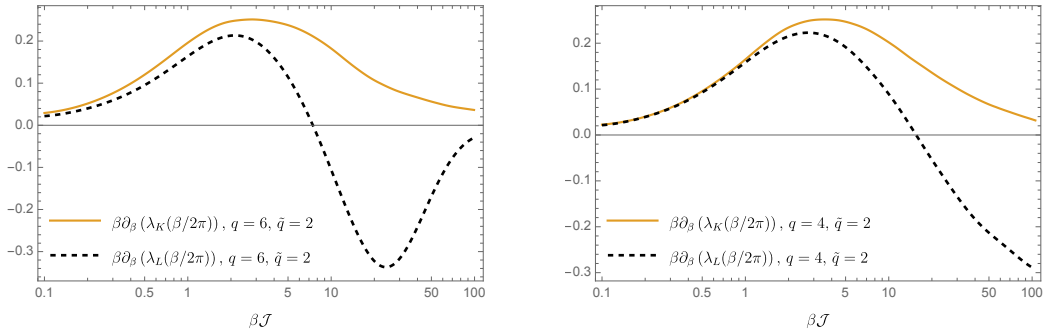

(a) $q=6,\ \tilde{q}=2$ (b) $q=4,\ \tilde{q}=2$

Fig. 36: Derivatives of Krylov and Lyapunov exponents as a function of $\beta\mathcal{J}$ for the deformed model with $s=0.2$. Plots are shown for different values of s. We observe that $\beta\partial_\beta\left(\lambda_K(\beta/2\pi)\right) \geq 0$, whilst this is not the case for the Lyapunov exponent.

6.4.2.2 Large q and $\tilde{q}=2$

There is one more example of a chaos-to-integrable RG flow, that can be solved analytically, at least perturbatively in the deformation parameter. This is the model with $q\to\infty$ and $\tilde{q}=2$. We need to be careful when taking the large q limit of this model. The relevant Schwinger-Dyson equation from (2.49), for $\tilde{q}=2$ becomes

$$\Sigma(\tau_1,\tau_2)=\mathcal{J}^2\left(\frac{2^{q-1}}{q}G(\tau_1,\tau_2)^{q-1}+s^2G(\tau_1,\tau_2)\right)\ . \tag{6.27}$$

As can be seen, the deformation would become dominant if we take the large q limit naively. Instead, we re-scale the coupling $s^2 \to \mathfrak{s}^2/q$ so that in the large q limit, using (2.40), we obtain,

$$\partial_\tau^2 g(\tau) = \mathcal{J}^2 \left(2e^{g(\tau)} + \mathfrak{s}^2\right) \ . \tag{6.28}$$

This equation does not have an analytic solution, but can be solved both perturbatively in $\mathfrak{s}$ [46] or numerically. For the perturbative solution, we expand $g(\tau)$ as,

$$g(\tau) = g^{(0)}(\tau) + \mathfrak{s}^2 \ g^{(1)}(\tau) + O((\beta\mathcal{J}\mathfrak{s})^4) \, . \tag{6.29}$$

The undeformed solution is given by (2.42), while $g^{(1)}(\tau)$ is given by [46],

$$g^{(1)}(\tau) = \left(\frac{\beta\mathcal{J}}{2\nu}\right)^2 \left[\alpha\left(\frac{\tau}{\beta}\right)\tan\left(\frac{\tau}{\beta}\right) + \log\cos\left(\frac{\tau}{\beta}\right) + \frac{\tau}{\beta}\tan\left(\frac{\tau}{\beta}\right) + B(\nu)\left(\frac{\tau}{\beta}\tan\left(\frac{\tau}{\beta}\right) + 1\right)\right] , \tag{6.30}$$

with

$$\begin{cases} \alpha(x) & = \int^x \mathrm{d}t \ \ \log\cos t = \frac{i}{2}\mathrm{Li}_2\left(-e^{2ix}\right) + \frac{ix^2}{2} - x\log\left(1+e^{2ix}\right) + x\log\cos(x) \ , \\ B(\nu) & = -\frac{-\alpha(-\nu)\tan\nu + \alpha(\nu)\tan\nu + 2\nu\tan\nu + 2\log\cos\nu}{2\nu\tan\nu + 2} \ . \end{cases} \tag{6.31}$$

The perturbative correction to the Lyapunov exponent to this order was computed in [46], and it is given by

$$\lambda_L^{(\text{pert.})} = \frac{2\pi}{\beta}\left(\frac{2\nu}{\pi} - \frac{\mathfrak{s}^2\nu}{2\pi}\frac{B(\nu) + \frac{19}{18} - \log 2}{\cos^2\nu} + \cdots\right) \ . \tag{6.32}$$

In principle, given that we have the analytic two-point function, we should be able to use either the moments method or look at the pole of the Wightman autocorrelator to compute λ_K. However, in this case, there are two difficulties. Since the solution is only perturbative in $\mathfrak{s}$ and the pole might depend on $\mathfrak{s}$, the pole method cannot be applied to the expansion directly since it will not capture the correct location of the pole in the two-point function. We could still use the moments method, but then the solution can only be trusted up to $\beta\mathcal{J} \sim 1/\mathfrak{s}$, where we do not expect to see a great deviation of the Krylov exponent from the Lyapunov exponent.

Instead of the perturbative solution, we directly solve (6.28) numerically and then compute both

the Lanczos coefficients and the Lyapunov exponent. The first step is to compute $g(\tau)$ numerically using a shooting method to solve (6.28), with thermal boundary conditions $g(0) = g(\beta) = 0$. Then, using the equation of motion (6.28) and derivatives of it, we can efficiently compute the moments of g, without any additional input other than the numerical value of $g(\tau = \beta/2)$. In this way, we can obtain up to around 16 Lanczos coefficients in the order of seconds and around 35 if one is patient. We fit the slope of the largest 3 even coefficients computed to obtain λ_K. To compute the Lyapunov exponent we follow the method described in [52], that does not need the explicit form of $g(\tau)$. In figure 37 we plot both λ_K and λ_L for $\mathfrak{s}^2 = 0.01$ and $\mathfrak{s}^2 = 0.08$, along with the corresponding perturbative Lyapunov exponents (6.32). We also include in this plot the analytic curve for $\lambda_L = \lambda_K$ in the undeformed model with $\mathfrak{s}^2 = 0$, see (6.12).

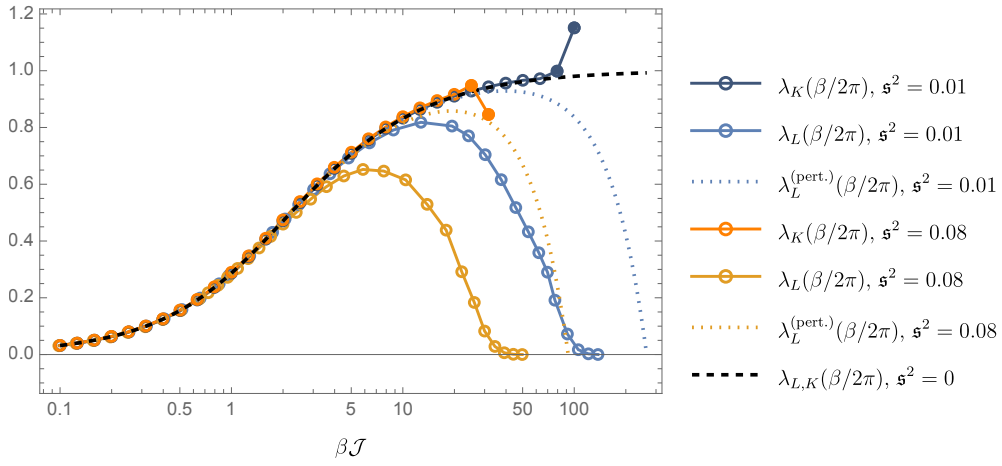

Fig. 37: Krylov and Lyapunov exponents for the $q \to \infty$ and $\tilde{q} = 2$ model. Plots are shown for $\mathfrak{s}^2 = 0, 0.01, 0.08$. The solid curves are numerical computations. The blacked dashed curve is the analytical $\lambda_L = \lambda_K$ for $\mathfrak{s}^2 = 0$, given by (6.12). Note that for the Krylov exponent curves with $\mathfrak{s}^2 > 0$, we indicate the first two points that are observed to deviate significantly from the $\mathfrak{s}^2 = 0$ curve by filled circles. These points should not be taken as valid Krylov exponents, as the Lanczos coefficients are not linear. The dotted lines are the pertubative Lyapunov exponents computed from (6.32). These are valid up to $\beta\mathcal{J} \sim 1/\mathfrak{s}$ and so do not agree with with the numerical computations beyond this point.

The Lyapunov exponent. We first note that the numerically computed Lyapunov exponents agree with the perturbative results only up to inverse temperatures $\beta\mathcal{J} \sim 1/\mathfrak{s}$, as expected from the perturbative analysis. At larger inverse temperatures, the two results disagree so we cannot draw further conclusions from the perturbative analysis. In particular, we see that the value at which $\lambda_L^{(\text{pert.})}$ hits zero [46], is not an accurate description of the inverse temperatures in which the actual Lyapunov exponent becomes very small.

Next we note that for fixed $\mathfrak{s}^2 > 0$, the numerically computed Lyapunov exponent initially increases with $\beta\mathcal{J}$ in line with the Lyapunov exponent of $\mathfrak{s}^2 = 0$ before reaching a maximum and then decreasing towards zero. Recall that in section 6.4.2.1, we observed that at finite q and large $\beta\mathcal{J}$ there is a power-law behaviour at large inverse temperatures that seems q and s dependent. In the regimes analysed here and in [47], the power seems to increase with q. Here we observe a much steeper decay towards zero, that does not seem to fit a power law, maybe in line with the large q limit taken. It seems that the Lyapunov exponent is reaching zero at a finite temperature in this case. As far as our numerics can assess, the lowest values of λ_L we managed to compute are as small as $\sim 10^{-6}$ for both values of $\mathfrak{s}$ analysed. It remains an interesting open question to understand if there is an actual chaotic-to-integrable phase transition at finite temperature in this model.

The Krylov exponent. For fixed $\mathfrak{s}^2 > 0$, the Krylov exponent also initially increases with $\beta\mathcal{J}$ in line with the Krylov exponent of $\mathfrak{s}^2 = 0$, with this behaviour continuing beyond the point that the corresponding Lyapunov exponent reaches its maximum. As in previous cases, we do not observe any non-monotonic behaviour for the Krylov exponent along the flow.

At around the inverse temperatures where the corresponding Lyapunov exponent reaches zero however, the Krylov exponent seems to sharply deviate from the $\mathfrak{s}^2 = 0$ curve. In figure 37 we indicate the first two points that are observed to deviate significantly from the $\mathfrak{s}^2 = 0$ curve by filled circles. Upon examining the Lanczos coefficients from and beyond this point we see significant staggering between even and odd coefficients and it is no longer clear that either the even or the odd coefficients grow linearly. Therefore, these points should **not** be taken as valid Krylov exponents.

As evidence, in figure 38 we contrast the Lanczos coefficients for $\mathfrak{s}^2 = 0.08$ at $\beta\mathcal{J} = 10$ and $\beta\mathcal{J} = 100$. For the latter case we computed an additional 19 coefficients to ensure we are capturing the asymptotic behaviour. Whilst at $\beta\mathcal{J} = 10$, the coefficients clearly grow linearly, at $\beta\mathcal{J} = 100$ it is possible to fit both linear and square root growth to the later coefficients (after taking into account the staggering of even and odd coefficients).

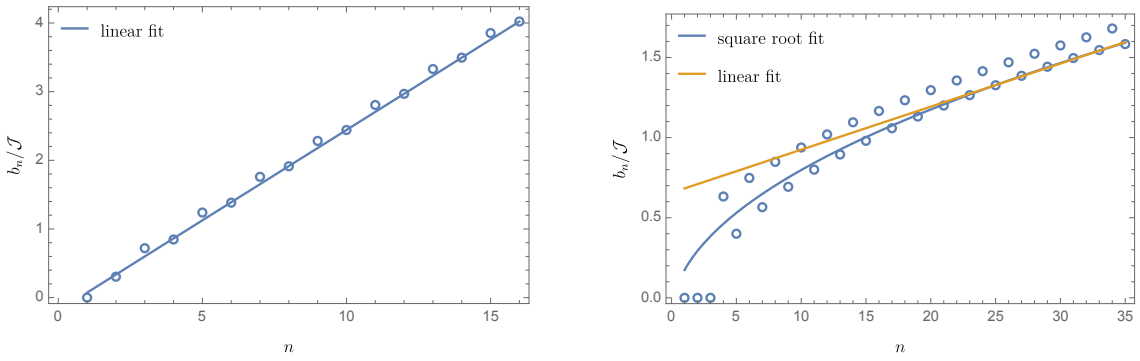

(a) $\beta\mathcal{J} = 10$ (b) $\beta\mathcal{J} = 100$

Fig. 38: The Lanczos cofficients for $\mathfrak{s}^2 = 0.08$ at (a) $\beta\mathcal{J} = 10$ and (b) $\beta\mathcal{J} = 100$. The late coefficients for $\beta\mathcal{J} = 10$ have a clear linear fit, $b_n/\mathcal{J} = 0.26\,n - 0.19$. At $\beta\mathcal{J} = 100$, the staggering is more pronounced. The late odd coefficients fit with both a square root fit, $b_n/\mathcal{J} = 0.29\sqrt{n} - 0.11$ and a linear one, $b_n/\mathcal{J} = 0.026\,n + 0.65$. Though not shown here, the late even coefficients can also be fit with both linear and square root behaviour.

It is suggestive that the Lanczos coefficients stop being conclusively linear at approximately the same inverse temperatures that the Lyapunov exponent becomes close to zero.[16] As far as our analysis reaches, we observe monotonic behaviour of the Krylov exponent up to temperatures where we cannot guarantee anymore the existence of a Krylov exponent. The interplay between Krylov methods and chaos-to-integrable phase transitions at finite temperature remains an interesting problem that deserves further investigation. We comment on this in the outlook.

[16] For the finite q to $\tilde{q} = 2$ examples of the previous subsection, the Lyapunov exponent follows instead a power law fall-off. This could be why we do not see the Lanczos coefficients stopping to be linear at finite q.

7 Conclusions and outlook

7.1 Summary of main results

In this thesis we have extended the study of the SYK model by carrying out a systetmatic analysis of deformed SYK models that exhibit tractable RG flows, employing a range of both analytical and numerical techniques. In section 4 we studied thermodynamic properties of the flows in a variety of regimes. At large q we established numerically that the zero temperature entropy carries a non-trivial dependence on model parameters $\mathfrak{n}$ and s. We also established numerically the relationship of the slope of the deep IR linear-in-temperature entropy with $\mathfrak{n}$ and s. We found the existence of flows between two near-fixed points for finite values of q for the first time. We provided evidence that the deep IR regime is captured by a Schwarzian action. We exhibited a novel, analytically tractable model in the $\mathfrak{n} = 1 + \varepsilon$ regime, with ε small. Finally we showed that the small temperature deformations away from the intermediate near-fixed point can be computed via conformal perturbation theory at both large q and finite q.

In section 5 we extended our analysis to consider multiple deformations. We established the use of conformal perturbation theory to describe multiple deformations, including those with imaginary couplings. We also provided evidence that the thermodynamic behaviour we observe in the large N limit persists at large but finite N for both unitary and non-unitary flows. Finally, we demonstrated how conformal perturbation theory can be used to engineer the IR theormydamics of the theory away from the first near confomal fixed point, opening up a far richer landscape of potential dilaton gravity duals beyond JT gravity. This allowed us to presented a finely tuned model that exhibits a region of negative linear-in-temperature entropy, a feature exhibited by dS_2 space.

In section 6 we turned our attention to signatures of chaos, computing and comparing Lyapunov and Krylov exponents in a variety of models. We started by studying the single SYK model. In the large q limit, it was already known that the Krylov exponent, λ_K, is exactly equal to the Lyapunov exponent λ_L, not only at infinite but also at finite temperature [26]. We computed the slope of the Lanczos coefficients to the next order in the $1/q$ expansion, and also numerically at finite q, finding an excellent agreement with the Lyapunov exponent both at finite and infinite temperature, reinforcing some already existing evidence that the bound $\lambda_L \leq \lambda_K$ might be precisely saturated, and thus provide a tighter bound to the Lyapunov exponent than the chaos bound, $\lambda_L \leq 2\pi/\beta$. We

then considered the deformed SYK models for which, in certain regimes, the Lyapunov exponent was known to have a non-monotonic behaviour, interpolating between two near-maximally chaotic regions or even decreasing to almost zero at very low temperatures when the deformation was integrable. We found that in all cases in which the Krylov exponent can be defined the bounds $\lambda_L \leq \lambda_K \leq 2\pi/\beta$ are satisfied. However, we also found that the computation of the Krylov exponent fails to capture the non-monotonic behaviour of the Lyapunov exponent. In particular, in cases where the deformation was integrable and $\lambda_L \to 0$ at low temperatures, the Krylov exponent shows maximal chaos $\lambda_K \to 2\pi/\beta$. We found one model, the deformed SYK with large q and $\tilde{q} = 2$, in which the Lanczos coefficients stop being linear at large n. It is interesting to note that this behaviour starts happening at inverse temperatures where the Lyapunov exponent becomes very small (or presumably, zero).

7.2 Outlook

Having established the deformed SYK models as a valuable setting to study holography and chaos, there are several new directions worth exploring in future work.

Non-Hermitian deformations

In the section 5, we provided strong evidence that non-Hermitian Hamiltonians can be used in the context of two-dimensional holography to microscopically describe certain gravitational scenarios. In attempting to realise a portion of dS_2 by flowing away from the AdS_2 near-fixed point, we reached the surprising conclusion that the deformation must be non-Hermitian. It is unclear to us what the role, if any, of non-Hermitian physics is for a microscopic picture of quantum de Sitter space. Nonetheless, several facts point to a departure from ordinary unitary physics for a quantum theory of de Sitter. The logarithm of the Euclidean path integral of de Sitter space, which has been postulated by Gibbons and Hawking [4] to compute the de Sitter horizon entropy, generically has an overall phase [134], and potentially fully fledged complexified saddles [135], rendering the partition function complex-valued. Edge-mode contributions from refined quantum features near the de Sitter horizon contribute negatively to the de Sitter partition function [136, 137]. The de Sitter horizon, moreover, is unlike a black hole horizon in that it does not evaporate and its interior does not harbor a singular spacelike slice. Instead, the interior of the de Sitter horizon

is an exponentially expanding region of spacetime that can harbor, at least naively, an arbitrary amount of quantum information–another potential indication that the static patch is a genuinely open system [138].

Given these ideas it would interesting to more firmly establish the validity of using a non-Hermitian Hamiltonian in our case. Generally, the use of non-Hermitian operators to understand physical systems has been the subject of significant research. For applications to the SYK see for example [112, 113, 139–142]. One direction of the existing literature on non-Hermitian physics has been to explore pseudo-Hermitian Hamiltonians, which allow for real spectra [143, 144]. However, this approach does not align with our objectives, as we necessitate complex spectra to invert the sign of heat capacity. Beyond pseudo-Hermiticity, non-Hermitian Hamiltonians have also garnered attention in their own right, as a potential means to describe dissipative systems. For reviews of the subject see for example, [145, 146].

A more complete picture is offered by Lindbladian time evolution [147, 148]. Here, one considers the dynamics for the density matrix ρ of a subsystem coupled to a large environment. The constraints are positivity, trace preservation, Hermiticity, and a Markovian environment. The Lindbladian equation can be expressed as

$$\dot{\rho} = -i[H, \rho] + \sum_i \left(L_i \rho L_i^\dagger - \frac{1}{2}\{L_i^\dagger L_i, \rho\} \right) \ . \tag{7.1}$$

The complex jump operators L_i encode the dissipative part of the system and H is the system Hamiltonian. For a derivation of this equation see appendix J. Lindbladian systems have already been studied in the context of the SYK model [98, 149–151], and could offer a natural framework to extend our analysis of de Sitter holography in the context of deformed SYK models. In addition to holographic considerations, quantum chaos has also been studied in the context of Lindbadlian systems, including Krylov complexity [152–155]. Such studies could provide a fruitful extension to our current understanding of these topics.

Engineering IR physics

In studying the thermal RG flows of the deformed SYK models we found several interesting features. Notably, the zero temperature entropy dependence on continuous model parameters $\mathfrak{n}$ and s found in section 4 warrants further investigation. It would be interesting to understand better the underlying

physics of this degenerate behaviour. It would also be interesting to find the analytical dependence on $\mathfrak{n}$ and s of the slope of the deep IR linear-in-temperature entropy. This could open up the possibility of engineering the deep IR thermodynamics of the flow along the lines of what was done in the neighbourhood the first conformal fixed point in section 5.

Borrowing the idea of engineering the thermodynamic properties of the RG flows, one could also ask whether it is possible to engineer the chaotic properties of the deformed SYK models, thus extending the non-monotonic behaviours of the Lyapunov exponent observed in section 6. One could perhaps use the SYK model with multiple deformations (5.1) to engineer a theory that has some particular desired non-maximal Lyapunov behaviour in the infrared. For example, one could imagine using parametrically separated couplings s_i, so that the behaviour of the Lyapunov becomes almost oscillatory as you move to lower temperatures.

A conjecture on the growth of the Krylov exponent

Going back to the results of this section 6, it seems tempting to conjecture that (as long as it is well-defined) the Krylov exponent has a monotonic behaviour along thermal RG flow. Namely, in quantum systems that obey unitary evolution at finite temperature,

$$\beta\partial_\beta\left(\frac{\lambda_K\beta}{2\pi}\right)\geq 0\ . \tag{7.2}$$

This conjecture is satisfied in all the examples considered in this thesis where the Krylov exponent could be computed, including the single SYK model. It would be interesting to test this conjecture in other models that exhibit chaos-to-integrable transitions, *e.g.,* [91, 92, 156–159]. In particular, it would be nice to see whether this conjecture holds at finite N, where the Lyapunov exponent has been computed up to $N\sim 60$ using Krylov methods for the single SYK [44] and exact diagonalisation is available up to around $N\sim 34$. Krylov complexity computations for the single SYK model have also been developed at finite N [132, 160], so it would be desirable to adapt them to include these deformed models. See [51] for some progress in this direction. At finite N, other quantities that probe late quantum chaos (such as the spectral form factor [41]) could also be used to characterise deformed SYK models, see [46] for some progress in this direction. In particular, the relation between the infrared sector that exhibits seemingly non-maximal chaos and holography seems like an interesting question to be explored [127, 161, 162]. Conjectures on operator growth have been

violated when tested in quantum field theory [79, 131, 163], so studying Krylov complexity in RG flows in QFT might be a natural avenue to test these ideas.

If the conjecture is true and the Krylov exponent is indeed monotonic, then, it would seem that λ_K behaves more as an entropy or a c-function, rather than as a quantum signature of chaos. In particular, it would mean that λ_K is not good at diagnosing chaos in quantum systems where the Lyapunov exponent has non-monotonic behaviour as a function of the energy scale, like, for instance, in systems where the Lyapunov exponent goes to zero at very low energies. See however the discussion in appendix I which suggests that the slope of early Lanczos coefficients could potentially capture additional properties of such flows.

Chaotic to integrable phase transitions

Finally in section 6 we further provided a concrete example where the Krylov exponent cannot be well-defined after some given inverse temperature. This was the deformed SYK with large q and $\tilde{q} = 2$, where observe staggering and no definite asymptotic behaviour in the Lanczos coefficients beyond this point. Given this occurs around inverse temperatures where the Lyapunov exponent becomes very small it would be desirable to further study this model to assess whether indeed there is a phase transition. If so, one would like to see whether the Krylov complexity stops being exponential and what is its characteristic behaviour at late times. Throughout section 6 we have assumed, following [26], that Krylov complexity C_K grows exponentially with time and that λ_K is given by 2α, α being the slope of the Lanczos coefficients at large n. One should compute the actual Krylov complexity to verify this is actually the case and understand what happens when there is a phase transition.

If we are to continue to make progress on the deep problems in theoretical physics, we must remain ambitious in our motivations whilst grounded in our calculations. Driven by the need for microscopic models of spacetime and a better understanding of chaos in quantum systems, we have identified a concrete set of models that have remarkably rich and intriguing behaviours in these contexts, whilst remaining tractable enough to extract precise insights. We hope the findings and numerical techniques presented in this thesis can help inspire further research in these fascinating fields.

A Derivation of the G and Σ action

In this appendix we describe how to derive the G and Σ action of the SYK model at large N. For a fermionic system there is no corresponding classical system that approximates the quantum system as $\hbar \to 0$. However we can define an action in terms of anti-commuting numbers, called Grassmann numbers, which can be quantised to produce fermionic quantum systems via a standard prescription. Such models therefore can be thought of as pseudo-classical models. In the case of the SYK, the pseudo-classical action expressed in Euclidean space is given by

$$S_E = \int d\tau \left(\frac{1}{2}\psi_i \partial_\tau \psi_i - \sum_{1 \leq i_1 < \cdots < i_q \leq N} J_{i_1 i_2 \cdots i_q} \psi_{i_1} \psi_{i_2} \cdots \psi_{i_q} \right) . \tag{A.1}$$

We will take $q = 4$ in what follows for notational simplicity but the results are easily extended to general q. The averaged partition function of the theory is then given by

$$\begin{aligned} \langle Z(\beta) \rangle_J &= \left\langle \int [D\psi] e^{-S_E(\psi(\tau))|_0^\beta} \right\rangle_J \\ &= \int \prod_{i<j<k<l} dJ_{ijkl}\, \mathbb{P}(J_{ijkl}) \int [D\psi] \exp\left\{ \int_0^\beta d\tau \left(-\frac{1}{2}\psi_i \partial_\tau \psi_i + \sum_{i<j<k<l} J_{ijkl} \psi_i \psi_j \psi_k \psi_l \right) \right\} , \end{aligned} \tag{A.2}$$

where in the last line we have used the fact that the J_{ijkl} are independent random variables. Recalling that our couplings are drawn from a Gaussian distribution with mean and variance given by (2.25), we have that

$$\mathbb{P}(J_{ijkl}) = \frac{1}{\sqrt{2\pi \left(\frac{12\mathcal{J}^2}{N^3} \right)}} e^{-\frac{1}{2} J_{ijkl}^2 \frac{N^3}{12\mathcal{J}^2}} . \tag{A.3}$$

We now integrate over the coupling constants. For example, to perform the integral over J_{1234} we note that

$$\begin{aligned}
&\int dJ_{1234}\ \frac{1}{\sqrt{2\pi\left(\frac{12\mathcal{J}^2}{N^3}\right)}}\exp\left\{-\frac{1}{2}J_{1234}^2\frac{N^3}{12\mathcal{J}^2}\right\}\exp\left\{\int_0^\beta d\tau\ J_{1234}\psi_1\psi_2\psi_3\psi_4\right\}\\
=&\int dJ_{1234}\ \frac{1}{\sqrt{2\pi\left(\frac{12\mathcal{J}^2}{N^3}\right)}}\exp\left\{-\frac{N^3}{24\mathcal{J}^2}\left[\left(J_{1234}-\int_0^\beta d\tau\ \frac{12\mathcal{J}^2}{N^3}\psi_1\psi_2\psi_3\psi_4\right)^2-\left(\int_0^\beta d\tau\ \frac{12\mathcal{J}^2}{N^3}\psi_1\psi_2\psi_3\psi_4\right)^2\right]\right\}\\
=&\exp\left\{\frac{N^3}{24\mathcal{J}^2}\left(\int_0^\beta d\tau\ \frac{12\mathcal{J}^2}{N^3}\psi_1\psi_2\psi_3\psi_4\right)^2\right\}\int dJ_{1234}\ \frac{\exp\left\{-\frac{N^3}{24\mathcal{J}^2}\left(J_{1234}-\int d\tau_0^\beta\ \frac{12\mathcal{J}^2}{N^3}\psi_1\psi_2\psi_3\psi_4\right)^2\right\}}{\sqrt{2\pi\left(\frac{12\mathcal{J}^2}{N^3}\right)}}\\
=&\exp\left\{\frac{6\mathcal{J}^2}{N^3}\left(\int_0^\beta d\tau\ \psi_1\psi_2\psi_3\psi_4\right)^2\right\}\ .
\end{aligned}\tag{A.4}$$

Performing the rest of the integrals in the same way we find that

$$\langle Z(\beta)\rangle_J=\int[D\psi]\ \exp\left\{\left(-\frac{1}{2}\int_0^\beta d\tau\ \psi_i\partial_\tau\psi_i\right)+\frac{6\mathcal{J}^2}{N^3}\sum_{i<j<k<l}\left(\int_0^\beta d\tau\ \psi_i\psi_j\psi_k\psi_l\right)^2\right\}\ .\tag{A.5}$$

The sum over fermions in the last term can of this expression can be re-written as

$$\begin{aligned}
&\sum_{i<j<k<l}\psi_i(\tau)\psi_j(\tau)\psi_k(\tau)\psi_l(\tau)\psi_i(\tau')\psi_j(\tau')\psi_k(\tau')\psi_l(\tau')\\
=&\sum_{i<j<k<l}[\psi_i(\tau)\psi_i(\tau')][\psi_j(\tau)\psi_j(\tau')][\psi_k(\tau)\psi_k(\tau')][\psi_l(\tau)\psi_l(\tau')]\\
=&\frac{1}{4!}\sum_{i\neq j\neq k\neq l}[\psi_i(\tau)\psi_i(\tau')][\psi_j(\tau)\psi_j(\tau')][\psi_k(\tau)\psi_k(\tau')][\psi_l(\tau)\psi_l(\tau')]\\
=&\frac{1}{4!}\left(\sum_{i=1}^N\psi_i(\tau)\psi_i(\tau')\right)^4\ ,
\end{aligned}\tag{A.6}$$

where in the second line and third lines we must be careful about the fact that we are dealing with anti-commuting (Grassmann) numbers; however since we do an even number of exchanges we don't pick up a sign. In the final line we are again using the fact that we are dealing with Grassmann numbers and so any term with a repeated factor of $\psi_i(\tau)$ or $\psi_i(\tau')$ drops out when we expand the

bracket. We therefore find

$$\langle Z(\beta)\rangle_J = \int [D\psi]\ \exp\left\{\left(-\frac{1}{2}\int_0^\beta d\tau\ \psi_i\partial_\tau\psi_i\right) + \frac{\mathcal{J}^2 N}{4}\int_0^\beta\int_0^\beta d\tau d\tau'\left(\sum_{i=1}^N \frac{\psi_i(\tau)\psi_i(\tau')}{N}\right)^4\right\}\ . \tag{A.7}$$

Now we introduce a bi-local field $G(\tau_1,\tau_2)$ into the integral using a delta function,

$$\begin{aligned}\langle Z(\beta)\rangle_J = \int_{APB}[D\psi]\int [DG(\tau,\tau')]\ \delta\left(NG(\tau,\tau') - \sum_{i=1}^N \psi_i(\tau)\psi_i(\tau')\right)\\ \exp\left\{\left(-\frac{1}{2}\int_0^\beta d\tau\ \psi_i\partial_\tau\psi_i\right) + \frac{\mathcal{J}^2 N}{4}\int_0^\beta\int_0^\beta d\tau d\tau' G(\tau,\tau')^4\right\}\ .\end{aligned} \tag{A.8}$$

We represent the delta function as an integral over another bi-local field $\Sigma(\tau,\tau')$,

$$\begin{aligned}&\delta\left(NG(\tau,\tau') - \sum_{i=1}^N \psi_i(\tau)\psi_i(\tau')\right)\\ &= \int [D\Sigma(\tau,\tau')]\ \exp\left\{-\frac{1}{2}\int_0^\beta\int_0^\beta d\tau d\tau' N\Sigma(\tau,\tau')\left(G(\tau,\tau') - \sum_{i=1}^N \frac{\psi_i(\tau)\psi_i(\tau')}{N}\right)\right\}\ ,\end{aligned} \tag{A.9}$$

where we are taking the integration contour for Σ to be parallel to the imaginary axis. We therefore have

$$\begin{aligned}\langle Z(\beta)\rangle_J = \int [D\psi][DG(\tau,\tau')][D\Sigma(\tau,\tau')]\ \exp\Big\{ -\frac{1}{2}\int_0^\beta\int_0^\beta d\tau d\tau' N\Sigma(\tau,\tau')\left(G(\tau,\tau') - \sum_{i=1}^N \frac{\psi_i(\tau)\psi_i(\tau')}{N}\right)\\ -\frac{1}{2}\int_0^\beta d\tau\ \psi_i\partial_\tau\psi_i + \frac{\mathcal{J}^2 N}{4}\int_0^\beta\int_0^\beta d\tau d\tau' G(\tau,\tau')^4\Big\}\ .\end{aligned} \tag{A.10}$$

We can now integrate out the fermionic fields. We show how to do the integral over one of the fermionic fields, say ψ_1,

$$\begin{aligned}&\int D\psi_1\ \exp\left\{\frac{1}{2}\int_0^\beta\int_0^\beta d\tau d\tau'\ \psi_1(\tau)\Sigma(\tau,\tau')\psi_1(\tau') - \frac{1}{2}\int_0^\beta d\tau\ \psi_1(\tau)\partial_\tau\psi_1(\tau)\right\}\\ &= \int D\psi_1\ \exp\left\{-\frac{1}{2}\int_0^\beta\int_0^\beta d\tau d\tau'\ \psi_1(\tau)\left[\delta(\tau-\tau')\partial_{\tau'} - \Sigma(\tau,\tau')\right]\psi_1(\tau')\right\}\\ &= \det\left(\delta(\tau-\tau')\partial_{\tau'} - \Sigma(\tau,\tau')\right)^{\frac{1}{2}}\\ &= \exp\left\{\frac{1}{2}\log\det(\delta(\tau-\tau')\partial_{\tau'} - \Sigma(\tau,\tau')\right\}\ .\end{aligned} \tag{A.11}$$

Integrating out all the fermionic fields in this way then gives the result

$$\langle Z(\beta)\rangle_J = \int [DGD\Sigma] e^{-NI[G,\Sigma]} \,, \tag{A.12}$$

where

$$I = -\frac{1}{2}\log\det\left(\delta(\tau-\tau')\partial_{\tau'} - \Sigma(\tau,\tau')\right) + \frac{1}{2}\int_0^\beta\int_0^\beta d\tau d\tau' \left(\Sigma(\tau,\tau')G(\tau,\tau') - \frac{\mathcal{J}^2}{2}G(\tau,\tau')^4\right) \,. \tag{A.13}$$

B Numerical computation of $\alpha(q)$ in a single SYK model

In section 2.3, we saw that the entropy of the single SYK model has a small temperature expansion given by

$$\frac{S}{N} = \left(S_0^{\text{free}} - \int_0^{1/q} dx\, \pi\left(\frac{1}{2}-x\right)\tan\pi x\right) + \frac{4\pi^2\alpha(q)}{\beta\mathcal{J}} + \cdots \,. \tag{B.1}$$

Here we describe how to compute the coefficient $\alpha(q)$ numerically. The first step is to numerically compute the large N entropy, S/N, of the model at a single low temperature point. We then subtract off the temperature independent piece of (B.1) and multiply the answer by $\beta\mathcal{J}/(4\pi^2)$ to obtain a value for $\alpha(q)$ up to corrections of order $(\beta\mathcal{J})^{-2}$. To find the entropy, we numerically solve the Schwinger-Dyson equations with $s = 0$, as shown in appendix 3.2. In figure 39 we plot the numerical values of $\alpha(q)$ and compare it with the two-sided Padé approximant, found in [90],

$$\alpha(q) = \frac{3(3\pi-2)q + \pi^2 - 18\pi + 24}{6q^2\left(2(3\pi-2)q + \pi^3 + 8\right)} \,. \tag{B.2}$$

Given the agreement with the numerics, we directly use (B.2) in our numerical computations.

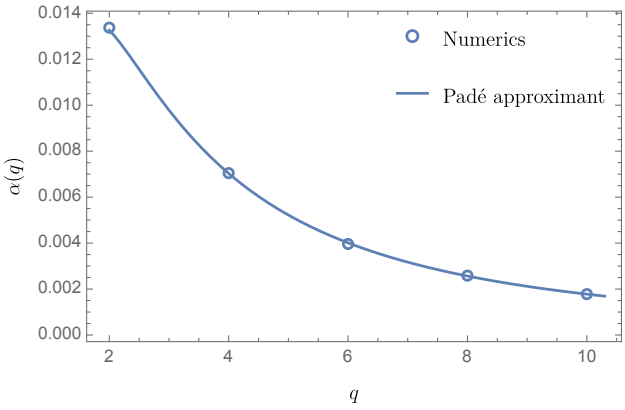

Fig. 39: The coefficient $\alpha(q)$ as a function of q. The circles are numerical computations while the solid blue curve is given by the Padé approximation (B.2). We used $\beta\mathcal{J} \sim 10^{2.3}$ for the numerical computations.

C Small s expansion for $\bar{\aleph}(s, \mathfrak{n})$

In this appendix, we provide an analytic form for $\bar{\aleph}(s, \mathfrak{n})$, when $\mathfrak{n} \geq 2$ and $s \ll 1$ by fitting the numerical data. For $\mathfrak{n} = 2$, we know $\bar{\aleph}(s, \mathfrak{n} = 2)$ analytically and it is given by $\bar{\aleph}$ in equation (2.58). It is straightforward to obtain

$$\bar{\aleph}(s, \mathfrak{n} = 2) \to \frac{1/2}{s} + \cdots , \tag{C.1}$$

in the small s expansion. Given the shape of the curves from the numerical results, we propose the following structure for general $\mathfrak{n}$ in the small s limit,

$$\bar{\aleph}(s, \mathfrak{n}) \to \frac{a(\mathfrak{n})}{s^{b(\mathfrak{n})}} + \cdots , \tag{C.2}$$

where $a(\mathfrak{n}), b(\mathfrak{n})$ can depend on $\mathfrak{n}$ but are independent of s.

To test this proposal and find the form of the functions $a(\mathfrak{n}), b(\mathfrak{n})$, we compute $\bar{\aleph}(s, \mathfrak{n})$ for small values of s such that $0.01 \leq s^2 \leq 0.02$ and different values of $\mathfrak{n}$. This is done numerically using the same methodology as described in section 4.2.1. The results for $\mathfrak{n} = 2, 3, 4, 5$ are shown in logarithmic scale in figure 40. The linear form of the plots supports the ansatz in equation (C.2).

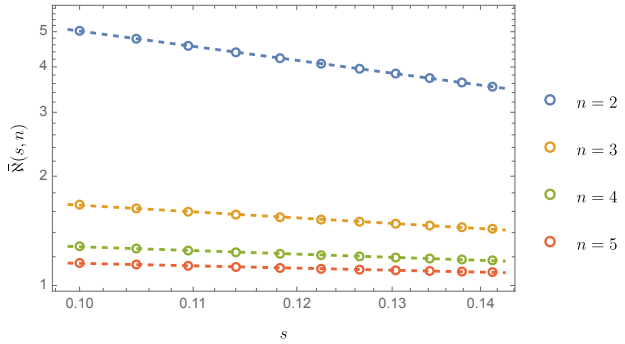

Fig. 40: Log-log plots of $\bar{\aleph}(s,\mathfrak{n})$ as function of s for different values of $\mathfrak{n}$. Circles correspond to numerical computations. Dashed lines are fitted curves for the ansatz $\bar{\aleph}(s,\mathfrak{n}) = \frac{a(\mathfrak{n})}{s^{b(\mathfrak{n})}}$.

For each $\mathfrak{n}$, we perform a fit on the data to find $a(\mathfrak{n})$ and $b(\mathfrak{n})$. For $\mathfrak{n}=2$, we find $a(\mathfrak{n}=2)=0.482$ and $b(\mathfrak{n}=2)=1.02$, which are close to the analytic values of $1/2$ and 1, respectively. We repeat the procedure for $2 \leq \mathfrak{n} \leq 10$. The results for $a(\mathfrak{n})$ and $b(\mathfrak{n})$ are shown in figure 41.

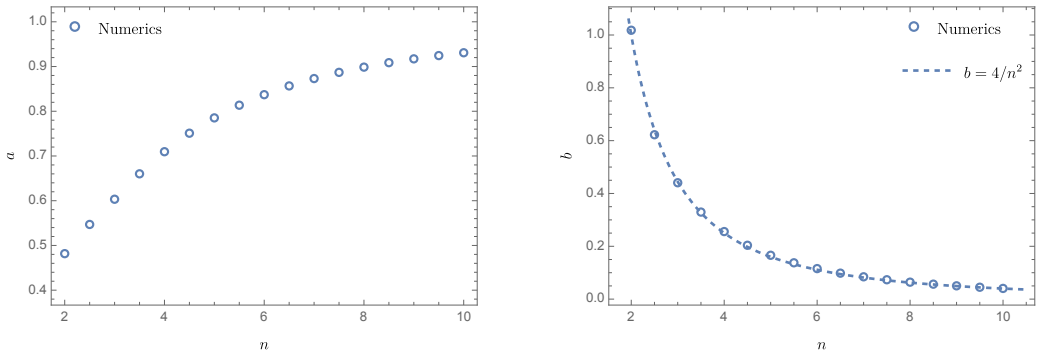

(a) (b)

Fig. 41: (a) Fitted values for $a(\mathfrak{n})$ in the ansatz $\bar{\aleph}(s,\mathfrak{n}) = \frac{a(\mathfrak{n})}{s^{b(\mathfrak{n})}}$ for small s. (b) Fitted values for $b(\mathfrak{n})$ in the ansatz $\bar{\aleph}(s,\mathfrak{n}) = \frac{a(\mathfrak{n})}{s^{b(\mathfrak{n})}}$ for small s.

Note that as $\mathfrak{n} \to \infty$, $a(\mathfrak{n}\to\infty) \to 1$ and $b(\mathfrak{n}\to\infty) \to 0$, so $\bar{\aleph}(s,\mathfrak{n}\to\infty) \to 1$, as expected from the considerations in section 4.2.1. Moreover, a simple fit in figure 41(b), shows that $b(\mathfrak{n}) \approx 4/\mathfrak{n}^2$. We conclude that

$$\bar{\aleph}(s,n) \to \frac{a(\mathfrak{n})}{s^{4/\mathfrak{n}^2}} + \cdots \quad \text{as} \quad s \to 0 \ , \tag{C.3}$$

with $1/2 \leq a(\mathfrak{n}) \leq 1$.

D Schwarzian action and entropy for the $q = 2$ SYK model

In this appendix we use the methodology to derive the Schwarzian action employed in sections 4.3.1 and 4.3.2 to correctly reproduce the linear-in-temperature entropy of the $q = 2$ SYK model at large N, which is known to be integrable.

For $q = 2$, we can solve the Schwinger-Dyson equations (2.29) exactly to find that at low temperatures [31]

$$\left.\frac{S}{N}\right|_{q=2} = \frac{\pi}{6}\frac{1}{\beta\mathcal{J}} + \cdots \ . \tag{D.1}$$

Note that the zero-temperature entropy vanishes for $q = 2$. We want to derive this formula from a Schwarzian action perspective. For that, we take $\Sigma \to \Sigma + \partial_\tau$ in (2.27) and write $I = I_{\rm CFT} + I_{\rm UV}$ [40, 81], where

$$I_{\rm CFT} = -\frac{1}{2}\log\det(-\Sigma) + \frac{1}{2}\int_0^\beta\int_0^\beta d\tau_1 d\tau_2 \left(\Sigma G - \mathcal{J}^2\frac{2^{q-1}}{q^2}G^q\right) \ , \tag{D.2}$$

$$I_{\rm UV} = \frac{1}{2}\int_0^\beta\int_0^\beta d\tau_1 d\tau_2 \delta(\tau_1-\tau_2)\partial_{\tau_2}G \ . \tag{D.3}$$

We then make an expansion of the saddle solution to $I_{\rm CFT}$ in powers of τ_{12}. It can be written in terms of soft modes $f(\tau_+)$, see (4.33). We can substitute this expansion into I_{UV}, which now becomes an integral over τ_{12} and τ_+. Carrying out the τ_{12} integral with a short time scale cutoff $\varepsilon/\mathcal{J}$, we are left with the following Schwarzian action,

$$I_{\rm Sch} = \left[\left(\frac{b(1-q)\varepsilon^{1-2\Delta}}{6q^2}\right)\frac{1}{\mathcal{J}}\right]\int_0^\beta d\tau_+ \ {\rm Sch}(f(\tau_+),\tau_+) = \left[\left(-\frac{1}{24\pi}\right)\frac{1}{\mathcal{J}}\right]\int_0^\beta d\tau_+ \ {\rm Sch}(f(\tau_+),\tau_+) \ , \tag{D.4}$$

where for the last equality we used that $b = 1/\pi$ and $\Delta = 1/2$, in the $q = 2$ model. Note that the cut off dependence drops out. Upon taking this Schwarzian action on-shell, we obtain that the entropy becomes

$$\left.\frac{S_{\rm Sch}}{N}\right|_{q=2} = \frac{\pi}{6}\frac{1}{\beta\mathcal{J}} \ , \tag{D.5}$$

which correctly reproduces (D.1).

E Spectra of non-Hermitian deformed SYK models with single deformation

For models with a single non-Hermitian deformation with purely imaginary s,

$$H_{\text{def}} = H_q + sH_{\tilde{q}} \ , \quad s := i\kappa \ , \kappa \in \mathbb{R} \ , \tag{E.1}$$

we can get an understanding of the structure of the spectrum by studying the action of the particle hole operator [41, 164],

$$P = K \prod_i^{N/2} \left(\chi_i^\dagger + \chi_i \right) \ . \tag{E.2}$$

Here, the operator K takes the complex conjugate, we have restricted to N being even and have defined

$$\chi_i \equiv \frac{1}{\sqrt{2}} \left(\psi_{2i} - i\psi_{2i+1} \right) , \quad i = 1, \ldots, N/2 \ . \tag{E.3}$$

The χ_i obey the anti-commutation relations

$$\{\chi_i, \chi_j^\dagger\} = \delta_{ij} \ , \qquad \{\chi_i, \chi_j\} = 0 \ , \qquad \{\chi_i^\dagger, \chi_j^\dagger\} = 0 \ . \tag{E.4}$$

By using these anti-commutation relations one can check that

$$P^2 = (-1)^{(\frac{N}{2})(\frac{N}{2}-1)/2} = \begin{cases} +1 & N/2 \bmod 4 = 0 \ , \\ +1 & N/2 \bmod 4 = 1 \ , \\ -1 & N/2 \bmod 4 = 2 \ , \\ -1 & N/2 \bmod 4 = 3 \ . \end{cases} \tag{E.5}$$

Moreover, depending on the number of fermion interactions, q, in the SYK Hamiltonian H_q we have the following (anti-)commutation relations

$$\begin{aligned} [H_q, P] = 0 \quad & \text{for } q = 4, 8, 12, \ldots \ , \\ \{H_q, P\} = 0 \quad & \text{for } q = 2, 6, 10, \ldots \ . \end{aligned} \tag{E.6}$$

To see these, note first note that one can check the following relation holds

$$P\psi_i = (-1)^{\frac{N}{2}-1}\psi_i P \quad \text{for } i = 1, \ldots, N \ . \tag{E.7}$$

Commuting H_q across P involves commuting an even number of fermions across P, resulting in no minus sign being picked up. However in the case of $q/2$ odd, the Hamiltonian (2.24) has a factor of i which causes a minus sign to be picked up due to the action of K, and (E.6) follows from this. Using (E.6) one can then verify the following cases:

Case 1: $q/2$ **even** $\tilde{q}/2$ **odd**: For an energy eigenstate $|E\rangle$ of H_{def} with eigenvalue E we have that

$$H_{\text{def}}(P|E\rangle) = E^*(P|E\rangle) \ , \tag{E.8}$$

and so the spectrum comes in complex conjugate pairs $(a + bi, a - bi)$.

Case 2: $q/2$ **odd** $\tilde{q}/2$ **even**: We find that

$$H_{\text{def}}(P|E\rangle) = -E^*(P|E\rangle) \ , \tag{E.9}$$

and the spectrum comes in pairs $(a + bi, -a + bi)$.

Case 3: $q/2$ **odd** $\tilde{q}/2$ **odd**: For each (right) eigenvector $|E^R\rangle$ of H_{def} with eigenvalue E we can define a left eigenvector $|E^L\rangle$ such that $H_{\text{def}}^\dagger|E^L\rangle = E^*|E^L\rangle$. Then we find

$$H_{\text{def}}(P|E^L\rangle) = -E(P|E^L\rangle) \ . \tag{E.10}$$

We therefore find that the spectrum comes in pairs $(a + bi, -a - bi)$.

Case 4: $q/2$ **even** $\tilde{q}/2$ **even**: We find that

$$H_{\text{def}}(P|E^L\rangle) = E(P|E^L\rangle) \ . \tag{E.11}$$

In this case whether or not we get degenerate eigenstates depends on whether $P|E^L\rangle$ equals $|E^R\rangle$ up to a phase, and this is found to depend on the value of N. In particular, for $N/2$ odd we must get a degeneracy. To see this we first note that the SYK Hamiltonian and the Hamiltonian of the deformed model preserve the parity of the Dirac fermion number operator

$$Q = \sum_i \left(\chi_i^\dagger \chi_i\right) \ . \tag{E.12}$$

Since for $N/2$ odd P must map a state with even parity to odd and vice versa, $P|E^L\rangle$ and $P|E^R\rangle$ must be distinct eigenstates. For the case $N/2$ even we cannot use this argument. Numerics confirm that only in the case $N = 0 \bmod 8$ is there no degeneracy. For all other cases, since $P^2 = \pm 1$, we find that the eigenstates come in degenerate pairs.

F Geodesics in dilaton gravity theories

In this appendix we present more details concerning the calculations of geodesics in a deformed dilaton gravity background, as described in section 5.5.2. Recall that the thermodynamic features of the deformed SYK models are captured by a dilaton gravity theory with Euclidean action given by (5.17) and general black hole solutions of the form (5.18). When parameterised by their distance, geodesics are found by varying the following length functional,

$$\mathcal{L} = \int ds \left(f(r)\dot{t}^2 + \frac{\dot{r}^2}{f(r)} \right) \ , \tag{F.1}$$

where the dot indicates a derivative with respect to the distance, s. Since the action does not explicitly depend on t we have a conserved quantity

$$f(r)\dot{t} = E \ . \tag{F.2}$$

We also have that our geodesics satisfy the constraint

$$1 = f(r)\dot{t}^2 + \frac{\dot{r}^2}{f(r)} \ . \tag{F.3}$$

Putting (F.2) into (F.3) we find

$$\dot{r} = \pm\sqrt{f(r) - E^2} \ , \tag{F.4}$$

where the sign determines whether the radial coordinate, r, is increasing or decreasing with increasing s. As in section 5.5.2, we consider a dilaton potential of the form

$$U(\phi) = 2\phi + \delta U(\phi) \ , \tag{F.5}$$

where $\delta U(\phi)$ is a smooth function of ϕ. For our argument we take $\delta U(\phi)$ to have compact support in some region $[r_1^*, r_2^*]$ for some $r_2^* > r_1^* > \tilde{\phi} r_h$, where r_h denotes the position of the horizon. The metric resulting from such a dilaton potential is given by

$$f(r) = r^2 - r_h^2 + g(r) \ , \qquad g(r) = \frac{1}{\tilde{\phi}} \int_{r_h}^{r} dr' \, \delta U(\tilde{\phi} r') \ . \tag{F.6}$$

The geodesic described in the main text has $E = 0$. In this case, $\dot{t} = 0$ and so the length of such a geodesic is given by

$$L = \int ds = 2 \int_{r_h}^{R_b} \frac{1}{\sqrt{r^2 - r_h^2 + g(r)}} \, dr \ , \tag{F.7}$$

from which the conclusions in the main text follow.

G Boundary two-point function of the deformed AdS_2 black hole

In this appendix we provide some more details for the comparison of the two-point function between the AdS_2 black hole and the deformed AdS_2 geometries that is described in section 5.5.3. In particular we derive the inequality (5.29).

AdS_2 black hole

We start by reviewing the form of the boundary two-point function for the AdS_2 black hole, whose metric is given by

$$ds^2 = f(r) dt^2 + \frac{dr^2}{f(r)} \ , \tag{G.1}$$

where $t \sim t + \beta$, $r > 1$ and $f(r) = r^2 - r_h^2$. Without loss of generality we will set $r_h = 1$ in what follows. Making the transformation $r = \coth z$ we bring the metric into the conformal frame

$$ds^2 = \frac{1}{\sinh^2 z}\left(dt^2 + dz^2\right) \ . \tag{G.2}$$

From [53] we have that the two-point function for light fields (as a perturbative expansion in the mass of the field) is given by

$$G_{\mathrm{AdS}_2}(\omega_n) = -\left(|\omega_n| + m^2 \int_{z_c}^{\infty} dy \ \frac{1}{\sinh^2 y} e^{-2|\omega_n|(y-z_c)} + \cdots\right) \ , \tag{G.3}$$

where $\omega_n = 2\pi n$ for $n \in \mathbb{Z}$ and we have set the boundary of the spacetime at some small value $z = z_c > 0$. Our conventions for the Fourier transform are

$$G(\tau) = \sum_{n\in\mathbb{Z}} G(\omega_n) e^{i\omega_n t/\beta}, \quad G(\omega_n) = \frac{1}{\beta}\int_0^{\beta} d\tau \ G(\tau) e^{-i\omega_n \tau/\beta} \ . \tag{G.4}$$

Deformed $\mathbf{AdS}_2$ black hole

We now add a deformation

$$f(r) = r^2 - 1 + \frac{1}{\tilde{\phi}}\int_1^r dr' \, \delta U(\tilde{\phi} r') = r^2 - 1 + g(r), \tag{G.5}$$

where we have defined

$$g(r) : \frac{1}{\tilde{\phi}}\int_1^r dr' \, \delta U(\tilde{\phi} r') \ . \tag{G.6}$$

If we make the coordinate transformation $r = \coth z$, we find that

$$f(r(z)) = \frac{1}{\sinh^2 z} + g(\coth z) = \frac{1}{\sinh^2 z} + h(z) \ , \tag{G.7}$$

where we have defined

$$h(z) := g(\coth z) \ . \tag{G.8}$$

Our metric then takes the form

$$ds^2 = \left(\frac{1}{\sinh^2 z} + h(z)\right) dt^2 + \frac{1}{\sinh^2 z \left(1 + h(z) \sinh^2 z\right)} dz^2 \ . \tag{G.9}$$

We now perform a further coordinate transformation to put the metric into its conformal frame. First we factor out the coefficient of dt^2 to give

$$ds^2 = \left(\frac{1}{\sinh^2 z} + h(z)\right) \left(dt^2 + \frac{1}{\left(1 + h(z) \sinh^2 z\right)^2} dz^2\right) \ . \tag{G.10}$$

We then make the transformation

$$\begin{cases} dx = \frac{1}{1+h(z)\sinh^2 z} dz \ , \\ x(z) = \int_{z_c}^{z} dz' \ \frac{1}{1+h(z')\sinh^2 z'} \ , \end{cases} \tag{G.11}$$

so that our metric now takes the form

$$ds^2 = \left(\frac{1}{\sinh^2(z(x))} + h(z(x))\right) \left(dt^2 + dx^2\right) \ . \tag{G.12}$$

From this we find that the two-point function in Fourier space is given by

$$G(\omega_n) = -\left(|\omega_n| + m^2 \int_0^\infty dy \ \left(\frac{1}{\sinh^2(z(y))} + h(z(y))\right) e^{-2|\omega_n| y} + \cdots\right) \ , \tag{G.13}$$

where we have used that $x = 0$ at the boundary $z = z_c$. We now change the variable of integration in (G.13) back to our variable z. That is, we substitute y for z where

$$\begin{cases} dy = \frac{1}{1+h(z)\sinh^2 z} dz \ , \\ y(z) = \int_{z_c}^{z} dz' \ \frac{1}{1+h(z')\sinh^2 z'} \ . \end{cases} \tag{G.14}$$

We then find that the two-point function is given by

$$G(\omega_n) = -\left(|\omega_n| + m^2 \int_{z_c}^\infty dz \ \left(\frac{1}{\sinh^2 z}\right) e^{-2|\omega_n| y(z)} + \cdots\right) \ . \tag{G.15}$$

We can re-write this as

$$G(\omega_n) = -\left(|\omega_n| + m^2 \int_{z_c}^{\infty} dz \, \left(\frac{1}{\sinh^2 z}\right) e^{-2|\omega_n|(z-z_c)} e^{2|\omega_n|((z-z_c)-y(z))} + \cdots\right) . \tag{G.16}$$

Noting that

$$\delta U(\phi) \geq 0 \Rightarrow g(r) \geq 0 \Rightarrow h(z) \geq 0 \ , \tag{G.17}$$

we then find

$$\begin{aligned} \delta U(\phi) \geq 0 &\Rightarrow \frac{1}{1 + h(z)\sinh^2 z} \leq 1 \\ &\Rightarrow y(z) \leq (z - z_c) \\ &\Rightarrow 1 \leq e^{2|\omega_n|((z-z_c)-y(z))} \ . \end{aligned} \tag{G.18}$$

This gives us the following inequality valid for $\delta U(\phi) \geq 0$

$$\begin{aligned} |G(\omega_n)| &\geq |\omega_n| + m^2 \int_{z_c}^{\infty} dz \, \left(\frac{1}{\sinh^2(z)}\right) e^{-2|\omega_n|(z-z_c)} + \cdots \\ &= |G_{\mathrm{AdS}_2}(\omega_n)| \ . \end{aligned} \tag{G.19}$$

H Krylov exponent from moments in the deformed SYK

In section 6.4.1.1 we computed the Krylov exponent at large q for the deformed SYK with $q = 2\tilde{q}$. This was done both by computing Lanczos coefficients as described in section 6.2.1, and from the pole of the autocorrelation function as described in section 6.2.2. In this case, with the moments method we are limited by numerical errors from the algorithm (6.3) to computing a maximum of 17 Lanczos coefficients and λ_K is computed from the slope of the last 3.

In the results shown in figure 31 we observe that for the first method there is a small deviation from $\lambda_K(\beta/2\pi) = 1$ during the transition between the two regions of near-maximal chaos which is not seen from the pole of the autocorrelation function. This happens, for instance, around $\beta\mathcal{J} \sim 10^{7.5}$ for $s = 0.001$.

We believe the deviation observed to be an artefact of not computing enough Lanczos coefficients before taking the slope. To demonstrate this in figure 42(a) we plot the Krylov exponent for the flow with $s = 0.001$ and different values of the number of Lanczos coefficients computed, $n_{\max}$. In each case λ_K is computed from the last 3 coefficients. We observe that as we increase $n_{\max}$

the deviation decreases. This is also shown in figure 42(b) which plots the maximum value of $\lambda_K(\beta/2\pi)$. We expect this trend to continue and that if enough coefficients were computed one would no longer observe a significant deviation from $\lambda_K(\beta/2\pi) = 1$ in this region, in agreement with the result from the pole of the autocorrelation function.

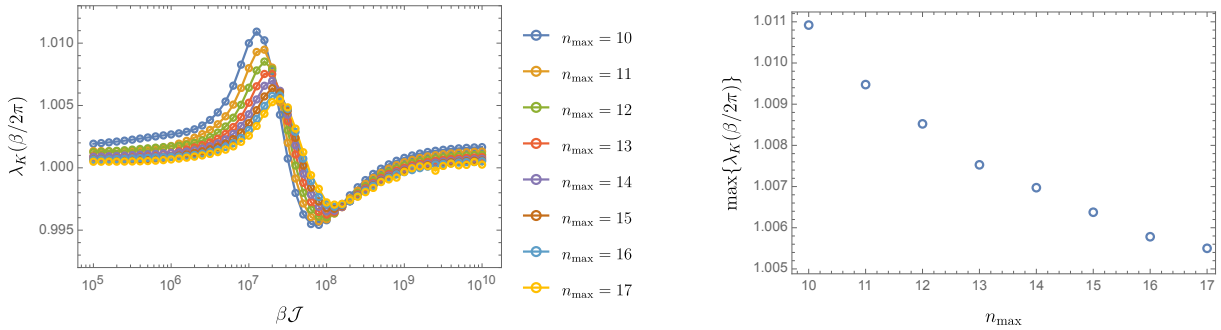

(a) (b)

Fig. 42: (a) The Krylov exponent, computed from the slope of the Lanczos coefficients, in the large q deformed model with $q/\tilde{q} = 2$ and $s = 0.001$. Each curve corresponds to a different number of coefficients computed, $n_{\max}$, before taking the slope of the last 3. (b) The maximum value of $\lambda_K(\beta/2\pi)$ in plot (a) for each value of $n_{\max}$.

I The slope of the first Lanczos coefficients in the deformed SYK

In section 6.4.1.1 it is shown that for the deformed SYK model at large q with $q = 2\tilde{q}$, the Krylov exponent does not detect the non-monotonic behaviour and sub-maximal chaos that the Lyapunov exponent shows between the two regimes of maximal chaos, see figure 31. If however, instead of looking at the asymptotic growth of the Lanczos coefficients at large n, we focus on the first few coefficients, we do observe a non-monotonic behaviour in this region. Surprisingly, up to an overall shift, the slope of just the first two Lanczos coefficients can be used to define a quantity that closely resembles the behaviour of the Lyapunov exponent. This is shown in figure 43, where we compute

$$\tilde{\lambda}_K = b_2 - b_1 - \left(\max_{\beta\mathcal{J}} \{b_2 - b_1\} - \frac{2\pi}{\beta} \right) , \tag{I.1}$$

and compare to the Lyapunov exponent for the same set of deformed SYK models as shown in figure 31. Though the match is not exact, it would be interesting to understand why this crude measure seems to be able to probe the region of sub-maximal chaos while λ_K is not.

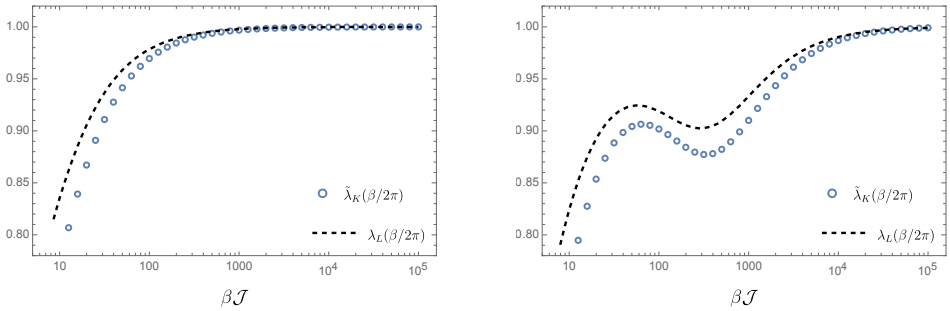

(a) $s = 1$

(b) $s = 0.1$

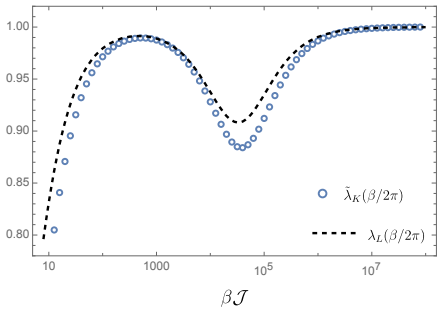

(c) $s = 0.01$

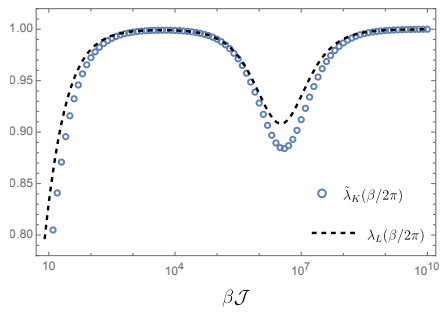

(d) $s = 0.001$

Fig. 43: $\tilde{\lambda}_K$ and Lyapunov exponent as a function of $\beta\mathcal{J}$ for the deformed model (2.47) in the large q limit with $q = 2\tilde{q}$. The blue dots are computed from the first two Lanczos coefficients which are found by the moments method described in section 6.2.1. The black dashed lines show the Lyapunov exponent, which is computed numerically. Plots are shown for different values of s.

J Open quantum systems and the Lindbladian

In the outlook of this thesis we speculate on the on open nature of a microscopic model of de Sitter space which leads us to consider the SYK model in the Lindbladian formalism. In this section we will review the basic concepts of open quantum systems and introduce the Lindblad master equation. For a more detailed introduction to open quantum systems we refer the reader to [165].

A system is said to be open if it can exchange energy and information with its environment. To describe such a system we will need to depart from the usual unitary time evolution that governs closed quantum systems. The basic idea will be to imagine the open system as a subsystem of a larger closed system that includes the environment. At any instance in time we can describe the state of the open system without reference to the environment by tracing out the environment degrees of freedom and leaving the system in a mixed state. The system is then described by a

reduced density matrix, $\rho(t)$. We would now like to derive the time evolution of $\rho(t)$ from general principles. We first note that the time evolution should be described by a map that takes density matrices to density matrices. This map should be Hemiticity preserving, trace preserving, and completely positive [17]. The most general such map is called a quantum channel and in general can be written in the so called Krauss representation

$$\mathcal{E}(\rho(t)) = \sum_i M_i(t)\rho(t)M_i^\dagger(t) \ , \tag{J.1}$$

where the operators $M_i(t)$ are called the Krauss operators and satisfy the completeness relation

$$\sum_i M_i^\dagger(t)M_i(t) = I. \tag{J.2}$$

The time evolution of our open system simplifies considerably if we make the further assumption of memorylessness of the environment called the Markovian assumption. Here we assume that the timescale of the environment is much shorter than the timescale of the evolution of the open system we are interested in. This means that the environment effectively "forgets" its correlations with the open system. Thus, under the Markovian assumption, the state of the open system after an infinitesmial time step at time $t + \Delta t$, only depends on the density matrix at time t and not on the entire history of the system. We can thus describe each time step by a quantum channel,

$$\rho(t + \Delta t) = \mathcal{E}_{dt}(\rho(t)) \ . \tag{J.3}$$

Writing the LHS of (J.3) to linear order in Δt and writing the quantum channel in terms of its Krauss operators we find

$$\rho(t) + \mathcal{L}(\rho(t))\Delta t + \mathcal{O}(\Delta t^2) = \sum_i M_i(t)\rho(t)M_i^\dagger(t) \ , \tag{J.4}$$

where we have defined the superoperator $\mathcal{L}(\rho) \equiv \dot{\rho}$, called the Lindbladian. Now keeping to linear

[17] If a map $\mathcal{E}_A$ maps positive linear operators acting on some Hilbert space $\mathcal{H}_A$ to other positive linear operators, we call it called positive. If additionally, upon extending the Hilbert space to $\mathcal{H}_A \otimes \mathcal{H}_B$ for any $\mathcal{H}_B$, the operator $\mathcal{E}_A \otimes I$ remains positive, then we say $\mathcal{E}_A$ is completely positive. This stronger condition ensures density operators of the open system remain positive when entangled with the environment

order we can, without loss of generality, re-write the Krauss operator as

$$\begin{aligned} M_1(t) &= I + (-iH(t) + K(t))\,\Delta t\ , \\ M_i(t) &= L_i(t)\sqrt{\Delta t} \quad \text{for } i > 1\ , \end{aligned} \tag{J.5}$$

where H and K are Hermitian operators and $L_i(t)$ are called jump operators. Upon fixing K in terms of the jump operators by using the completeness relation (J.2), we find that the Lindbladian can be written as

$$\mathcal{L}(\rho) = -\mathrm{i}[H(t), \rho] + \sum_{i=1}^{N} \left(L_i(t)\rho L_i^\dagger(t) - \frac{1}{2}\left\{ L_i^\dagger(t) L_i(t), \rho \right\} \right)\ . \tag{J.6}$$

Here we can view $H(t)$ as the system Hamiltonian and the first term as the usual Hamiltonian term describing unitary evolution. The additional terms involving the jump operators $L_i(t)$ capture the interactions between the system and the environment.

References

[1] D. Bernoulli, *Hydrodynamica, sive de viribus et motibus fluidorum commentarii*. Sumptibus Johannis Reinholdi Dulseckeri; Typis Joh. Deckeri, typographi Basiliensis, 1738, 10.3931/e-rara-3911.

[2] J. C. Maxwell, *On the dynamical theory of gases*, *Philosophical Transactions of the Royal Society of London* **157** (1867) 49.

[3] L. Boltzmann, *Weitere studien über das wärmegleichgewicht unter gasmolekülen*, *Sitzungsberichte der Kaiserlichen Akademie der Wissenschaften, Mathematisch-Naturwissenschaftliche Classe* **66** (1872) 275.

[4] G. W. Gibbons and S. W. Hawking, *Action Integrals and Partition Functions in Quantum Gravity*, *Phys. Rev. D* **15** (1977) 2752.

[5] J. D. Bekenstein, *Black holes and entropy*, *Phys. Rev. D* **7** (1973) 2333.

[6] S. W. Hawking, *Particle Creation by Black Holes*, *Commun. Math. Phys.* **43** (1975) 199.

[7] G. 't Hooft, *Dimensional reduction in quantum gravity*, *Conf. Proc. C* **930308** (1993) 284 [gr-qc/9310026].

[8] L. Susskind, *The World as a hologram*, *J. Math. Phys.* **36** (1995) 6377 [hep-th/9409089].

[9] J. M. Maldacena, *The Large N limit of superconformal field theories and supergravity*, *Adv. Theor. Math. Phys.* **2** (1998) 231 [hep-th/9711200].

[10] D. A. Galante, *Modave lectures on de Sitter space & holography*, *PoS* **Modave2022** (2023) 003 [2306.10141].

[11] A. Linde, *Eternally existing self-reproducing chaotic inflanationary universe*, *Physics Letters B* **175** (1986) 395.

[12] A. H. Guth, *Eternal inflation and its implications*, *Journal of Physics A: Mathematical and Theoretical* **40** (2007) 6811–6826.

[13] J. Polchinski, *The Black Hole Information Problem*, in *Theoretical Advanced Study Institute in Elementary Particle Physics: New Frontiers in Fields and Strings*, pp. 353–397, 2017, 1609.04036, DOI.

[14] D. Marolf, *The black hole information problem: past, present, and future*, *Reports on Progress in Physics* **80** (2017) 092001.

[15] S. Weinberg, *The cosmological constant problem*, *Rev. Mod. Phys.* **61** (1989) 1.

[16] S. M. Carroll, *Spacetime and Geometry: An Introduction to General Relativity*. Cambridge University Press, 7, 2019, 10.1017/9781108770385.

[17] Planck collaboration, *Planck 2018 results. VI. Cosmological parameters*, *Astron. Astrophys.* **641** (2020) A6 [1807.06209].

[18] F. Haake, *Quantum Signatures of Chaos*, Springer Series in Synergetics. Springer, Berlin, 2010, 10.1007/978-3-642-05428-0.

[19] R. Cooke and I. Grattan-Guinness, *Alexandr mikhailovich lyapunov, thesis on the stability of motion (1892)*, in *Landmark Writings in Western Mathematics 1640-1940*, (The Netherlands), Elsevier Science & Technology, (2005).

[20] A. I. Larkin and Y. N. Ovchinnikov, *Quasiclassical Method in the Theory of Superconductivity*, *Soviet Journal of Experimental and Theoretical Physics* **28** (1969) 1200.

[21] J. Maldacena, S. H. Shenker and D. Stanford, *A bound on chaos*, *JHEP* **08** (2016) 106 [1503.01409].

[22] L. D'Alessio, Y. Kafri, A. Polkovnikov and M. Rigol, *From quantum chaos and eigenstate thermalization to statistical mechanics and thermodynamics*, *Adv. Phys.* **65** (2016) 239 [1509.06411].

[23] H.-J. Stčkmann, *Quantum Chaos: An Introduction*. Cambridge University Press, 1999.

[24] L. Susskind, *Three Lectures on Complexity and Black Holes*, SpringerBriefs in Physics, Springer, 10, 2018, 1810.11563, DOI.

[25] S. Chapman and G. Policastro, *Quantum computational complexity from quantum information to black holes and back*, *Eur. Phys. J. C* **82** (2022) 128 [2110.14672].

[26] D. E. Parker, X. Cao, A. Avdoshkin, T. Scaffidi and E. Altman, *A Universal Operator Growth Hypothesis*, *Phys. Rev. X* **9** (2019) 041017 [1812.08657].

[27] A. Krylov, *De la résolution numérique de l'équation servant à déterminer dans des questions de mécanique appliquée les fréquences de petites oscillations des systèmes matériels*, *Bulletin de l'Académie des Sciences de l'URSS. Classe des sciences mathématiques et naturelles* **4** (1931) 491.

[28] P. Nandy, A. S. Matsoukas-Roubeas, P. Martínez-Azcona, A. Dymarsky and A. del Campo, *Quantum Dynamics in Krylov Space: Methods and Applications*, 2405.09628.

[29] S. Sachdev and J. Ye, *Gapless spin fluid ground state in a random, quantum Heisenberg magnet*, *Phys. Rev. Lett.* **70** (1993) 3339 [cond-mat/9212030].

[30] A. Kitaev, "A simple model of quantum holography." 2015.

[31] J. Maldacena and D. Stanford, *Remarks on the Sachdev-Ye-Kitaev model*, *Phys. Rev. D* **94** (2016) 106002 [1604.07818].

[32] K. Jensen, *Chaos in AdS_2 Holography*, *Phys. Rev. Lett.* **117** (2016) 111601 [1605.06098].

[33] J. Maldacena, D. Stanford and Z. Yang, *Conformal symmetry and its breaking in two dimensional Nearly Anti-de-Sitter space*, *PTEP* **2016** (2016) 12C104 [1606.01857].

[34] J. Engelsöy, T. G. Mertens and H. Verlinde, *An investigation of AdS_2 backreaction and holography*, *JHEP* **07** (2016) 139 [1606.03438].

[35] G. Sárosi, *AdS_2 holography and the SYK model*, *PoS* **Modave2017** (2018) 001 [1711.08482].

[36] Y. Sekino and L. Susskind, *Fast Scramblers*, *JHEP* **10** (2008) 065 [0808.2096].

[37] J. Polchinski and V. Rosenhaus, *The Spectrum in the Sachdev-Ye-Kitaev Model*, *JHEP* **04** (2016) 001 [1601.06768].

[38] M. Berkooz, P. Narayan, M. Rozali and J. Simón, *Higher Dimensional Generalizations of the SYK Model*, *JHEP* **01** (2017) 138 [1610.02422].

[39] D. J. Gross and V. Rosenhaus, *The Bulk Dual of SYK: Cubic Couplings*, *JHEP* **05** (2017) 092 [1702.08016].

[40] A. Kitaev and S. J. Suh, *The soft mode in the Sachdev-Ye-Kitaev model and its gravity dual*, *JHEP* **05** (2018) 183 [1711.08467].

[41] J. S. Cotler, G. Gur-Ari, M. Hanada, J. Polchinski, P. Saad, S. H. Shenker et al., *Black Holes and Random Matrices*, *JHEP* **05** (2017) 118 [1611.04650].

[42] M. Blake, H. Lee and H. Liu, *A quantum hydrodynamical description for scrambling and many-body chaos*, *JHEP* **10** (2018) 127 [1801.00010].

[43] D. A. Roberts, D. Stanford and A. Streicher, *Operator growth in the SYK model*, *JHEP* **06** (2018) 122 [1802.02633].

[44] B. Kobrin, Z. Yang, G. D. Kahanamoku-Meyer, C. T. Olund, J. E. Moore, D. Stanford et al., *Many-Body Chaos in the Sachdev-Ye-Kitaev Model*, *Phys. Rev. Lett.* **126** (2021) 030602 [2002.05725].

[45] M. Blake and H. Liu, *On systems of maximal quantum chaos*, *JHEP* **05** (2021) 229 [2102.11294].

[46] A. M. García-García, B. Loureiro, A. Romero-Bermúdez and M. Tezuka, *Chaotic-Integrable Transition in the Sachdev-Ye-Kitaev Model*, *Phys. Rev. Lett.* **120** (2018) 241603 [1707.02197].

[47] J. Kim and X. Cao, *Comment on "Chaotic-Integrable Transition in the Sachdev-Ye-Kitaev Model"*, *Phys. Rev. Lett.* **126** (2021) 109101 [2004.05313].

[48] A. M. García-García, B. Loureiro, A. Romero-Bermúdez and M. Tezuka, *Reply to Comment on "Chaotic-Integrable Transition in the Sachdev-Ye-Kitaev Model"*, *Phys. Rev. Lett.* **126** (2021) 109102 [2007.06121].

[49] A. Lunkin, A. Kitaev and M. Feigel'man, *Perturbed Sachdev-Ye-Kitaev model: a polaron in the hyperbolic plane*, 2006.14535.

[50] D. K. Nandy, T. Cadez, B. Dietz, A. Andreanov and D. Rosa, *Delayed Thermalization in Mass-Deformed SYK*, 2206.08599.

[51] H. G. Menzler and R. Jha, *Krylov localization as a probe for ergodicity breaking*, 2403.14384.

[52] J. Jiang and Z. Yang, *Thermodynamics and Many Body Chaos for generalized large q SYK models*, *JHEP* **08** (2019) 019 [1905.00811].

[53] D. Anninos and D. A. Galante, *Constructing AdS_2 flow geometries*, *JHEP* **02** (2021) 045 [2011.01944].

[54] D. Anninos, D. A. Galante and S. U. Sheorey, *Renormalisation group flows of deformed SYK models*, *JHEP* **11** (2023) 197 [2212.04944].

[55] J. C. Louw, L. M. van Manen and R. Jha, *Thermodynamics and dynamics of coupled complex SYK models*, 2312.14644.

[56] D. Anninos and D. M. Hofman, *Infrared realization of ds2 in ads2*, *Classical and Quantum Gravity* **35** (2018) 085003.

[57] D. Anninos, D. A. Galante and D. M. Hofman, *De sitter horizons & holographic liquids*, *Journal of High Energy Physics* **2019** (2019) 38.

[58] L. Susskind, *Entanglement and Chaos in De Sitter Holography: An SYK Example*, *Journal of Holography Applications in Physics* **1** (2021) 1 [2109.14104].

[59] A. A. Rahman, *dS JT Gravity and Double-Scaled SYK*, 2209.09997.

[60] V. Narovlansky and H. Verlinde, *Double-scaled SYK and de Sitter Holography*, 2310.16994.

[61] A. Avdoshkin and A. Dymarsky, *Euclidean operator growth and quantum chaos*, *Phys. Rev. Res.* **2** (2020) 043234 [1911.09672].

[62] Y. Gu, A. Kitaev and P. Zhang, *A two-way approach to out-of-time-order correlators*, *JHEP* **03** (2022) 133 [2111.12007].

[63] P. Caputa, J. M. Magan and D. Patramanis, *Geometry of Krylov complexity*, *Phys. Rev. Res.* **4** (2022) 013041 [2109.03824].

[64] V. Balasubramanian, P. Caputa, J. M. Magan and Q. Wu, *Quantum chaos and the complexity of spread of states*, *Phys. Rev. D* **106** (2022) 046007 [2202.06957].

[65] P. Caputa, J. M. Magan, D. Patramanis and E. Tonni, *Krylov complexity of modular Hamiltonian evolution*, *Phys. Rev. D* **109** (2024) 086004 [2306.14732].

[66] A. Bhattacharya, P. Nandy, P. P. Nath and H. Sahu, *On Krylov complexity in open systems: an approach via bi-Lanczos algorithm*, *JHEP* **12** (2023) 066 [2303.04175].

[67] A. Bhattacharya, R. N. Das, B. Dey and J. Erdmenger, *Spread complexity for measurement-induced non-unitary dynamics and Zeno effect*, *JHEP* **03** (2024) 179 [2312.11635].

[68] P. Caputa, H.-S. Jeong, S. Liu, J. F. Pedraza and L.-C. Qu, *Krylov complexity of density matrix operators*, *JHEP* **05** (2024) 337 [2402.09522].

[69] A. Bhattacharya, R. N. Das, B. Dey and J. Erdmenger, *Spread complexity and localization in $\mathcal{PT}$-symmetric systems*, 2406.03524.

[70] S. Chapman, S. Demulder, D. A. Galante, S. U. Sheorey and O. Shoval, *Krylov complexity and chaos in deformed SYK models*, 2407.09604.

[71] E. Witten, *Deformations of JT Gravity and Phase Transitions*, 2006.03494.

[72] D. Anninos and E. Harris, *Interpolating geometries and the stretched dS_2 horizon*, 2209.06144.

[73] O. Bohigas, M. J. Giannoni and C. Schmit, *Characterization of chaotic quantum spectra and universality of level fluctuation laws*, *Phys. Rev. Lett.* **52** (1984) 1.

[74] E. P. Wigner, *Characteristic vectors of bordered matrices with infinite dimensions*, *Annals of Mathematics* **63** (1955) 548.

[75] C. E. Porter, *Statistical theories of spectra: Fluctuations*, 1965.

[76] M. Mehta, *Random Matrices and the Statistical Theory of Energy Levels*. Academic Press, New York, 1991.

[77] G. W. Anderson, A. Guionnet and O. Zeitouni, *An Introduction to Random Matrices*. Cambridge University Press, Cambridge, 2010.

[78] A. Romero-Bermúdez, K. Schalm and V. Scopelliti, *Regularization dependence of the OTOC. Which Lyapunov spectrum is the physical one?*, *JHEP* **07** (2019) 107 [1903.09595].

[79] A. Avdoshkin, A. Dymarsky and M. Smolkin, *Krylov complexity in quantum field theory, and beyond*, *JHEP* **06** (2024) 066 [2212.14429].

[80] H. A. Camargo, V. Jahnke, K.-Y. Kim and M. Nishida, *Krylov complexity in free and interacting scalar field theories with bounded power spectrum*, *JHEP* **05** (2023) 226 [2212.14702].

[81] V. Rosenhaus, *An introduction to the SYK model*, *J. Phys. A* **52** (2019) 323001 [1807.03334].

[82] D. A. Trunin, *Pedagogical introduction to the Sachdev–Ye–Kitaev model and two-dimensional dilaton gravity*, *Usp. Fiz. Nauk* **191** (2021) 225 [2002.12187].

[83] D. Chowdhury, A. Georges, O. Parcollet and S. Sachdev, *Sachdev-Ye-Kitaev models and beyond: Window into non-Fermi liquids*, *Rev. Mod. Phys.* **94** (2022) 035004 [2109.05037].

[84] S. Sachdev, *Bekenstein-Hawking Entropy and Strange Metals*, *Phys. Rev. X* **5** (2015) 041025 [1506.05111].

[85] E. A. Cruz and G. Tarnopolsky, *Precise Low-Temperature Expansions for the Sachdev-Ye-Kitaev model*, 2206.13547.

[86] D. Stanford and E. Witten, *Fermionic Localization of the Schwarzian Theory*, *JHEP* **10** (2017) 008 [1703.04612].

[87] D. Anninos, D. M. Hofman and S. Vitouladitis, *One-dimensional Quantum Gravity and the Schwarzian theory*, *JHEP* **03** (2022) 121 [2112.03793].

[88] M. Berkooz, P. Narayan and J. Simon, *Chord diagrams, exact correlators in spin glasses and black hole bulk reconstruction*, *JHEP* **08** (2018) 192 [1806.04380].

[89] M. Berkooz, M. Isachenkov, V. Narovlansky and G. Torrents, *Towards a full solution of the large N double-scaled SYK model*, *JHEP* **03** (2019) 079 [1811.02584].

[90] G. Tarnopolsky, *Large q expansion in the Sachdev-Ye-Kitaev model*, *Phys. Rev. D* **99** (2019) 026010 [1801.06871].

[91] M. Berkooz, N. Brukner, Y. Jia and O. Mamroud, *From Chaos to Integrability in Double Scaled SYK*, 2403.01950.

[92] M. Berkooz, N. Brukner, Y. Jia and O. Mamroud, *A Path Integral for Chord Diagrams and Chaotic-Integrable Transitions in Double Scaled SYK*, 2403.05980.

[93] T. G. Mertens and G. J. Turiaci, *Solvable models of quantum black holes: a review on Jackiw–Teitelboim gravity*, *Living Rev. Rel.* **26** (2023) 4 [2210.10846].

[94] R. Jackiw, *Lower Dimensional Gravity*, *Nucl. Phys. B* **252** (1985) 343.

[95] C. Teitelboim, *Gravitation and Hamiltonian Structure in Two Space-Time Dimensions*, *Phys. Lett. B* **126** (1983) 41.

[96] V. Y. Pan and Z. Q. Chen, *The complexity of the matrix eigenproblem*, in *Symposium on the Theory of Computing*, 1999, https://api.semanticscholar.org/CorpusID:2974790.

[97] W. Cheney and D. Kincaid, *Numerical Mathematics and Computing*. Thomson Brooks/Cole, Belmont, CA, 6th ed., 2007.

[98] L. Sá, P. Ribeiro and T. Prosen, *Lindbladian dissipation of strongly-correlated quantum matter*, *Phys. Rev. Res.* **4** (2022) L022068 [2112.12109].

[99] L. Sá, *Signatures of dissipative quantum chaos*, phd thesis, University of Lisboa, 11, 2023.

[100] A. Castro Neto and E. Fradkin, *The thermodynamics of quantum systems and generalizations of zamolodchikov's c-theorem*, *Nuclear Physics B* **400** (1993) 525.

[101] M. Zabzine, *A Finite temperature generalization of Zamolodchikov's C theorem*, hep-th/9705015.

[102] T. Appelquist, A. G. Cohen and M. Schmaltz, *A New constraint on strongly coupled gauge theories*, *Phys. Rev. D* **60** (1999) 045003 [hep-th/9901109].

[103] L. V. Delacretaz, A. L. Fitzpatrick, E. Katz and M. T. Walters, *Thermalization and hydrodynamics of two-dimensional quantum field theories*, *SciPost Phys.* **12** (2022) 119 [2105.02229].

[104] J. de Boer, E. P. Verlinde and H. L. Verlinde, *On the holographic renormalization group*, *JHEP* **08** (2000) 003 [hep-th/9912012].

[105] S. de Haro, S. N. Solodukhin and K. Skenderis, *Holographic reconstruction of space-time and renormalization in the AdS / CFT correspondence*, *Commun. Math. Phys.* **217** (2001) 595 [hep-th/0002230].

[106] J. Maldacena and X.-L. Qi, *Eternal traversable wormhole*, 1804.00491.

[107] A. M. García-García, T. Nosaka, D. Rosa and J. J. M. Verbaarschot, *Quantum chaos transition in a two-site Sachdev-Ye-Kitaev model dual to an eternal traversable wormhole*, *Phys. Rev. D* **100** (2019) 026002 [1901.06031].

[108] D. J. Gross and V. Rosenhaus, *A Generalization of Sachdev-Ye-Kitaev*, *JHEP* **02** (2017) 093 [1610.01569].

[109] D. Anninos, T. Anous and R. D'Agnolo, *Marginal deformations & rotating horizons*, *JHEP* **12** (2017) 095 [1707.03380].

[110] J. Yoon, *SYK Models and SYK-like Tensor Models with Global Symmetry*, *JHEP* **10** (2017) 183 [1707.01740].

[111] Y. Gu, A. Kitaev, S. Sachdev and G. Tarnopolsky, *Notes on the complex Sachdev-Ye-Kitaev model*, *JHEP* **02** (2020) 157 [1910.14099].

[112] C. Liu, P. Zhang and X. Chen, *Non-unitary dynamics of Sachdev-Ye-Kitaev chain*, *SciPost Phys.* **10** (2021) 048 [2008.11955].

[113] A. M. García-García, L. Sá and J. J. M. Verbaarschot, *Symmetry Classification and Universality in Non-Hermitian Many-Body Quantum Chaos by the Sachdev-Ye-Kitaev Model*, *Phys. Rev. X* **12** (2022) 021040 [2110.03444].

[114] Y. Gu, X.-L. Qi and D. Stanford, *Local criticality, diffusion and chaos in generalized Sachdev-Ye-Kitaev models*, *JHEP* **05** (2017) 125 [1609.07832].

[115] A. Goel, H. T. Lam, G. J. Turiaci and H. Verlinde, *Expanding the Black Hole Interior: Partially Entangled Thermal States in SYK*, *JHEP* **02** (2019) 156 [1807.03916].

[116] D. Anninos, T. Anous and F. Denef, *Disordered Quivers and Cold Horizons*, *JHEP* **12** (2016) 071 [1603.00453].

[117] W. Fu, D. Gaiotto, J. Maldacena and S. Sachdev, *Supersymmetric Sachdev-Ye-Kitaev models*, *Phys. Rev. D* **95** (2017) 026009 [1610.08917].

[118] I. Affleck and A. W. W. Ludwig, *Universal noninteger 'ground state degeneracy' in critical quantum systems*, *Phys. Rev. Lett.* **67** (1991) 161.

[119] A. Jevicki and K. Suzuki, *Bi-Local Holography in the SYK Model: Perturbations*, *JHEP* **11** (2016) 046 [1608.07567].

[120] S. R. Das, A. Ghosh, A. Jevicki and K. Suzuki, *Near Conformal Perturbation Theory in SYK Type Models*, *JHEP* **12** (2020) 171 [2006.13149].

[121] M. Tikhanovskaya, H. Guo, S. Sachdev and G. Tarnopolsky, *Excitation spectra of quantum matter without quasiparticles I: Sachdev-Ye-Kitaev models*, *Phys. Rev. B* **103** (2021) 075141 [2010.09742].

[122] A. Belin and J. de Boer, *Random statistics of OPE coefficients and Euclidean wormholes*, *Class. Quant. Grav.* **38** (2021) 164001 [2006.05499].

[123] D. J. Gross and V. Rosenhaus, *All point correlation functions in SYK*, *JHEP* **12** (2017) 148 [1710.08113].

[124] D. Grumiller and R. McNees, *Thermodynamics of black holes in two (and higher) dimensions*, *JHEP* **04** (2007) 074 [hep-th/0703230].

[125] D. Anninos and D. M. Hofman, *Infrared Realization of dS_2 in AdS_2*, *Class. Quant. Grav.* **35** (2018) 085003 [1703.04622].

[126] H. Maxfield and G. J. Turiaci, *The path integral of 3D gravity near extremality; or, JT gravity with defects as a matrix integral*, *JHEP* **01** (2021) 118 [2006.11317].

[127] D. Anninos, D. A. Galante and D. M. Hofman, *De Sitter Horizons & Holographic Liquids*, *JHEP* **07** (2019) 038 [1811.08153].

[128] D. Anninos, D. A. Galante and B. Mühlmann, *Finite Features of Quantum De Sitter Space*, 2206.14146.

[129] A. Kitaev, *A simple model of quantum holography*, *KITP strings seminar and Entanglement program* (2015) [http://online.kitp.ucsb.edu/online/entangled15].

[130] M. G. Viswanath V.S., *The recursion method Application to many-body dynamics*. Springer, 1994.

[131] A. Dymarsky and M. Smolkin, *Krylov complexity in conformal field theory*, *Phys. Rev. D* **104** (2021) L081702 [2104.09514].

[132] S.-K. Jian, B. Swingle and Z.-Y. Xian, *Complexity growth of operators in the SYK model and in JT gravity*, *JHEP* **03** (2021) 014 [2008.12274].

[133] B. Bhattacharjee, P. Nandy and T. Pathak, *Krylov complexity in large q and double-scaled SYK model*, *JHEP* **08** (2023) 099 [2210.02474].

[134] J. Polchinski, *The phase of the sum over spheres*, *Phys. Lett. B* **219** (1989) 251.

[135] D. Anninos, T. Bautista and B. Mühlmann, *The two-sphere partition function in two-dimensional quantum gravity*, *JHEP* **09** (2021) 116 [2106.01665].

[136] D. Anninos, F. Denef, Y. T. A. Law and Z. Sun, *Quantum de Sitter horizon entropy from quasicanonical bulk, edge, sphere and topological string partition functions*, *JHEP* **01** (2022) 088 [2009.12464].

[137] D. Anninos and E. Harris, *Three-dimensional de Sitter horizon thermodynamics*, 2106.13832.

[138] R. Loganayagam and O. Shetye, *Influence phase of a dS observer. Part I. Scalar exchange*, *JHEP* **01** (2024) 138 [2309.07290].

[139] A. M. García-García and V. Godet, *Euclidean wormhole in the Sachdev-Ye-Kitaev model*, *Phys. Rev. D* **103** (2021) 046014 [2010.11633].

[140] A. M. García-García, Y. Jia, D. Rosa and J. J. M. Verbaarschot, *Dominance of Replica Off-Diagonal Configurations and Phase Transitions in a PT Symmetric Sachdev-Ye-Kitaev Model*, *Phys. Rev. Lett.* **128** (2022) 081601 [2102.06630].

[141] P. Zhang, S.-K. Jian, C. Liu and X. Chen, *Emergent Replica Conformal Symmetry in Non-Hermitian SYK_2 Chains*, *Quantum* **5** (2021) 579 [2104.04088].

[142] S.-K. Jian, C. Liu, X. Chen, B. Swingle and P. Zhang, *Measurement-Induced Phase Transition in the Monitored Sachdev-Ye-Kitaev Model*, *Phys. Rev. Lett.* **127** (2021) 140601 [2104.08270].

[143] C. M. Bender and S. Boettcher, *Real spectra in nonHermitian Hamiltonians having PT symmetry*, *Phys. Rev. Lett.* **80** (1998) 5243 [physics/9712001].

[144] C. M. Bender, D. C. Brody and H. F. Jones, *Complex extension of quantum mechanics*, *Phys. Rev. Lett.* **89** (2002) 270401 [quant-ph/0208076].

[145] Y. Ashida, Z. Gong and M. Ueda, *Non-Hermitian physics*, *Adv. Phys.* **69** (2021) 249 [2006.01837].

[146] D. A. Lidar, *Lecture Notes on the Theory of Open Quantum Systems*, 1902.00967.

[147] V. Gorini, A. Kossakowski and E. C. G. Sudarshan, *Completely Positive Dynamical Semigroups of N Level Systems*, *J. Math. Phys.* **17** (1976) 821.

[148] G. Lindblad, *On the generators of quantum dynamical semigroups*, *Communications in Mathematical Physics* **48** (1976) 119.

[149] A. Kulkarni, T. Numasawa and S. Ryu, *Lindbladian dynamics of the Sachdev-Ye-Kitaev model*, *Phys. Rev. B* **106** (2022) 075138 [2112.13489].

[150] A. M. García-García, L. Sá, J. J. M. Verbaarschot and J. P. Zheng, *Keldysh Wormholes and Anomalous Relaxation in the Dissipative Sachdev-Ye-Kitaev Model*, 2210.01695.

[151] K. Kawabata, A. Kulkarni, J. Li, T. Numasawa and S. Ryu, *Dynamical quantum phase transitions in Sachdev-Ye-Kitaev Lindbladians*, *Phys. Rev. B* **108** (2023) 075110 [2210.04093].

[152] A. Bhattacharya, P. Nandy, P. P. Nath and H. Sahu, *Operator growth and Krylov construction in dissipative open quantum systems*, *JHEP* **12** (2022) 081 [2207.05347].

[153] C. Liu, H. Tang and H. Zhai, *Krylov complexity in open quantum systems*, *Phys. Rev. Res.* **5** (2023) 033085 [2207.13603].

[154] B. Bhattacharjee, X. Cao, P. Nandy and T. Pathak, *Operator growth in open quantum systems: lessons from the dissipative SYK*, *JHEP* **03** (2023) 054 [2212.06180].

[155] N. S. Srivatsa and C. von Keyserlingk, *Operator growth hypothesis in open quantum systems*, *Phys. Rev. B* **109** (2024) 125149 [2310.15376].

[156] M. Berkooz, A. Sharon, N. Silberstein and E. Y. Urbach, *Onset of quantum chaos in disordered CFTs*, *Phys. Rev. D* **106** (2022) 045007 [2111.06108].

[157] M. Berkooz, A. Sharon, N. Silberstein and E. Y. Urbach, *Onset of Quantum Chaos in Random Field Theories*, *Phys. Rev. Lett.* **129** (2022) 071601 [2207.11980].

[158] E. Rabinovici, A. Sánchez-Garrido, R. Shir and J. Sonner, *Krylov localization and suppression of complexity*, *JHEP* **03** (2022) 211 [2112.12128].

[159] E. Rabinovici, A. Sánchez-Garrido, R. Shir and J. Sonner, *Krylov complexity from integrability to chaos*, *JHEP* **07** (2022) 151 [2207.07701].

[160] E. Rabinovici, A. Sánchez-Garrido, R. Shir and J. Sonner, *Operator complexity: a journey to the edge of Krylov space*, *JHEP* **06** (2021) 062 [2009.01862].

[161] J. Yoon, *A Bound on Chaos from Stability*, 1905.08815.

[162] K. Jensen, *Scrambling in nearly thermalized states at large central charge*, 1906.05852.

[163] A. Kundu, V. Malvimat and R. Sinha, *State dependence of Krylov complexity in 2d CFTs*, *JHEP* **09** (2023) 011 [2303.03426].

[164] W. Fu and S. Sachdev, *Numerical study of fermion and boson models with infinite-range random interactions*, *Phys. Rev. B* **94** (2016) 035135 [1603.05246].

[165] J. Preskill, *Lecture notes for physics 229: Quantum information and computation*, 1998.